FOREST COVER CHANGE AND POST-FIRE RESPONSE IN THE SOUTHERN ROCKY MOUNTAINS

by

Kyle C. Rodman

B.A., University of Colorado Colorado Springs – 2011

M.S., Northern Arizona University – 2015

A thesis submitted to the

Faculty of the Graduate School of the

University of Colorado in partial fulfillment

of the requirements for the degree of

Doctor of Philosophy

Department of Geography

2019

This thesis entitled:

Forest Cover Change and Post-Fire Response in the Southern Rocky Mountains

written by Kyle C. Rodman

has been approved by the Department of Geography

_____

Thomas T. Veblen

_____

Barbara P. Buttenfield

_____

Stefan Leyk

Date _____

The final copy of this thesis has been examined by the signatories, and we find that both the content and the form meet acceptable presentation standards of scholarly work in the above-mentioned discipline.

ABSTRACT

Rodman, Kyle C. (Ph.D., Geography)

FOREST COVER CHANGE AND POST-FIRE RESPONSE IN THE SOUTHERN ROCKY MOUNTAINS

Thesis directed by Distinguished Professor Thomas T. Veblen.

Forests are some of the Earth's most important ecosystems. They are sanctums of biodiversity, play a key role in nutrient cycling, and provide countless ecosystem services to humans. Recent studies have identified broad-scale changes in forest cover across the globe. A richer understanding of these changes can be developed by identifying specific causal mechanisms, placing recent shifts in forest cover in a historical context, and by using knowledge of the past and present to make inferences about the future. The goal of our research was to better understand the past, present, and future of forested ecosystems in the northern Front Range of Colorado (NFR) and in the Southern Rocky Mountains Ecoregion (SRME). In particular, this dissertation focused on the roles of historical land use, wildfire activity, and post-fire recovery in observed and projected changes in conifer forests.

To quantify the extent to which forest cover in the NFR changed 1938-2015 and to provide insight into possible potential drivers, we used high-resolution historical (c. 1938) and contemporary (2015) aerial photography to classify forested area across a 2932 km2 study area. We found that historical patterns of land use, as well as historical and contemporary fire activity

and subsequent post-fire recovery, played key roles in 20th-century changes in forest cover across the NFR. To better characterize the drivers of limited conifer recovery in low-elevation forests, we surveyed post-fire conifer seedling abundance, tree establishment, and seed cone production across 15 wildfires in southern Colorado and northern New Mexico. We then used these data to quantify potential bottlenecks to post-fire conifer recovery. Lastly, we combined these data with similar surveys in the SRME performed by three former graduate students in Colorado and Arizona. Using the combined dataset, we modeled the extent to which a warming climate is limiting post-fire recovery of two widespread conifer species and projected that further declines in resilience are likely through 2100. Our findings reinforce the historical importance of wildfire, anthropogenic impacts, and abiotic factors in the dynamics of forested landscapes in the southern Rocky Mountains. These same factors will remain important throughout the upcoming century.

DEDICATION

This dissertation is dedicated to Teresa Cotten, Lee Rodman, Dori Rodman, Howard Lankford, Jamie Cotten-Walker, Carita Rodman, Hubert Rodman, and Ana Miller-Ter Kuile. I wouldn't be here without your unwavering support, love, and inspiration.

ACKNOWLEDGEMENTS

I owe many thanks to my advisor Tom Veblen for sharing his vast knowledge of forests in North and South America and for pushing me intellectually and academically. I have been blessed to work in a lab with a number of tremendously talented, interesting, and kind people including Robbie Andrus, Rachel Chai, Teresa Chapman, Brian Harvey, Julia Kelly, Jennifer Landesmann, and Sara Saraceni. Thanks to my committee members Mike Battaglia, Babs Buttenfield, Stefan Leyk, and Carol Wessman for helpful feedback and keen scientific insight. Tania Schoennagel, Rosemary Sherriff, Alan Tepley, and Solomon Dobrowski provided additional feedback or contributed data for various portions of this dissertation. Teresa Chapman, Sara Saraceni, Monica Rother, Andreas Wion, Miranda Redmond, Mike Battaglia, Marin Chambers, Paula Fornwalt, Zack Holden, Jessi Ouzts, and Tom Kolb have all been helpful collaborators in this work. Katie Lage helped in accessing and understanding the aerial photography collections at the University of Colorado Boulder. The Department of Geography has been an amazing and supportive place to work and I value each of the friendships I have developed with students, faculty, and staff. Darla Shatto and Karen Weingarten provided crucial support at many steps throughout this process. Geography is where it's at.

Thanks to Andrew Sánchez Meador, David Huffman, Kristen Waring, Margaret Moore, Dave Havlick, Eric Billmeyer, Tom Huber, Curt Holder, and Mark Hesse for teaching me about the natural world and for pulling me in the right direction. Thanks also to my many friends and former co-workers at RMFI for helping shape the way I think about science, nature, and the land around us. Over the last four years, Ryan Lima, Tim Bryant, Brent Nelson, and the Flagstaff crew kept me sane by getting me out on some amazing adventures. Adam Mahood, Tasha Snow,

Joe Tuccillo, Sarah Posner, Josh Vonloh, Dan Allen and many others helped to do the same here in Boulder.

The work in this dissertation would not have been possible without financial support from the Australian Research Council, the National Science Foundation, the Joint Fire Science Program, Boulder Open Space and Mountain Parks, the John Marr Ecology Fund, the Colorado Mountain Club Foundation, and the University of Colorado. Many employees of the U.S. Forest Service, the Vermejo Park Ranch, the Tercio Ranch, and the Trinchera-Blanca ranch gave permission to access and sample our research sites. A special thanks to Amanda Benton, Craig Taggart, Aaron Swallow, Lora Arciniega, Gabriel Romero, Gretchen Fitzgerald, Frank Nemick, Paul Crespin, Dennis Carril, and Alex Rudney. For help with field data collection and laboratory work, I am indebted to Kelsey Bohanon, Aaron Broughton, Kristina Cowell, Molly Day, Katherine Feldmann, Mike Greene, Angela Gonzalez, Ana Miller-ter Kuile, Josh Vonloh, Katie Weimer, Brenna Wider, and Jake Zatz.

Lastly, thanks to each member of my large and complicated family. We've been through a lot together, but you all helped me get through it.

CONTENTS

TABLES

FIGURES

CHAPTER 1

INTRODUCTION

1.1 Justification

Forests cover just 30 percent of the Earth's land area, yet they provide habitat for more than 80 percent of terrestrial wildlife species (Bonan 2008, FAO 2015). Forests are also some of the most economically valuable ecosystems to humans, supplying myriad ecosystem services such as carbon sequestration, timber production, and water resource protection (Costanza et al. 1997, Bonan 2008). Recent shifts in global forest area have been documented using a range of techniques (Hansen et al. 2013, Keenan et al. 2015, Song et al. 2018); human land use and anthropogenic climate change are now widely recognized as important drivers of these changes. The characterization of disturbance dynamics and successional processes helps to describe the mechanisms and consequences of forest change and to provide insight into what the future may hold.

An understanding of specific drivers of ecosystem change is needed to better manage, protect, and conserve forests. These drivers of change can operate at a wide range of temporal scales; while a forest can persist beyond human time scales, it can also disappear in an instant and take decades to recover. Integrative research that combines historical ecology, contemporary observations, and forward modeling approaches helps to better describe the complexities of the causal mechanisms of forest change. In this dissertation, we utilized historical datasets (i.e., tree-ring methods, historical aerial photographs, records of past land use), contemporary field

surveys, and future climate projections, to develop a more holistic picture of the past, present, and future of coniferous forests in the Southern Rocky Mountains.

1.2 Background

1.2.1 Forests and Disturbance Dynamics in the Southern Rocky Mountains

The Southern Rocky Mountains Ecoregion (SRME) spans 144,462 km² area in southern Wyoming, Colorado, and northern New Mexico, USA, and forested ecosystems cover 56.3% of the total area (Homer et al. 2015). Across this broad area, vegetation differs substantially in composition, structure, and in its relationship with disturbance. In the southern and western portions of the study area, lower-elevation forests (Piñon-juniper woodlands) are dominated by two-needle piñon pine (*Pinus edulis*) and several juniper species (*Juniperus* spp). In the early 2000s, extreme drought stress and outbreaks of piñon ips (the bark beetle *Ips confusus*) triggered widespread mortality of piñon pine throughout these low elevation forests and woodlands (Breshears et al. 2005). Historical fire activity in piñon-juniper woodlands was typically infrequent and stand-replacing (Baker and Shinneman 2004), though frequent surface fires may have occurred in piñon-juniper savanna sites, or those with thick, continuous grass cover (Romme et al. 2009a). In the south and west portions of the SRME, Gambel oak (*Quercus gambelii*) is also an important component of low-mid elevation forests, intermixing with piñon-juniper vegetation at its lower extent, and ponderosa pine (*Pinus ponderosa* var. *scopulorum*) at its upper extent. Gambel oak exhibits a range of fire-adaptive traits, including the ability to resprout following mortality of the aboveground stems, as well as thick bark in larger size-classes that permits survival of large stems during low-severity surface fires (Abella and Fulé 2008, Kaufmann et al. 2016). Gambel oak is predicted to benefit from climate warming through increases in climatically suitable habitat throughout the region (Rehfeldt et al. 2006) and because

increases in fire activity allow for long-term site occupancy in high severity fire patches (Guiterman et al. 2017).

Ponderosa pine and mixed-conifer forests span much of the middle elevations in the SRME. Pure stands of ponderosa pine are common in the southern and eastern portion of the region, but are less common on the western slope. Mixed-conifer forests are composed of ponderosa pine as well as Douglas-fir (*Pseudotsuga menziesii* var. *glauca)*, white fir (*Abies concolor* var. *concolor*), lodgepole pine (*Pinus contorta* var. *latifolia*), quaking aspen (*Populus tremuloides*), Gambel oak, and blue spruce (*Picea pungens*). Mixed-conifer forests also include other species in the genera *Abies*, *Juniperus*, *Picea*, *Pinus*, and *Populus* that vary in importance throughout the region. Western spruce budworm (*Choristoneura freemani*), Douglas-fir bark beetle (*Dendroctonus pseudotsugae*), and mountain pine beetle (*D. ponderosae*) are all important insect pests that can cause tree mortality in ponderosa pine and mixed-conifer forests (Romme et al. 2006). Western spruce budworm and Douglas-fir bark beetle preferentially attack Douglas-fir (Hadley and Veblen 1993), while mountain pine beetle is most associated with mortality in pine species (e.g., lodgepole pine, ponderosa pine, and limber pine – *Pinus flexilis*). Throughout the 2000s, mountain pine beetle caused widespread tree mortality in lodgepole pine forests throughout the SRME (Chapman et al. 2012). The historical effects of fire are widely-variable in ponderosa pine and mixed-conifer forests sometimes leading to divergent views of its role in structuring the landscape (Kaufmann et al. 2006, Veblen et al. 2012). However, it is generally agreed that frequent, low-severity fire was most common at low-elevation sites (Williams and Baker 2012a, Sherriff et al. 2014, Brown et al. 2015), and those that are adjacent to, or intermixed with, grasslands (Gartner et al. 2012).

In the highest elevation forests, the spruce-fir zone, dominant tree species include lodgepole pine, subalpine fir (*Abies lasiocarpa*), Engelmann spruce (*Picea engelmannii*), limber pine, bristlecone pine (*Pinus aristata*), and quaking aspen. White pine blister rust, a tree disease caused by the invasive fungus *Cronartium ribicola*, has the potential to drive widespread mortality of limber and bristlecone pine throughout this zone (Geils et al. 2010). Though mountain pine beetle activity has declined in recent years, spruce beetle (*Dendroctonus rufipennis*) activity has increased, leading to extensive mortality of Engelmann spruce in the northern and southwestern portions of the SRME (Hart et al. 2017). Wildfires are typically infrequent (> 200 years between events), large (> 1000 ha), and severe in spruce-fir forests, occurring only in times of extreme drought (Sibold and Veblen 2006, Sibold et al. 2006). Lodgepole pine, limber pine, and aspen are the most common early-seral species, and can give way to Engelmann spruce and subalpine fir over time on more productive sites (Veblen 1986). Across most elevational zones, riparian sites tend to be dominated by a mixture of broadleaf deciduous species (i.e., *Populus* spp. and *Salix* spp.).

1.2.2 Human Land Use Change and Wildfire in the Southern Rocky Mountains

Euro-American settlement in the southern portion of the SRME began in the late 1500s with the development of Spanish outposts in current-day New Mexico (Liebmann et al. 2016), but Native American communities were present in many areas for at least 11,000 years before present (Waters and Stafford Jr. 2007). Native peoples likely used fire to drive game throughout portions of the region (Veblen and Donnegan 2005, Baker 2009), though the overall effects of these activities on forests are not well understood. Native American activities may have increased fire activity in some areas, while decreasing fire activity in others (Liebmann et al. 2016). The removal of Native American communities through war and disease triggered

afforestation and shifts in fire regimes in some areas (Liebmann et al. 2016). Widespread Euro-American settlement in the Southern Rocky Mountains occurred much later c. late 1850s and coincided with the occurrence of the 1859 gold rush. This rapid increase in mining activity and industrialization triggered large fire years in forests of the heavily-mined northern Front Range (Veblen et al. 2000, Rodman et al. 2019). Logging impacts were also widespread. Logging activities in the late 1800s and early 1900s selectively-targeted larger, older trees for timber. Thus, few trees in national forests of the Colorado Front Range predate this 1850s period (Veblen and Donnegan 2005). Though widespread mining did not occur in some portions of the Southern Rocky Mountains, the impacts of these anthropogenic activities are obvious in repeat photographs in the northern Front Range and the San Juan Mountains (Veblen and Lorenz 1991, Zier and Baker 2006). Logging, grazing, and organized fire suppression reduced fire activity in many ponderosa pine and dry mixed-conifer forests throughout the region, though the initiation of fire exclusion varied from the 1850s to the 1920s depending on the location (Swetnam and Baisan 1996, Veblen et al. 2000, Fulé et al. 2009, Brown et al. 2015, Tepley and Veblen 2015). Rapid exurban development occurred in the SRME throughout the 1900s, particularly after 1950, and led to a drastic increase in the number of homes in fire-prone areas (Theobald and Romme 2007, Platt et al. 2011). The long-term impacts of each of these processes are important to understand because they help to better contextualize historical forest conditions, recent forest changes, and the natural ranges of variability that are often targeted with ecological restoration.

Since 1984, the area burned in large wildfires in the western United States (Dennison et al. 2014) and in the Southern Rocky Mountains has increased (Picotte et al. 2016). Anthropogenically-driven climate warming has lengthened fire seasons and increased fuel aridity (Jolly et al. 2015, Westerling 2016) and may account for 50 percent or more of the increase in

area burned in large wildfires since 1984 (Abatzoglou and Williams 2016). Fire activity is expected to continue to increase in the near-future (Liu et al. 2013), and the Rocky Mountain region is especially susceptible to these increases (Spracklen et al. 2009). While increased temperatures and drought stress influence wildfire activity directly, they can also negatively influence post-fire recovery, compounding the initial impacts of these disturbances (Enright et al. 2015, Stevens-Rumann et al. 2018, Davis et al. 2019). Forest response to disturbance is a key metric when assessing ecosystem resilience (the ability to recover to a relatively similar state following an disturbance; Holling 1973, Millar and Stephenson 2015), and remains a crucial research need within the context of a warmer, drier future (Turner 2010). Research focusing on post-fire recovery processes in coniferous forests has rapidly expanded in recent years (Table 1.1). However, this type of research can be improved through the better incorporation of interannual climate variability, the explicit consideration of different components of regeneration (e.g., seed cone production, seedling establishment, site suitability), the use of higher-resolution spatial data that better matches the operational scales of post-fire recovery processes, and the consideration of a range of future climate projections.

1.3 Research Aims

This dissertation focuses on the dynamic nature of forested ecosystems in the northern Front Range of Colorado and across the Southern Rocky Mountains. In Chapter 2, a manuscript published in the journal *Ecosphere* and co-authored with Thomas Veblen, Sara Saraceni, and Teresa Chapman, we quantified changes in forest extent from 1938-2015 in a 2,932 km^2 area in the northern Front Range of Colorado using high-resolution aerial imagery. We then compared patterns of forest gain and loss with records of human land use, characteristics of the biophysical environment, historical and modern fire history, and tree ring reconstructions of past climate. In

Chapter 3, a manuscript submitted to the journal *Ecological Applications* and co-authored with Thomas Veblen, Teresa Chapman, Monica Rother, Andreas Wion, and Miranda Redmond, we assessed potential limitations to post-fire recovery across 15 recent (1988-2010) wildfires in northern New Mexico and southern Colorado. In this study, we used a novel combination of field inventories, tree ring methods, image classification, and GIS modeling to quantify spatial and temporal variability in seed cone production, seed availability, seedling establishment, climate suitability, and post-fire seedling abundance across each landscape. In Chapter 4, a manuscript co-authored with Michael Battaglia, Marin Chambers, Paula Fornwalt, Zachary Holden, Thomas Kolb, Monica Rother, Jessica Ouzts, and Thomas Veblen, we combined two regionally-extensive datasets describing post-fire conifer seedling establishment and abundance. Using these data, we modeled the combined influence of terrain, interannual climate variability, and spatial variability in climate on post-fire recovery in montane forests of the Southern Rocky Mountains, reconstructing historical patterns of recovery and projecting future trends based on a range of climate projections.

Table 1.1. A summary of relevant studies that focused on the post-fire recovery of coniferous forests across the western United States. “Seedling Presence/Abundance” indicates if a study quantified post-fire recovery using field surveys of conifer seedling presence or abundance. “Ages” indicates if a study presented ages of seedlings using either tree-ring methods or plot remeasurements. “Seed” indicates if a study collected site-specific data on seed or seed cone production following fire. “Spatial Modeling” indicates if a study made projections of post-fire recovery throughout at least one fire, or if the study made inferences at the fire-level using GIS and/or remotely sensed datasets. “Climate or Proxy” indicates that a study used either gridded climate data, or proxies for climate (e.g., elevation, aspect) in an analysis of post-fire recovery. “GCMs” indicates if a study incorporated projections of future climate into an analysis in some way.

Article	State(s)	Seedling Presence/ Abundance	Ages	Seed	Spatial Modeling	Climate or Proxy	GCMs
Bonnet et al. (2005)	South Dakota	Y	N	N	N	N	N
Savage and Mast (2005)	Arizona, New Mexico	Y	Y[a]	N	N	N[b]	N
Donato et al. (2006)	Oregon	Y	N	N	N	N	N
Shatford et al. (2007)	California, Oregon	Y	Y[a]	N	N	N[b]	N
Keyser et al. (2008)	South Dakota	Y	N	N	N	N[b]	N
Donato et al. (2009)	Oregon	Y	N	N	Y	Y	N
Haire and McGarigal (2010)	New Mexico	Y	N	N	Y	Y	N
Roccaforte et al. (2012)	Arizona	Y	N	N	N	N	N
Dodson and Root (2013)	Oregon	Y	N	N	N	Y	N
Feddema et al. (2013)	New Mexico	N	Y[a]	N	N	Y	Y
Harvey et al. (2013)	Wyoming	Y	N	N	N	N	N
Savage et al. (2013)	New Mexico	Y	Y[a]	N	N	Y	N
Harvey et al. (2014a)	Wyoming	Y	N	N	N	N	N
Harvey et al. (2014b)	Idaho, Montana	Y	N	N	N	Y	N
Ritchie and Knapp (2014)	California	Y	N	N	N	N	N
Ouzts et al. (2015)	Arizona, New Mexico	Y	N	N	N	N[c]	N
Chambers et al. (2016)	Colorado	Y	N	N	Y	Y	N
Donato et al. (2016)	Wyoming	Y	N	N	Y	Y	N
Harvey et al. (2016)	Montana, Wyoming	Y	N	N	N	Y	N
Kemp et al. (2016)	Idaho, Montana	Y	N	N	N	Y	N
Rother and Veblen (2016)	Colorado	Y	N	N	N	Y	N
Stevens-Rumann and Morgan (2016)	Idaho	Y	N	N	N	Y	N
Welch et al. (2016)	California	Y	N	N	Y	Y	N

Coop et al. (2016)	New Mexico	Y	N	N	N	N[c]	N
Owen et al. (2017)	Arizona	Y	N	N	Y	Y	N
Rother and Veblen (2017)	Colorado	N	Y	N	N	Y	N
Tepley et al. (2017)	California, Oregon	Y	Y[a]	N	Y	Y	Y
Ziegler et al. (2017)	Colorado, South Dakota	Y	N	N	Y	Y	N
Haffey et al. (2018)	Arizona, New Mexico	Y	N	N	Y	Y	N
Roccaforte et al. (2018)	Arizona	Y	N	N	N	N	N
Shive et al. (2018)	California	Y	N	N	Y	Y	N
Stevens-Rumann et al. (2018)	Western U.S.	Y	N	N	N	Y	N
Stoddard et al. (2018)	Arizona	Y	N	N	N	N[b]	N
Davis et al. (2019)	Western U.S.	Y	Y	N	N	Y	N
Kemp et al. (2019)	Idaho, Montana	Y	N	N	N	Y	Y
Hankin et al. (2019)	Idaho, Montana	N	Y	N	N	Y	N
Young et al. (2019)	California	Y	N	N	N	Y	N
Rodman et al. *In Review*; Chapter 3	Colorado, New Mexico	Y	Y	Y	Y	Y	N
Chapter 4	Colorado, New Mexico, Wyoming	Y	Y	N	Y	Y	Y

[a]: Ages of seedlings were presented using tree-ring methods or repeated measurements that do not permit annual-resolution estimates of establishment.
[b]: Climate or climate proxies (e.g., elevation, aspect) were not directly included in the analysis, but recovery was qualitatively compared to climate records.
[c]: Climate or climate proxies (e.g., elevation, aspect) were included in the analysis, but results of these analyses were not discussed or interpreted.

CHAPTER 2

WILDFIRE ACTIVITY AND LAND USE DROVE 20TH CENTURY CHANGES IN FOREST COVER IN THE COLORADO FRONT RANGE

2.1 Introduction

Studies using forest inventories and remotely sensed data have identified declines in global forest area c. 1990s-2010s (Hansen et al. 2013, Keenan et al. 2015), though longer-term trends may differ in direction and magnitude (Song et al. 2018). Forests provide countless ecosystem services to humans, are sanctums of biodiversity, and play a key role in nutrient cycling (Stocker et al. 2013, FAO 2015), thus an understanding of the causes of forest change is an important research priority. Forest change is rarely a result of a single factor acting alone. The causes of land cover change vary across complex landscapes, and multiple potential drivers should be considered (Black et al. 2003). The attribution of forest cover change to specific natural and anthropogenic factors, at sufficient timescales to observe both abrupt losses and gradual recovery, is likely to improve conservation planning and the understanding of global change.

Wildfire is one of the most important terrestrial disturbances (Bowman et al. 2009) and is a key determinant of the global distribution of forest vegetation (Bond et al. 2005). The effects of wildfire activity on forest cover change are complex because fire is expected to influence forest cover through both initial losses and subsequent recovery. From 1984 to 2015, warming and drying trends contributed to increases in the area burned in large wildfires across much of the

western U.S. (Abatzoglou and Williams 2016). These increases in wildfire activity have occurred in tandem with poor post-fire recovery in many western conifer forests (Stevens-Rumann et al. 2018). Seed tree - and therefore seed availability - is one of the primary drivers of post-fire recovery, particularly in forests composed of seed obligate species without fire-adapted canopy seed banks (Bonnet et al. 2005, Haire and McGarigal 2010, Harvey et al. 2016). Due to dispersal limitations, sites in the interior of large, high-severity patches may take decades or centuries to regain forest cover (Chambers et al. 2016, Baker 2018). Furthermore, a warm and dry climate can inhibit post-fire recovery of forests (Stevens-Rumann et al. 2018). Recent wildfire activity, combined with poor post-fire recovery, may be leading to forest cover declines through the western US at the onset of the 21st century.

The longer-term history of fire activity also plays an important role in forest cover change. Slow recovery and conversion to non-forest cover types have been noted at varying spatial scales following 18th and 19th century fires in some coniferous forests in the Rocky Mountains (Stahelin 1943, Kaufmann et al. 2000, Huckaby et al. 2001). Thus, increases in the extent or density of some subalpine forests over the last century (e.g., Cocke et al. 2005, Zier and Baker 2006) may be partially explained by slow, yet continuous forest recovery following widespread high-severity fires in the 18th and 19th centuries. Forest cover increases have also been documented in some lower elevation montane forests where formerly frequent surface fires have declined during the 20th century (Schoennagel et al. 2004, Hessburg et al. 2005). Therefore, changes in fire occurrence during the 18th-20th centuries could account for a trend of increasing forest cover through different mechanisms (slow post-fire recovery from past severe fires vs. decreased thinning effects of surface fires) that are likely to vary in importance across the elevation gradient from lower elevation montane forests to higher elevation subalpine sites.

In addition to contemporary and historical fire activity, other factors have also played influential roles in forest cover change across the western U.S. over the past century. For example, moisture availability and changes in land use have been noted as important correlates with changes in dry forests of the northwest and southwest U.S. since the late 1800s (Merschel et al. 2014, Johnston 2017, Rodman et al. 2017). Extractive logging of large diameter trees has altered stand structure in many coniferous forests in the western U.S.; in some cases late 20th century forest cover may still be responding to timber extraction in the 19th and early 20th centuries (Naficy et al. 2010, Merschel et al. 2014, Collins et al. 2017). Historical mining activity also led to increases in soil disturbance, logging, and fire activity in many parts of the western U.S. in the late 1800s and early 1900s (Gruell 1983, 2001, Veblen and Lorenz 1991, Hessburg and Agee 2003, Dethier et al. 2018). More recently, exurban housing development has occurred throughout portions of the U.S. (Theobald and Romme 2007, Platt et al. 2011, Radeloff et al. 2018), leading to forest fragmentation (Radeloff et al. 2005).

To effectively disentangle the potential drivers of forest cover change, detailed data covering a range of ecosystem types, ownership designations, and human land uses are needed. Though the satellite record can provide maps of vegetation change since approximately 1972 (i.e., the launch of Landsat 1), these data lack both temporal depth and high spatial resolution, which is particularly important when studying long-lived tree species and areas of sparse forest cover. Aerial surveys of agricultural and forested lands began throughout the United States in the 1930s (Matthews 2005), and these photographs provide extensive records of land cover at a high (< 2 m) spatial resolution (Morgan et al. 2010). These data have been used in quantitative assessments of historical forest change in the western U.S. (e.g., Hessburg et al. 1999, Coop and

Givnish 2007, Lydersen and Collins 2018), and of the anthropogenic and biophysical factors influencing these changes (Asner et al. 2003, Black et al. 2003).

We used historical and contemporary aerial photography to quantify changes in forest cover across a study area in the northern Front Range (NFR) of Colorado c. 1938-2015. The NFR (Fig. 2.1) is a region that has been shaped by human activities and by wildfire over the last several centuries (Veblen and Donnegan 2005, Addington et al. 2018), and provides both a data- and disturbance-rich case study of the potential causes of forest change throughout a complex landscape. Fire history (Sibold et al. 2006, Sherriff et al. 2014), historical stand densities (Battaglia et al. 2018), climate and tree growth (Villalba et al. 1994, Veblen et al. 2000, Lukas et al. 2014), and patterns of exurban development (Platt et al. 2011) are well-documented in this region, permitting a thorough analysis of the potential drivers of vegetation change throughout the 20th century. To date, there have been no landscape-scale studies which have attempted to characterize the relative influences of land-use, the abiotic environment, and wildfire to observed shifts in forest cover in the NFR. Indeed, there are few studies in similar conifer forest ecosystem in the western U.S. that have quantified changes in forest cover and implemented robust research designs to assess the contributions of *multiple* driving factors to 20th century forest change across broad biophysical gradients. Specifically, we asked the following questions: *1) How has the extent of forest cover changed across the NFR c. 1938-2015? 2) How do elevation, topographic heat load index, land ownership, and historical land use relate to spatial patterns of increase and decrease in forest cover? 3) How do changes in forest cover through the 20th century relate to known fire history across a range of fire regime types?*

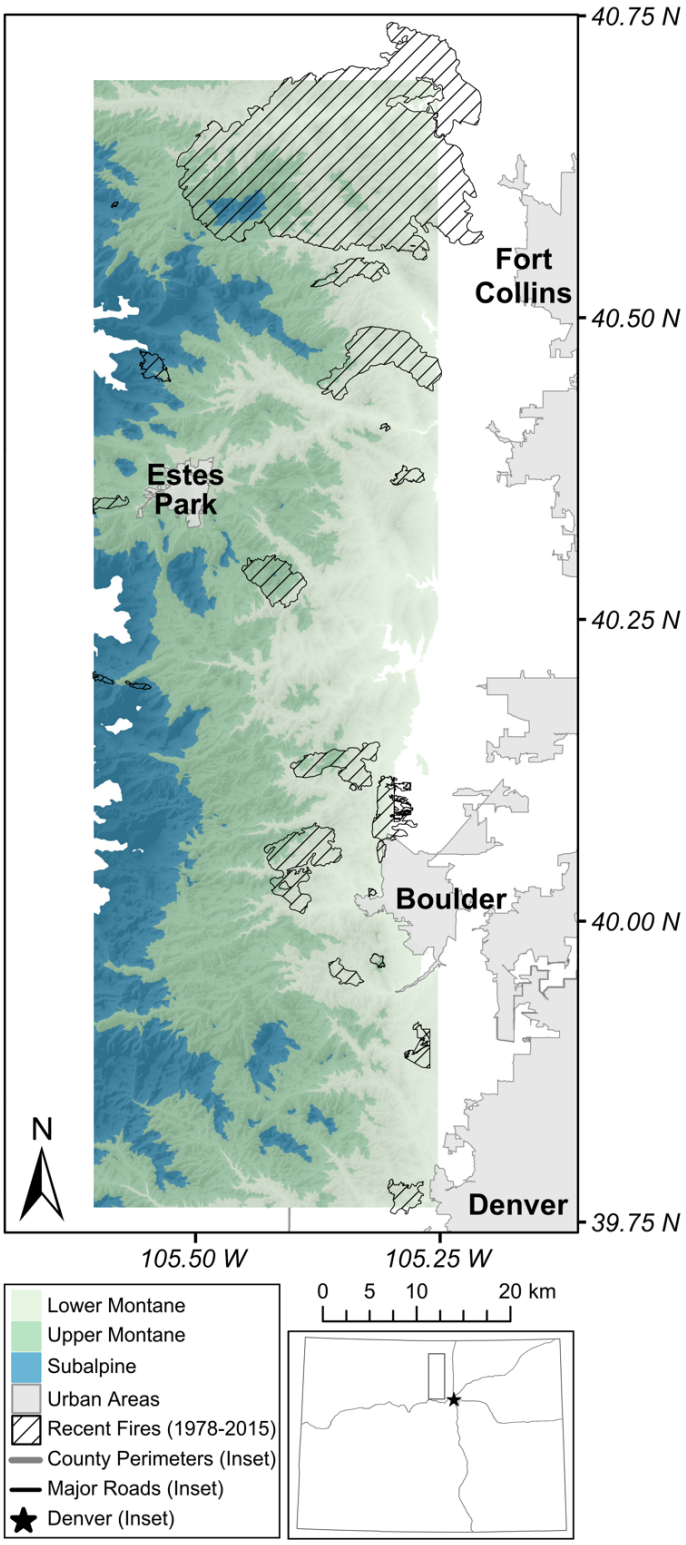

Fig. 2.1. Overview of study area, locations of urban areas, and recent wildfires (1978-2015) in the northern Front Range of Colorado. Background color shows the spatial distribution of the different life zones (lower montane [1,700-2,400 m], upper montane [2,400-2,800 m], and subalpine [2,800-3,500 m]).

2.2 Study Area

2.2.1 Climate and Vegetation

Our study area covers 2,932 km^2 on the eastern slope of the northern Front Range (NFR) of Colorado, USA (Fig. 2.1). Elevations range c. 1,600-4,200 m and climate varies substantially along this gradient, with lower sites being much warmer and drier than sites found at high elevations. Across elevations, minimum temperatures in January range -17 to -5 °C and July maximums range 14 to 32 °C (PRISM 2018). Average precipitation is 400-1,300 mm/year, with spring months (March-May) being the wettest (35% of annual totals; PRISM 2018). The proportion of precipitation occurring as snowfall increases with elevation and snow depth typically peaks in April (Kittel et al. 2015). Recently, increases in temperature have been noted throughout much of Colorado (1.1 C° from 1977-2006), including the NFR (Lukas et al. 2014).

Native vegetation in the study area begins with short grass prairie at the lowest sites (< 1,700 m), transitioning into lower montane forests (1,700-2,400 m) principally dominated by ponderosa pine (*Pinus ponderosa*) with scattered Douglas-fir (*Pseudotsuga menziesii*) and Rocky Mountain juniper (*Juniperus scopulorum*) (Peet 1981, Addington et al. 2018). Upper montane forests range c. 2,400-2,800 m and are dominated by ponderosa pine, Douglas-fir, and lodgepole pine (*Pinus contorta*). At the highest forested sites (subalpine; 2,800-3,500 m), lodgepole pine, limber pine (*Pinus flexilis*), subalpine fir (*Abies lasiocarpa*), and Engelmann spruce (*Picea engelmannii*) are the dominant tree species, giving way to alpine vegetation at c. 3,500 m. Colorado blue spruce (*Picea pungens*) and several broad-leafed, deciduous tree species (e.g., narrowleaf cottonwood [*Populus angustifolia*] and willows [*Salix* spp.]) are common in riparian areas. Quaking aspen (*Populus tremuloides*) is also present in scattered locations either as a post-fire seral component, or as the persistent dominant species in some areas (Peet 1981).

2.2.2 Disturbance History

In low-elevation montane forests and interspersed grassland sites (below 2,260 m) in the NFR, fires were relatively frequent and of low- to moderate-severity prior to the 20th century (Sherriff et al. 2014, Brown et al. 2015). In contrast, middle and upper-elevation montane forests (2,260-2,800 m) were historically characterized by a mixed-severity fire regime, in which higher-severity patches of mortality (> 70% of canopy trees; 50 ha or larger) were more common (Schoennagel et al. 2011, Sherriff et al. 2014). Subalpine forests (2,800-3,500 m) typically burned infrequently (> 200 year intervals) and in large (> 1,000 ha) high-severity patches during exceptionally dry years (Buechling and Baker 2004, Sibold and Veblen 2006). Surface fires affected only 1-3% of the forested area in the subalpine zone (Sibold et al. 2006), although fire-scar records do indicate more frequent small fires at the ecotone of forest with rocky alpine sites (Sherriff et al. 2001).

The mid-late 1800s were a time of heightened fire activity across all zones in the NFR, concurrent with widespread droughts throughout the Rockies and expanding Euro-American settlement (Veblen et al. 2000, Sherriff et al. 2001, Kitzberger et al. 2007, Sherriff and Veblen 2008, Schoennagel et al. 2011; Fig. 2.2). Following this period, fire activity in the NFR was fairly limited c. 1920 – 2000 likely due to a combination of direct fire suppression, fuel reduction due to livestock grazing, lack of combustible fuels in higher elevation, recently burned sites, and potentially less suitable climatic conditions for fire ignition and spread (Veblen et al. 2000, Sibold et al. 2006, Sherriff and Veblen 2008). Recent increases in fire activity have occurred since 1984 following a relatively fire quiescent period for most of the 20th century (Fig. 2.2).

Insects and pathogens are also important components of stand dynamics in the NFR. In this region, western spruce budworm (*Choristoneura freemani*), Douglas-fir bark beetle

(*Dendroctonus pseudotsugae*), and mountain pine beetle (MPB; *Dendroctonus ponderosae*) are the most important potentially lethal insect pests of the lower and upper montane zones, whereas mountain pine beetle, spruce beetle (*Dendroctonus rufipennis*), and western balsam fir bark beetle (*Dryocoetes confusus*) are the primary lethal insects of the subalpine zone. Outbreaks of many of these insect species have occurred during the 1938-2015 time period of this study (Hadley and Veblen 1993, Chapman et al. 2012). Although such outbreaks have killed large numbers of trees in some areas (e.g., MPB in the 1970s and the early 2000s), post-outbreak release of advance regeneration and new tree establishment typically lead to rapid forest recovery (i.e., at a decadal scale; Veblen et al. 1991, Hadley and Veblen 1993, Collins et al. 2011).

2.2.3 Land Use History

Human land use in the NFR has shifted over the last two centuries in ways that are likely to have influenced forest cover during the 1938-2015 study period. The mid-late 1800s and early 1900s were associated with the removal of Native American communities (and their associated land-use practices; Simmons 2000), and with increases in logging, mining, and ranching impacts from Euro-Americans (Veblen and Lorenz 1986, Veblen and Donnegan 2005, Dethier et al. 2018). The decline in Native American populations likely led to declines in intentional burning in certain areas, though historical ignitions due to lightning and humans are difficult to separate (Veblen et al. 2000). Past logging and mining have had complex impacts on forests in the NFR. Timber extraction and surface mining initially reduce forest cover. However, the longer-term effects of logging and mining depend on rates of succession and whether the site is converted to another land use such as ranching or residential development.

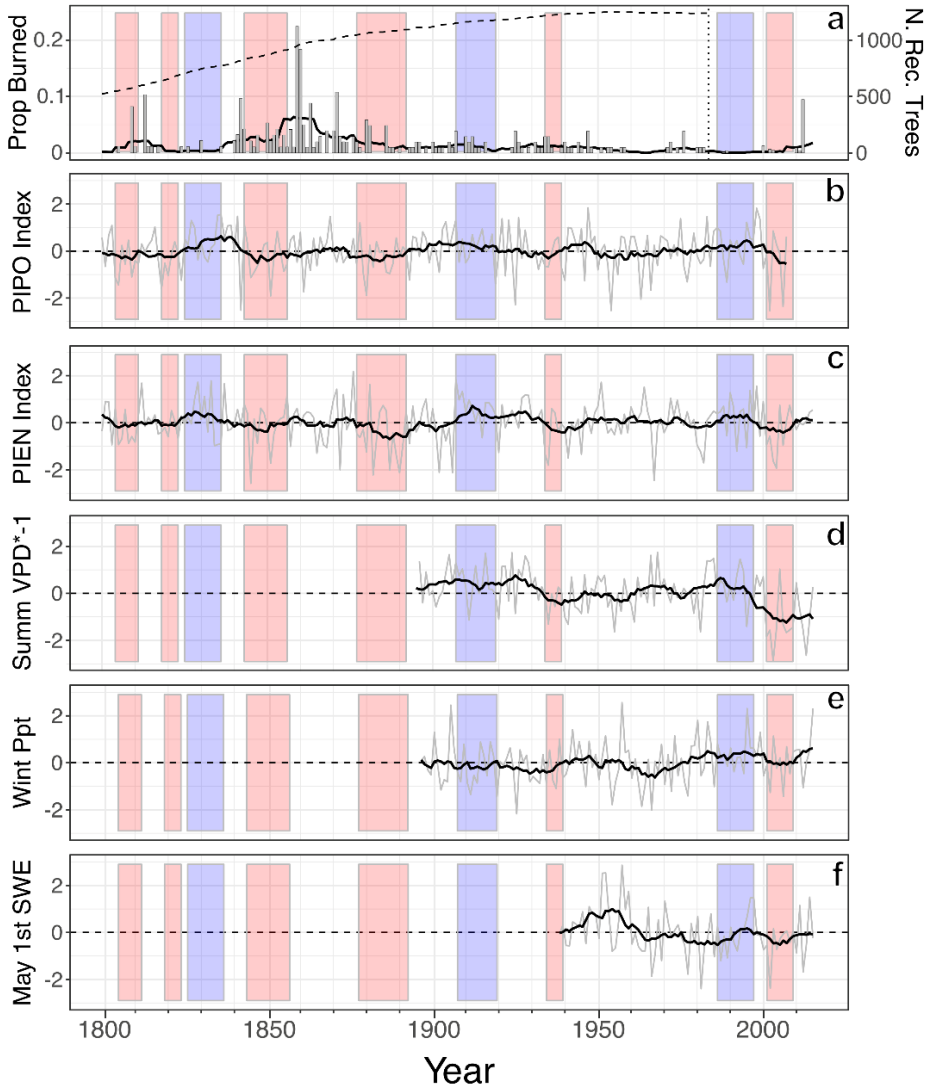

Fig. 2.2. Variability in wildfire activity, tree growth, and climate 1800-2015 in the study area in the northern Front Range of Colorado. Prior to 1984, proportion burned (a) is given as the proportion of montane fire history sites recording spreading fire in a given year (min two trees and 10% of trees within a site). For 1984-2015, proportion burned is based on the percent surface area of the montane zone (1,700-2,800 m) within Monitoring Trends in Burn Severity fire perimeters in each year. Sample depth (dashed line) gives the total number of fire-scarred recorder trees (across all sites) in a given year. Variability in tree growth is derived from residual tree ring chronologies of ponderosa pine (PIPO; b) and Engelmann spruce (PIEN; c). Summer vapor pressure deficit (VPD; d) is an indicator of summer (Jun-Aug) drought stress, while winter precipitation (PPT; e) is the sum of Nov-Dec (prior year) and January-May (focal year) precipitation across the study area. Snow water equivalent (SWE; f) is derived from a long-term record (1938-2015) of snow depth and water content collected May 1st each year within the study area. All tree ring and climate values (b-f) were re-scaled using z-score transformations. Grey lines and bars give annual values, while black lines show 10-year moving averages. Regional pluvials (blue overlay) and droughts (red overlay) were defined as extended periods (five or more years) in which moving 10-year moving averages of growth were above or below (respectively) the long-term mean for both ponderosa pine and Engelmann spruce.

Although fuels reduction due to livestock grazing contributed to decreased fire spread at some sites as early as the 1860s (e.g., Veblen et al. 2000, Brown et al. 2015), widespread fire exclusion in the NFR dates from approximately 1920 when automobile roads allowed effective access to the rugged topography of the region (Veblen and Lorenz 1986, Veblen and Donnegan 2005). The more direct effects of early settlers on fire activity ranged from intentionally set fires during the early settlement and mining era (e.g., 1840s-1890s) to more effective fire suppression and exclusion at permanently settled sites in lower elevations (Veblen and Lorenz 1986, Veblen and Donnegan 2005). Exurban development has been widespread in the NFR since c. 1940, with home construction shifting over time from predominantly grass covered valley bottoms to forested slopes more prone to higher-severity fires (Platt et al. 2011). The effects of this development include forest removal for home sites and changes in fire frequency - more aggressive fire suppression but also an increased risk of human set fires.

2.3 Methods

2.3.1 Interannual and Interdecadal Trends in Climate, Wildfire, and Tree Growth

To provide important context for observed trends in forest cover throughout the study area, we compiled data describing interannual and interdecadal variability in climate, tree growth, and wildfire activity 1800-2015 (Appendix A). We characterized climate using gridded spatial data describing summer drought stress (i.e., vapor pressure deficit) and annual winter precipitation 1896-2015 (PRISM 2018), as well as field-derived measurements of snow depth and density 1938-2015 (snow water equivalent from the University Camp snow course ([40.03 N, -105.57 W], 3,140 m; NRCS 2016). These components of climate are important to many forest processes in the Southwest U.S. and Southern Rocky Mountains (e.g., Williams et al. 2012, Andrus et al. 2018). We also used tree ring chronologies from ponderosa pine and

Engelmann spruce (Villalba et al. 1994, Veblen et al. 2000) – two dominant conifers in the montane zone and subalpine zone, respectively – to extend the temporal coverage of the climate record to 1800. Lastly, we developed an index of fire activity in the montane zone using field-derived fire history data (1800-1983; Sherriff et al. 2014) and recent wildfire perimeters (1984-2015; Eidenshink et al. 2007). To visualize interdecadal trends in climate, tree growth, and wildfire activity, we also calculated 10-year moving averages of all annual values.

2.3.2 Image Acquisition and Digitization

The historical air photos used in this study were captured in flights of the NFR commissioned by the US Forest Service and Soil Conservation Service in 1938 and 1940 as part of broad-scale timber and resource inventories. These images have an approximate cartographic scale of 1:20,000, and over 1,700 individual scenes were scanned and digitized at 600 ppi by technicians from the University of Colorado library system. The average spatial resolution of these data is 1.1 m. Of the digitized images available through the University of Colorado, we selected a subset of 308 based on the availability of pre-existing fire history and stand age data (e.g., Sibold et al. 2006, Sherriff et al. 2014). This subset was primarily captured in 1938 and the 1940 images represent only 8.6% of the final study area (Table 2.1), therefore we refer to these data as "1938 imagery" for simplicity. For comparison with historical imagery, we also acquired county-level mosaics of NAIP (National Agriculture Imagery Program) imagery from the area that were collected in fall 2015 (Table 2.1). These data have a 1 m spatial resolution and three spectral bands – one each in the red, green, and blue wavelengths (NAIP 2015). To use similar methods with 1938 and 2015 imagery, we created a single panchromatic band (the mean of red, green, and blue values) from NAIP data prior to image processing and classification.

Table 2.1. Collection dates and areas of coverage for historical and contemporary imagery throughout the northern Front Range of Colorado.

	Flight Date	Area (ha)	Life Zones Covered
Initial Imagery	5/8/38	39,602.8	Lower Montane
	10/25/38	62,828.8	Lower/Upper Montane
	10/26/38	140,236.0	Upper Montane/Subalpine
	10/29/38	25,200.5	Subalpine
	10/7/40	1,283.9	Lower Montane
	10/9/40	24,022.4	Lower/Upper Montane
NAIP	8/25/15	26,216.1	Subalpine
	9/8/15	180,274.7	All
	9/19/15	74,958.1	All
	9/20/15	11,725.9	Subalpine

2.3.3 Image Processing

To aid in the identification of forested areas in the 1938 and 2015 images, we used a series of image processing steps to add supplemental information describing the texture and context surrounding each c. 1 m pixel. During these steps, we identified locally dark pixels (indicative of individual trees surrounded by bright grassland) and quantified local standard deviation in brightness using moving windows at multiple scales (*sensu* Coburn and Roberts 2004; Fig. 2.3; Appendix A). We combined these two layers with the original greyscale imagery to create three-band composite imagery (Fig. 2.3d). The combination of brightness, local minima, and standard deviation emphasizes differences in spectral reflectance that facilitate the separation of different forest structures (e.g., individual trees and dense stands) from non-forested areas.

We projected each of the 1938 images to NAD 83, UTM 13N (the same projection as the NAIP images), and georeferenced them using metadata that described the approximate center location of each frame, scanning resolution, and cartographic scale. Next, we mosaicked the 1938 imagery by merging overlapping areas along each N-S flight line, then merging adjacent flight lines into a single photomosaic. Lastly, we co-registered this mosaic to 2015 NAIP

imagery using 4,955 tie points that were homogeneously distributed throughout the image. We assessed the accuracy of this co-registration using an independent set of tie points (n = 100). These points were located at the nearest identifiable feature to 100 randomly located points throughout the mosaic. Mean horizontal error of these points was 23.6 m (standard deviation = 17.2). Though larger than values of c. 7-16 m reported by two similar studies (e.g., Platt and Schoennagel 2009, Lydersen and Collins 2018), this alignment is reasonable considering the larger size of our study area. Still, change detection and further analyses were performed at an aggregated spatial resolution to account for this offset (described below).

2.3.4 Image Segmentation and Classification

Following image processing and mosaicking, we performed image segmentations and developed supervised classifications of the three-band composite imagery for each date (1938 and 2015). These classifications were based on a hybrid approach of pixel- and object-based image analysis, where we used image segmentation to enhance pixel-level classification accuracy (i.e., "enhanced pixel classification" *sensu* Radoux and Bogaert 2017). First, we segmented three-band composites from each date (Fig. 2.3d) using the "segment mean shift" algorithm in ArcGIS v. 10.4 (ESRI 2016). We prioritized spectral similarity over spatial scale during segmentation parameter selection, which resulted in segments ranging in size from individual trees to entire forest stands. Next, we included a hillshade model (derived from a 10 m digital elevation model and resampled to c. 1 m; 1938 imagery) and a red-green index (RGI; 2015 imagery) as additional bands to help account for topographic differences in illumination. RGI is a proxy for vegetation health in imagery covering the visible portion of the electromagnetic spectrum (Gartner et al. 2015); as a ratio of two bands, RGI is relatively insensitive to differences in illumination. We used a hillshade model as ancillary data in the 1938

classification because this serves as an additional way to account for topographic differences in illumination in panchromatic imagery. Finally, we assigned c. 1 m pixels in each set of imagery to forest or non-forest classes using support vector machines (SVMs; Fig. 2.3e). SVMs are a statistical learning algorithm that can identify non-linear decision boundaries between classes in multi-dimensional space (Hastie et al. 2009) and are commonly used in image classification.

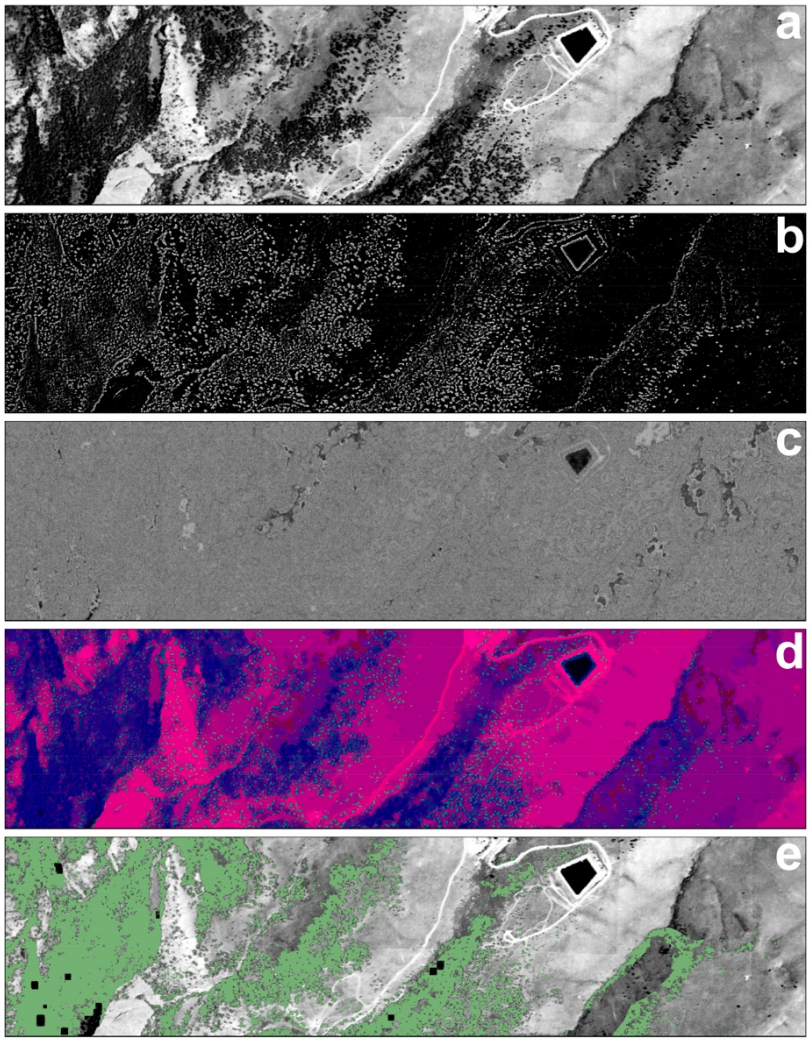

Fig. 2.3. Image classification workflow for an area near Boulder, CO (39.99 N, 105.29 W). Original imagery (a) was processed using an expanding window method to identify pixels darker than their surroundings (b), and to quantify local standard deviation (c). Next, these three images were merged to create a three-band composite, which we segmented to identify areas of relatively homogenous brightness, contrast, and variance (d). We then classified the segmented imagery using support vector machines to separate forest and non-forest cover types (e; forest shown in green). Following classification, we detected and removed shadows and bodies of water from the forest class by thresholding dark pixels with low local variance.

Following classification, we post-processed classified maps using thresholds of brightness and local standard deviation to identify and remove large shadows that could be misclassified as forest (Appendix A). We also masked lakes and reservoirs (USGS 2018), urban areas (from spatial data available through local government offices), and elevations above 3,500 m (which have very little or no forest cover) from the final classifications. Of the total study area, 93.9% (2,713.2 km^2) was left unmasked and included in further analyses.

2.3.5 Data Aggregation

To account for co-registration error and to permit additional analyses of the potential drivers of forest change, we aggregated the resolution of the 1 m classified maps to 250 m in each date. We selected a 250 m cell size (6.25 ha) because this extent is several times larger than our estimated co-registration error and corresponds to the coarsest-resolution dataset used in later analyses (i.e., Sohl et al. 2016). This 250 m resolution is also relevant for land managers, approximating the size of individual treatment units that are used in planning forest management activities in the NFR (Addington et al. 2018). Henceforth, we refer to these 250 m cells as 'grid cells'. We performed this data aggregation by summing the areas of forest and non-forest (from the classified 1 m maps) in each grid cell; we then calculated forest cover in each grid cell as the sum of classified forest area divided by the sum of classified forest and non-forest area. This resulted in two maps of forest cover (1938 and 2015) with continuous values (0-100% in each grid cell) which were later used in change detection (as described below). To limit the influence of grid cells that had little overlap with the study area, we excluded cells with more than 50% of the area masked or beyond the extent of imagery (i.e., no data). Though this criterion removed 15.4% of initial grid cells from later analysis, these cells contained less than 1% of the total classified area. Lastly, to provide a more detailed characterization of variability in forest cover

throughout the study area, we calculated the percentage of grid cells in different forest cover classes (20% bins) in both 1938 and 2015.

2.3.6 Accuracy Assessment and Uncertainty Modeling

We performed global and local accuracy assessments to quantify the classification accuracy of the SVMs, as well as the spatial variability in accuracy throughout the study area. For the global accuracy assessment (*sensu* Congalton 1991, Olofsson et al. 2014), we used manual photointerpretation at 2,000 randomly located points throughout each image (1938 and 2015), and compared photointerpretation ("reference") to predictions from the SVM classification. We then calculated user's, producer's, and overall accuracies following the protocol of Olofsson et al. (2014). Overall accuracy was 90.2% for the 1938 imagery and 89.4% for the 2015 imagery (Table A1). It should be noted however, that the reliability of photointerpretation in the 2015 classification is generally higher (because the 1938 imagery was of a slightly coarser resolution and was not perfectly preserved) and estimates of classification accuracy in 1938 are less certain than those in 2015.

To develop local accuracy assessments, we used the 2,000 manual photointerpretation points, segmented and unsegmented pixel values at each point, and SVM-predicted classes to develop binomial generalized linear models (GLMs) of correct/incorrect classification (*sensu* Leyk and Zimmermann 2004, 2007; Appendix A). Adjusted deviance squared values (following Guisan and Zimmermann 2000) for the final GLMs were 0.32 for 1938 imagery and 0.28 for the 2015 imagery. We then used these GLMs to predict the probability of correct classification in each 1 m pixel in the 1938 and 2015 imagery. Following GLM predictions, we calculated overall classification accuracy, forest accuracy, and non-forest accuracy as the predicted values from 1 m pixels within each 250 m grid cell. Overall accuracy was calculated as the mean GLM-

predicted probability of a correct classification across all classified pixels in a grid cell, while forest and non-forest accuracies were the mean values for all pixels assigned (in final SVM classifications) to each class in each grid cell (Fig. A1a-d).

Accurate results of change detection analyses are contingent upon proper thematic representations of cover types (i.e., classification accuracy) and upon spatial alignment between datasets (i.e., co-registration error; Leyk et al. 2018). To identify grid cells that had directional changes in forest cover (1938-2015) that exceeded the potential influence of inaccurate classification and co-registration error, we merged our local accuracy assessments with Monte Carlo simulations of error in image alignment (Appendix A). Monte Carlo simulations consisted of 200 random shifts of the 1938 imagery to quantify the sensitivity of forest cover estimates to co-registration error. We then combined accuracy assessments and Monte Carlo simulations using the following formulas to calculate potential ranges of forest cover for each grid cell for each date:

$$LowerForest_{1938} = (\%Acc_{Forest} * ForestArea_{6th})/ClassifiedArea_{6th}$$

$$UpperForest_{1938} = (ForestArea_{195th} + (NonForestArea_{195th} * (1 - \%Acc_{NonForest})))/ClassifiedArea_{195th}$$

$$LowerForest_{2015} = (\%Acc_{Forest} * ForestArea)/ClassifiedArea$$

$$UpperForest_{2015} = (ForestArea + (NonForestArea * (1 - \%Acc_{NonForest})))/ClassifiedArea$$

Where *LowerForest* and *UpperForest* are the lower and upper estimates for forest cover at a given date ($_{1938}$ or $_{2015}$), *%Acc* is the estimated classification accuracy for a given cover type, *ForestArea* and *NonForestArea* are the total area classified (by SVMs) as forest and non-forest, respectively, and *ClassifiedArea* is the total area classified as either cover type. Subscripts $_{6}$ and $_{195}$ correspond to the 6th and 195th ranked estimates of forest cover (95% bounds) across the Monte Carlo simulations of co-registration error for the 1938 imagery. All values in the above

formulas were specific to each grid cell, thus identifying potential ranges of forest cover in each 250 m area at each date (1938 or 2015).

We determined that a grid cell had experienced a significant change in forest cover 1938-2015 if the potential ranges of forest cover in 1938 and 2015 did not overlap. In other words, if a maximum estimate of 1938 forest cover was lower than the minimum estimate of 2015 forest cover, a grid cell was classified as Forest Gain. Similarly, if the maximum estimate of 2015 forest cover was lower than minimum estimate of 1938 canopy cover, a grid cell was classified as Forest Loss. If the error bounds for the two dates overlapped, a cell was then classified as Little Change (generally less than 15% net change in forest cover). Following this, we manually reclassified 1,331 Forest Loss grid cells (3.0% of the total area) to Little Change because designation as Forest Loss in these cells was primarily due to lighting conditions in the 1938 imagery (i.e., overestimates of 1938 forest cover due to topographic shading).

2.3.7 Potential Drivers of Change in Forest Cover

To assess the relative influences of several known drivers of change in forest cover, we performed a Random Forest analysis to predict forest change class (i.e., Little Change, Forest Gain, Forest Loss) in each grid cell as a function of 13 landscape variables relating to land use, land management, ownership designation, the abiotic environment, spatially modelled historical fire regime class, and recent wildfire activity (Table 2.2, Appendix A). We did not include gridded climate data in this analysis, instead using elevation and heat load index (derived from slope, aspect, and latitude; McCune and Keon 2002) as proxies for average moisture availability. Because the study area spans a single mountain range, elevation and aspect are strongly tied to climate and describe much of the variability in site moisture and vegetation (Peet 1981).

We performed the analysis of these 13 landscape variables and their relationship with forest change class in each grid cell using the *ranger* (Wright and Ziegler 2017), *mlr* (Bischl et al. 2016), and *caret* (Kuhn 2008) packages in R. We also tested for multicollinearity of predictors using the *rfUtilities* package (Evans et al. 2011). During model fitting, we tuned hyperparameters (i.e., "mtry" - the number of variables available for splitting and "ntree" - the total number of trees) for the final Random Forest analysis using five-fold cross-validation across a range of parameter values; selected values were "mtry" of 6, and "ntree" of 300. For ease of interpretation, permutation-based variable importance (mean decrease in accuracy) was relativized so as to sum to 1 ("relative importance"). We also characterized final model fit using percent classification accuracy from 100-fold cross-validation. While we present final results of these analyses at a 250 m resolution, we also quantified forest cover change, performed uncertainty thresholding, and completed an additional Random Forest analysis at a 1 km-resolution using the same set of 13 predictors to assess the extent to which our results may be sensitive to spatial scale.

Table 2.2. Variables included in Random Forest analysis used to identify potential drivers of forest cover change (1938-2015) in the study area in the northern Front Range of Colorado.

Category	Variable	Definition	Reason for Inclusion	Source(s)
Human Impacts	Density of Mine Sites	Kernel estimate of mine site density surrounding each grid cell.	Historical mining activity influenced forests through increased logging activity and anthropogenic ignitions.	USGS (2005)
	Land Cover Class 1938	Land cover class in each grid cell from 1938 backcast model of land cover.	Initial land cover in the study period could have important influences on forest cover change due to initial cover type and prior land-use legacies.	Sohl et al. (2016)

	Proportion Developed Land	Proportion of each grid cell that was classified as developed in 2011 National Land Cover Dataset (classes 21-24).	Development, particularly in the wildland urban interface, increased rapidly through the study area in the 20th century.	Homer et al. (2015)
	Proportion Treated	Proportion of each grid cell that was treated using mechanical thinning and/or prescribed fire prior to September 2015.	Silvicultural treatments are commonly used throughout forests in the western United States to reduce hazardous fuels around homes and to reduce forest densities.	Caggiano (2017)
	Road Density	Linear meters of road within each grid cell.	Road density provides a proxy for development intensity and access to forested lands.	USCB (2017)
Ownership Designation	Proportion City/County Open Space Land	Proportion of each grid cell that is city- or county-managed open space.	City and county open space lands receive high levels of recreational use. Slightly different management strategies are likely on these lands than other designations.	COMaP (2010)
	Proportion NPS Land	Proportion of each grid cell that is managed by the U.S. National Park Service.	U.S. National Park Service lands are more highly regulated, less likely to have experienced extractive logging in the early 1900s, and have lower rates of silvicultural treatment than many other designations.	COMaP (2010)
	Proportion Private Land	Proportion of each grid cell that is privately owned.	Private lands likely have different management strategies and land use than do public lands in the study area, typically being smaller, more developed, and more highly fragmented.	COMaP (2010)
	Proportion USFS Land	Proportion of each grid cell that is managed by the U.S. Forest Service.	U.S. Forest Service lands in the area are likely to experience heavy recreational use and more substantial rates of silvicultural treatment than many other land designations.	COMaP (2010)
Physical Environment	Elevation (m)	Mean elevation of each grid cell, as derived from 10 m digital elevation	Elevation is the strongest proxy for average climate in the	USGS (1999)

		model (DEM) of study area.	study area. Elevation is highly correlated with both temperature and precipitation.	
	Heat Load	Mean heat load (combination of aspect, slope, and latitude) of grid cell as derived from 10 m DEM. Higher values indicate generally higher levels of direct sun from the southwest.	Heat load provides an estimate of incoming radiant intensity in an area and is an important control on local climate.	McCune and Keon (2002)
Wildfire	Proportion Burned (1978-2015)	Proportion of each grid cell that burned between 1978 and 2015 (time-period in which reliable fire perimeter data is available).	Recent studies have noted increases in area burned and limited post-fire recovery in many sites through western United States.	Eidenshink et al. (2007); USGS (2018)
	Proportion Low-Severity	Proportion of each grid cell that was spatially modelled to have burned frequently and at low severity (few trees killed in each fire) as the dominant fire regime prior to 1920.	Areas with historically frequent, low-severity fire regimes are those believed to be most affected by 20th century fire exclusion and are those in which restoration and fuels reduction objectives are believed to be most convergent.	Sherriff et al. (2014)

2.3.8 Comparison with Fire History

In addition to the Random Forest model spanning the study area, we compared net forest change across specific montane and subalpine stands with previously collected field data describing fire history. Previous studies in the montane and subalpine zones of the NFR have compiled a combined total of 1,938 samples of fire-scarred trees and 13,832 tree ages from increment cores in an effort to reconstruct past fire activity and stand-origin dates (Veblen et al. 2000, Sherriff and Veblen 2006, 2007, 2008, Sibold et al. 2006, Schoennagel et al. 2011, Gartner et al. 2012). Using these records, one of the most extensive datasets yet assembled to characterize fire history in a single region, we performed two separate analyses to quantify forest cover change within: 1) montane stands historically characterized by distinctly different fire regimes (low- vs. mixed-severity), and 2) subalpine stands with differing time since last stand-

replacing fire. For each of these analyses, we performed a sensitivity assessment as described in *Accuracy Assessment and Uncertainty Modeling* to quantify potential ranges of forest cover.

Sites in the NFR with a history of frequent, low-severity fire likely experienced a greater deviation from their natural ranges of variability during the fire-suppression era (c. 1920-present) than did sites with mixed- or high-severity fire regimes (Sherriff et al. 2014). For this reason, sites with a history of low- and moderate-severity fire are typically the highest priority for forest management activities such as mechanical thinning and low-intensity prescribed fire (Addington et al. 2018). To assess differences in the magnitude of 20th century forest cover change by historical fire regime class in fire-excluded sites throughout the montane zone, we compared net change in forest cover using a stand-specific procedure for forests dominated by a frequent, low-severity fire regime (n = 6; 435.2 ha classified) with cover change in those dominated by a less frequent mixed-severity fire regime (n = 67; 3,618.8 ha classified). Stands were classified as low- or mixed-severity using a combination of tree establishment data and fire-scarred samples in a previous study of the montane zone in the Colorado Front Range (Sherriff et al. 2014). The difference in sample sizes between fire regime classes reflects the relative proportions of the modern landscape characterized by the respective fire regimes as well as the accessibility to study areas not impacted by logging and exurban development (a factor that guided initial plot selection). These locations were a subset of the original fire history sites described in Sherriff et al. (2014); we selected forest stands that were the most intensively surveyed (i.e., including site-specific fire histories and/or stand age data), overlapped the area of the imagery, and did not overlap recent fire perimeters (1978-2015). For this analysis, sites within recent fire perimeters were removed because the focus of the montane fire history analysis was to quantify 20th century montane forest change resulting from fire exclusion and/or longer term post-fire recovery.

In forests characterized by infrequent, high-severity fires (e.g., subalpine forests in the NFR), stand attributes such as tree density and crown cover vary with time since fire (Veblen 1986, Aplet et al. 1988, Donnegan and Rebertus 1999). Therefore, forest cover change c. 1938-2015 could be expected to differ according to stand age. To test this idea, we compared 20th century forest cover change to stand age (time since last fire) in a 5076.2 ha area in Rocky Mountain National Park – the area of overlap between our imagery and the area studied by Sibold et al. (2006). Sibold et al. (2006) reconstructed fire history of individual forest stands greater than c. 8 ha using stand-origin methods supplemented with evidence from fire-scarred trees. The study area of this fire history reconstruction spans c. 2,500-3,500 m in elevation, though > 75% is in the subalpine zone (> 2,800 m) and the vast majority is influenced by higher-severity fire (Sibold et al. 2007). For this analysis, we binned stands by age class and time since last known fire as follows: 1) prior to 1650 (stands without any recorded fire since 1650; 11.3% of the total), 2) 1650-1850 (stands originating after burning in 1650-1850 and prior to Euro-American settlement of the region; 30.4%), 3) 1850-1900 (stands originating in 1850-1900 during a period of enhanced fire activity and drought; 48.5%), 4) 1900-1938 (stands originating following fires early in the 20th century but before initial imagery; 7.0%), and 5) 1938-2015 (stands that originated following fires during the study period, 2.9%).

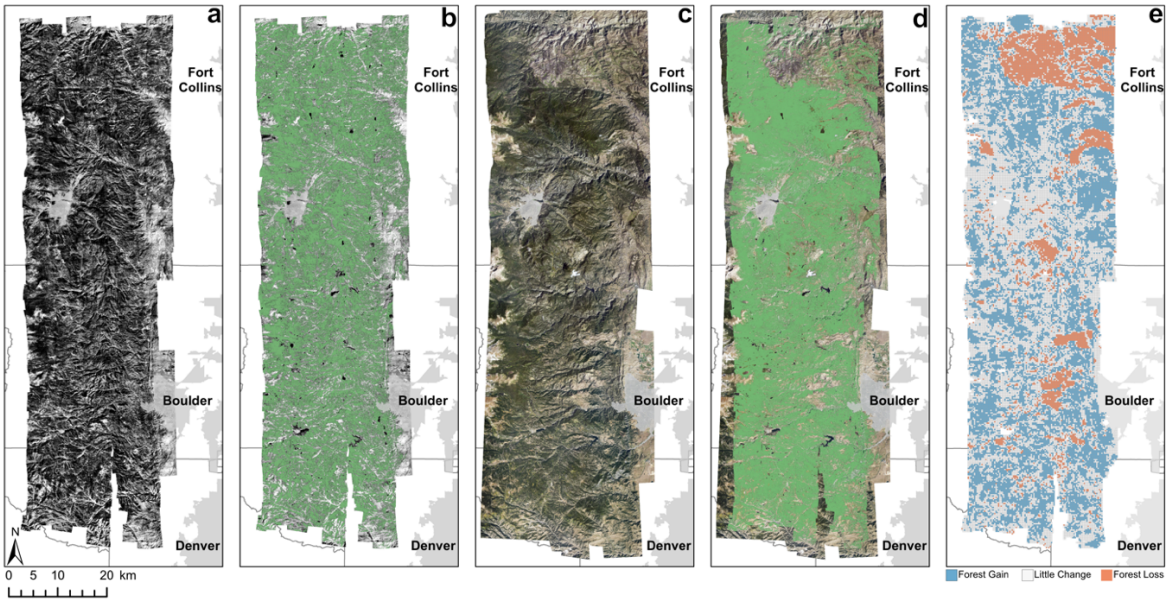

Fig. 2.4. Summary of image classification and change detection results across the study area in the northern Front Range of Colorado. We classified forest cover (forest/non-forest) for each 1 m pixel in 1938 (a, b) and 2015 (c, d), and then compared percent forest cover at an aggregated scale between 1938 and 2015. Grid cells (250 m) that showed gains (blue), or losses (orange) of forest cover were classified based on directional changes in forest cover that exceeded the influence of inaccurate classification and sensitivity to co-registration error (e).

2.4 Results

2.4.1 Changes in Forest Cover and Contributing Factors

Between 1938 and 2015, forest cover increased from 56.5% to 64.3% throughout the NFR, a net gain of 7.8% (Fig. 2.4, Table A2). However, there was notable spatial variability in forest cover change. Across the study area, 13.0% of 250 m grid cells were classified as Forest Loss, 39.4% were classified as Forest Gain, and 47.6% experienced Little Change (Fig. 2.4, Table A2). Increases in cover were greatest in the subalpine zone (16%), and were more limited in the upper montane (7.4%) and lower montane zones (4.5%). The percentage of total area in different cover classes also varied among zones in 1938 and 2015 (Fig. 2.5). While lower montane stands had a relatively uniform distribution across cover classes, the upper montane and subalpine zones had a greater percentage of stands with high canopy cover (i.e., > 60% cover; Fig. 2.5).

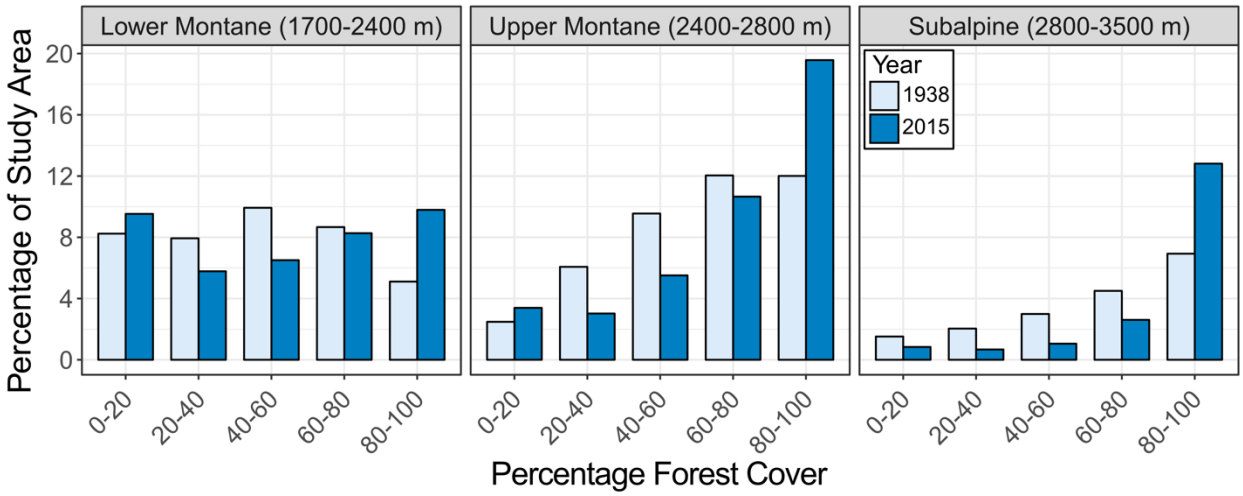

Fig. 2.5. Variability in forest cover across the study area in the northern Front Range of Colorado by life zone (lower montane, upper montane, and subalpine). Values represent the percentage of 250 m grid cells in the study area with differing levels of forest cover (20% bin width) at each date (1938 and 2015).

Of the total classified area (forest/non-forest) in the NFR, 14.3% overlapped with recent (1978-2015) fire perimeters. More than 70% of this fire activity occurred in the lower montane zone, which helps to explain lower increases in forest cover throughout this zone when compared to the upper montane and subalpine. Within recent fire perimeters, forest cover decreased from 56.6% to 19.7%, a net loss of 36.9%. So, while forest cover generally increased in the northern Front Range (NFR) of Colorado 1938-2015, a proportion of these longer-term increases in cover has been offset by recent fire activity in the lower montane zone. The years of peak fire activity between 1800 and 2015 occurred in 1859 and 1860, where 22.5% and 18.4% of fire history sites in the montane zone recorded fire, respectively (Fig. 2.2a). Given that these two years were not abnormally dry (Fig. 2.2b, 2.2c) and that the sites recording fire were primarily within the upper montane area utilized for mining (Veblen et al. 2000), the sharp rise in fire activity probably reflects increased anthropogenic ignitions - 1859 marks the year of widespread increases in intensive mining activity throughout the study area. In the 1938-2015 period, 2012 was the largest year for fire activity, with fire perimeters intersecting 9.5% of the montane zone (Fig.

2.2a). This year had above-average summer drought stress, below-average winter precipitation, and below-average spring snowpack (May 1st SWE; Fig. 2.2). These periods of historical and contemporary fire activity had important influences on 20th century changes in forest cover.

The Random Forest analysis indicated that the proportion of area recently burned (1978-2015) was the largest single contributor to forest cover change (Fig. 2.6a). When at least 70% of a grid cell intersected a recent fire perimeter, the cell was more likely to belong to the Forest Loss class than to other categories (Fig. 2.6b). In total, 78.1% of Forest Loss grid cells overlapped 1978-2015 fire perimeters. Elevation and proportion low-severity fire – related variables given the historical prevalence of frequent, low-severity fire at lower elevations – were the second and fourth most important predictors of forest cover change, respectively. Grid cells between c. 1700-2250 m and those historically dominated by low-severity fire (according to the spatial model in Sherriff et al. 2014) showed increased probabilities of membership in the Forest Gain class (Fig. 2.6c, 2.6e). Grid cells at the highest and lowest elevations (i.e., upper treeline and persistent grasslands), as well as mid-upper montane sites had lower probabilities of Forest Gain, but with some variability (Fig. 2.4, Fig. 2.6c). Grid cells with moderate to high heat load indices (HLI; i.e., SW slopes with average to above average levels of direct insolation) showed greater probabilities of Forest Gain than did cooler, NE-facing grid cells (Fig. A2). This relationship was consistent across elevations, with the exception of the grassland ecotone (< 1,700 m) where cool and wet sites (i.e., HLI < 0.7) were most likely to be classified as Forest Gain. At the grassland ecotone, 70% of grid cells with HLI < 0.7 were classified as Forest Gain, as compared to 25.8% of grid cells on warm/dry sites (HLI > 0.7). Mine site density was the third ranked predictor overall, and the most important predictor related to land use, though effects varied nonlinearly from low to high mine densities (Fig. 2.6a, 2.6d). Grid cells with no

recorded mine locations in the vicinity (kernel density of mines = 0/grid cell) were most likely to belong to the Little Change class. In contrast, areas with low to moderate mining density (0-0.125) had higher probabilities of Forest Gain. Sites with the highest mine densities (> 0.125) showed increased probabilities of membership to the Little Change class (Fig. 2.6a, 2.6d).

Among the predictors with lower importance, general trends still existed (Fig. 2.6a, Fig. A2). For example, silvicultural treatments, primarily fuels mitigation conducted between 2006 and 2015, led to decreased probabilities of Forest Gain (Fig. A2). Silvicultural treatments (c. 2006-2015) occurred on c. 6% of the classified area throughout the NFR and were more common in the montane zone. Surprisingly, the differences in forest cover change among current land ownership classes and 1938 land cover types were relatively minor (Fig. 2.6a, Fig. A2). Similarly, proportion of developed land and road density were not strong predictors of forest change in our model (Fig. 2.6a), likely because some of these areas were developed prior to 1938 or because some of this development took place in previously non-forested areas and thus did not lead to deforestation.

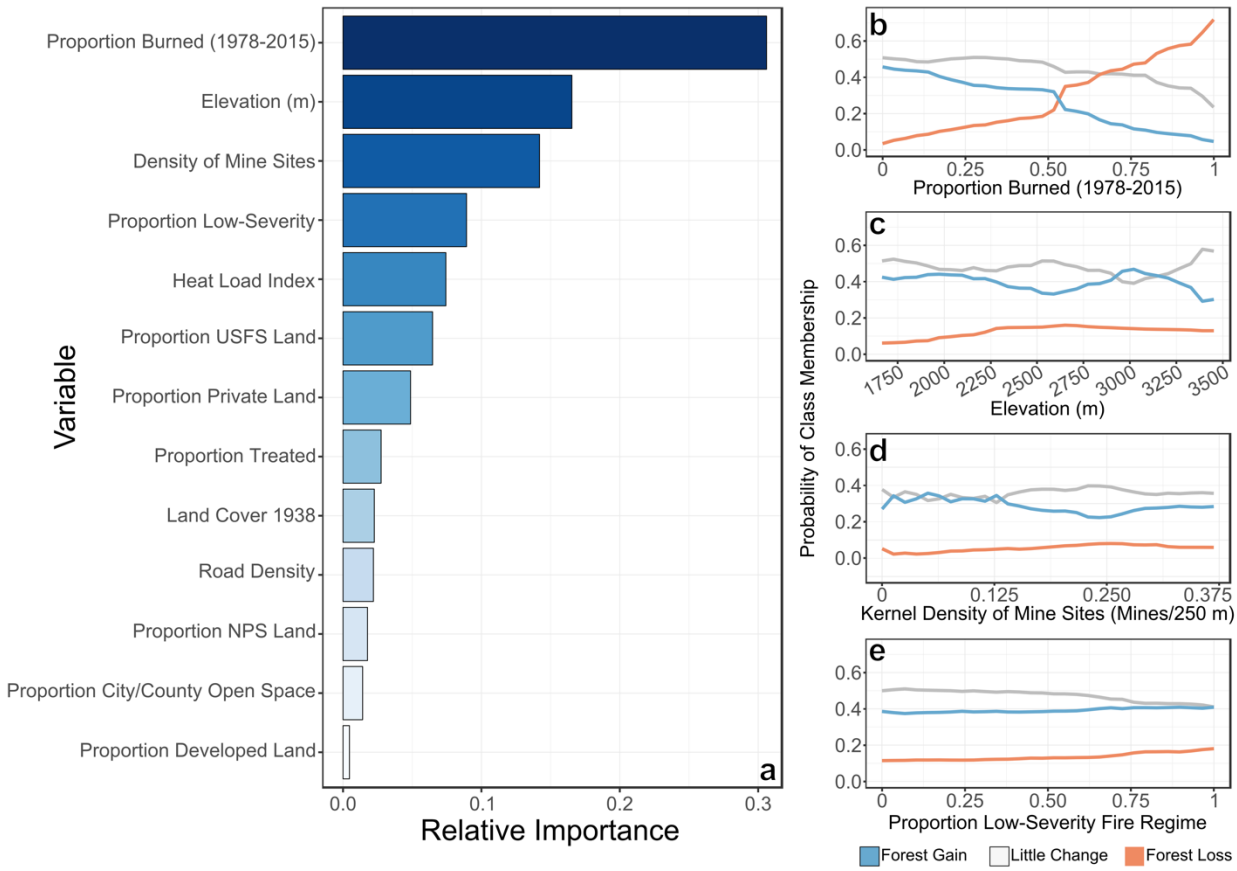

Fig. 2.6. Random Forest analysis (250 m resolution) of several potential drivers of forest cover change in the northern Front Range of Colorado, 1938-2015. Variable importance plot (a) gives the relative importance of each variable to the ensemble model, and partial dependence plots (b-e) show the marginal effects of each of the top four predictors across their respective ranges. Partial dependence plots for the remaining predictors are given in Fig. A2.

Cross-validation of the Random Forest model (at 250 m resolution) indicated that overall classification accuracy was 66.3% and that accuracy was highest for the Forest Loss class (Table A3). We also noted that our analyses of forest change were relatively insensitive to aggregation to a 1 km resolution. At this scale, 13.6% of 1 km cells were classified as Forest Loss, 44.9% were classified as Forest Gain, and 41.5% were classified as Little Change. The Random Forest analysis at a 1 km resolution yielded relatively similar rankings of variable importance, similar patterns in partial dependence (Fig. A3), and similar classification accuracy (65.2%) to analyses at the 250 m resolution. As might be expected, fine-scale drivers such as heat load index became less important at the coarser spatial resolution of 1 km (Fig. A3a) than they were at a 250 m

resolution (Fig. 2.6a). Patterns in the partial dependence of forest cover change on mine density (Fig. A3c) and on spatially modelled fire regime class (e.g., proportion of low-severity fire; Fig. A3e) also became more apparent at the 1 km resolution.

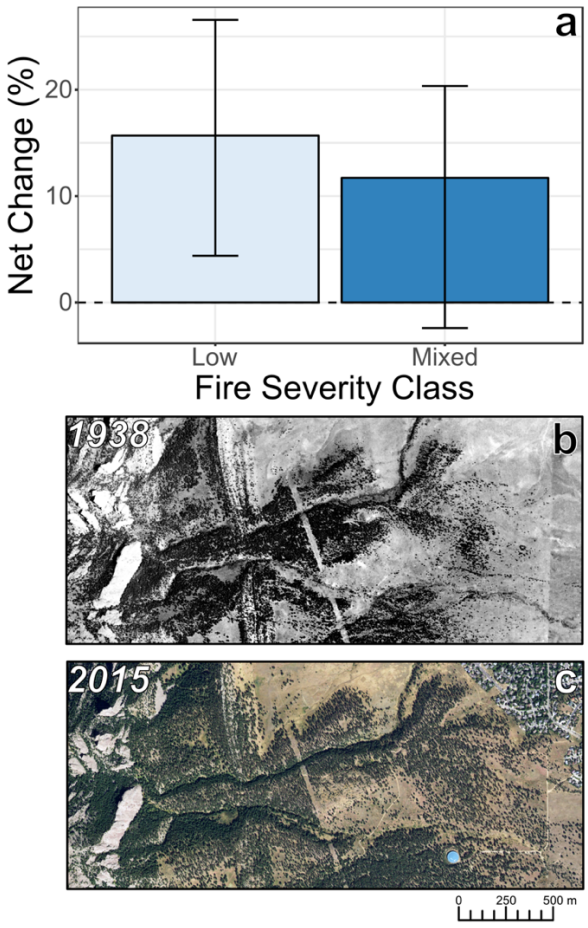

Fig. 2.7. Net change in forest cover 1938-2015 by historical fire regime class in 73 fire-excluded montane stands in the northern Front Range of Colorado with stand-specific fire history reconstructions. Stands in the low-severity class were historically characterized by frequent surface fires, while stands in the mixed-severity class experienced occasional stand-replacing patches of wildfire and tend to exist at middle elevations in the study area. Values given are area-weighted change in forest cover across all stands, and error bars represent the sensitivity of forest cover change to inaccurate classification and co-registration error. Example image pair (b, c) illustrates forest expansion into grasslands, as well as recent suburban development at a site typified by frequent, low-severity surface fires prior to 1920 (39.96 N, 105.27 W).

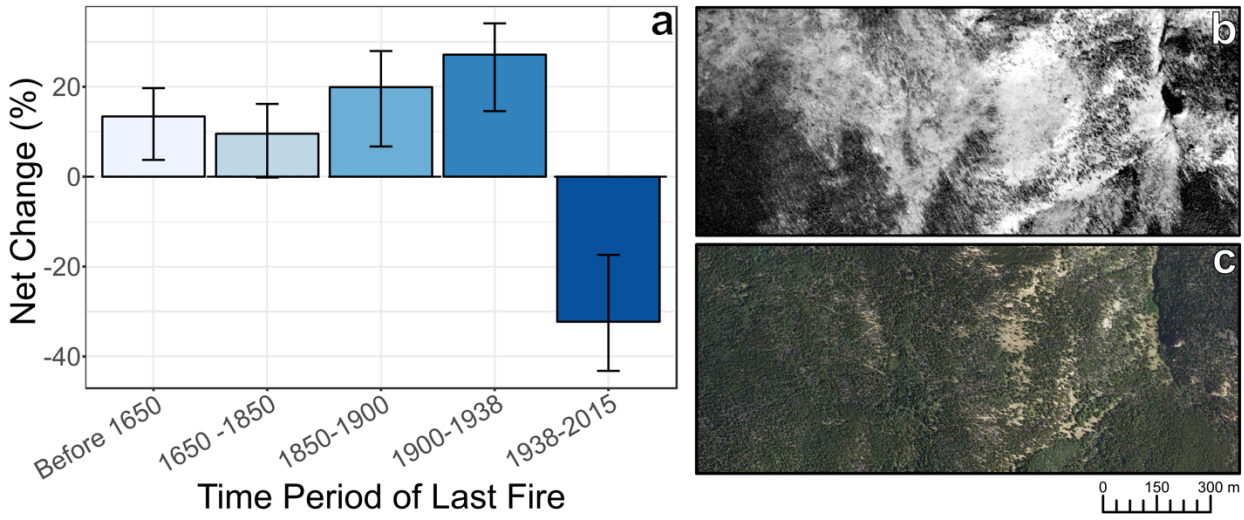

Fig. 2.8. Net change in forest cover (1938-2015) as it relates to time since last stand-replacing wildfire in higher elevation forest stands within a c. 5,000 ha area of Rocky Mountain National Park, CO (a). Error bars represent the sensitivity of each value to inaccurate classification and co-registration error. Areas in the 1938-2015 class are within a single wildfire that took place in 1978 (the Ouzel Fire). Example image pair (b, c) shows a subarea with a recorded fire that occurred in the late 1800s and subsequent recovery through the 20th century (40.31 N, 105.59 W). Fires in the subalpine zone typically burn infrequently (> 200 years) and at high-severity.

2.4.2 Comparison of Changes in Forest Cover with Fire History

In the comparison of forest cover change and stand-specific fire history (i.e., as opposed to the spatially modeled area) in the montane zone, we documented that fire-excluded stands with a history of frequent, low-severity surface fire (prior to 1920) showed greater increases in forest cover 1938-2015 (15.7% net change) than did stands with a history of mixed-severity fire (11.7% net change), corroborating results of the Random Forest analysis with respect to trends by elevation and spatially modelled fire regime (Fig. 2.7, Table A2). Sites within the low-severity class were primarily at lower elevations or in close proximity to grasslands.

In higher elevation forests (primarily subalpine) in a subset of Rocky Mountain National Park with previously reconstructed fire history, forest cover change showed variation with time since fire (Fig. 2.8, Table A2). Younger stands – those that burned 1850-1938 – showed greater increases in forest cover than did older stands (i.e., sites with the last fire prior to 1850). These

results are likely due to continued but slow post-fire recovery in areas that burned in the century prior to the initial imagery c. 1938 (Fig. 2.8b-c). In the 1938 imagery, locations with clearly identifiable fires dating from the 1800s and early 1900s were evident elsewhere in the upper montane and subalpine zones of the NFR; many of these burned sites returned to forest cover in 2015. Taken together, these results suggest that continued post-fire recovery from high-severity events in the late 1800s and early 1900s, and a near-absence of subalpine fires in the 20th century, are some of the major causes for the widespread increases in forest cover at higher elevations 1938-2015. The decline in forest cover for subalpine areas that burned 1938-2015 (Fig. 2.8a; -31.9% net change) was driven by a 143 ha subset of the 1978 Ouzel Fire that overlapped with our imagery and the study area of Sibold et al. (2006).

2.5 Discussion

We quantified 20th century forest cover change in the northern Front Range of Colorado, a complex landscape spanning broad gradients in the abiotic environment, disturbance regimes, and in human influence. We then linked changes in forest cover to data describing elevation, heat load index, historical and contemporary fire history, and land use. The NFR experienced extensive changes in forest cover 1938-2015, but reasons for these changes are spatially varying and a complex combination of drivers was related to the observed changes in forest cover. However, we note three general findings:

2.5.1 Changes in Forest Cover Were Influenced by Abiotic Factors and Human Influences

Consistent with previous studies in the NFR and in California, USA (Platt and Schoennagel 2009, Lydersen and Collins 2018), we noted that forest cover changes varied with elevation and that mesic, N-facing grid cells (with lower heat load indices) showed lower increases in cover through the 20th century than did grid cells with other aspects. In many cases,

these more mesic slopes were covered by dense forest stands in the initial imagery, which limited potential increases. However, this relationship shifted at the lowest elevations. Similar to the findings of Mast et al. (1997), we found that N-facing slopes at the grassland ecotone were more likely to experience Forest Gain than were S-facing slopes in these elevations. It is logical that forest cover on S-facing sites at lower treeline is moisture-limited and thus forest cover remained low at these sites throughout the 20th century. Similarly, in Arizona and New Mexico, USA, increases in tree density during the fire exclusion era were more limited in xeric, moisture stressed sites (Rodman et al. 2017), indicative of broad-scale climatic controls on tree growth and establishment. Moisture stress may be less limiting to establishment at higher elevations in the montane zone (Chambers et al. 2016, Rother and Veblen 2016); instead, time since disturbance may be a more important driver of forest cover change at these higher sites.

Mining activity was the dominant historical anthropogenic impact on forest cover changes in the NFR. Mining activity beginning in the mid-1800s led to surface disturbance rates at least 50 times that of the natural rate of soil disturbance prior to the 19th century (Dethier et al. 2018). Mining brought with it the removal of large diameter trees for railroad ties and timber, as well as increases in anthropogenic ignitions, all having important influences on forests (Veblen and Lorenz 1986, 1991, Veblen and Donnegan 2005). For example, 1859 and 1860 were the years of most widespread fire activity throughout the NFR c. 1800-2015 and 1859 marks the onset of intensive mining in the region (Veblen et al. 2000, Dethier et al. 2018). Throughout the NFR, areas with low to moderate mining density showed greater probabilities of Forest Gain through the 20th century, likely due to recovery from 1800s logging and burning. However, areas with the highest mining densities were more likely to demonstrate Little Change 1938-2015. We hypothesize that this effect could be attributed to two factors. First, areas of highest mining

density were more often privately owned and had higher densities of roads in both 1938 and 2015 than many other areas in the NFR. Therefore, persistent fragmentation due to residential development and road construction is one likely mechanism for lower probabilities of Forest Gain on these intensively-mined sites. Second, severe ground disturbance and seed source limitations (due to substantial removal of large-diameter timber) may have led to prolonged forest recovery in sites with high mining density, even those without persistent development or road networks. This relationship between mining density and forest cover change is complex and merits further investigation.

Like many areas throughout the western U.S., forest thinning and fire hazard mitigation have been prominent goals in forests in the NFR since the early 2000s (Caggiano 2017, Addington et al. 2018). Though silvicultural treatments were only documented in 6% of the NFR, these treatments influenced forest change in certain areas. For example, treatments were most common in the montane zone and, where present, led to decreased probabilities of Forest Gain 1938-2015. We did not perform analyses that separated silvicultural treatments by intensity or time since treatment, both of which are factors that would be likely to influence our results and would be useful in future studies. Similarly, we did not include data on sanitation or salvage harvests related to mountain pine beetle outbreaks in the 1970s or extractive logging prior to this time (Veblen and Donnegan 2005) and the influence of these events on forest change c. 1938-2015 is difficult to assess. However, establishment of younger cohorts has been noted following historical logging and it is likely that these mid-20th century management activities would lead to an altered forest age structure (Veblen and Donnegan 2005) rather than a conversion of forest to non-forest c. 1938-2015.

Land ownership influences forest cover change in a multitude of ways, such as differences in patterns of development, the intensity of fire suppression activities, and differences in the degree of silvicultural treatment by land ownership category. Developed private lands make up the vast majority of the wildland urban interface (Theobald and Romme 2007), an area where fire suppression activities are particularly intense (Gorte 2013). Forest management activities also differ across management units. For example, Easterday et al. (2018) noted substantial differences in 20th century forest change by land ownership designation in California, likely as a result of differing long-term management strategies. In the NFR, rates of silvicultural treatment varied by ownership and were highest on city/county owned lands (12.2% of total city/county area), intermediate on US Forest Service lands (6%) and private lands (3.8%), and lowest on National Park Service lands (0.6%). Widespread and consistent implementation of silvicultural treatments has been difficult in the NFR due to the fragmented nature of land ownership and potential treatment inconsistencies across ownership designations (Calkin et al. 2014). While silvicultural treatment, land ownership, and development intensity were not the most important variables in our analyses, we do not exclude potential influences from these factors given their known influence on ecological systems.

2.5.2 20th Century Changes in Forest Cover Varied by Life Zone and Historical Fire Regime

While forest cover increased 7.8% through the entire study area from 1938-2015, these increases were most pronounced in the subalpine zone and unburned portions of the lower montane zone. These findings align with what is known about patterns of historical fire activity and tree establishment across life zones in the NFR over the last two centuries. We noted that lower montane stands that were historically dominated by a frequent, low-severity fire regime (< 2,260 m; Sherriff et al. 2014) showed greater increases in forest cover c. 1938-2015 (15.7% net

gain in forest cover) than did mid-upper montane sites with a history of mixed-severity fire (11.7%). Stand age data indicate that abundant tree establishment occurred during the early 1900s throughout the lower montane zone (Sherriff and Veblen 2006, Battaglia et al. 2018). Because it may take several years for tree crowns to expand to a size that could be classified in the 1938 imagery (i.e., > 2 m crown diameter), some of this early 1900s establishment likely appeared to be forest cover increase during the 1938-2015 period of our study. In contrast, upper montane sites in the study area experienced abundant tree establishment in the mid-late 1800s following widespread mixed-severity fires and logging (Mast et al. 1998, Ehle and Baker 2003, Schoennagel et al. 2011, Battaglia et al. 2018). Thus, some of these mid-upper montane sites may have already appeared as closed forest and relatively dense stands in 1938, limiting potential increases 1938-2015. Still, continued establishment has occurred in some areas of the upper montane zone into the 2000s (Sherriff and Veblen 2006, Schoennagel et al. 2011), particularly areas experiencing past logging (Battaglia et al. 2018) or with low initial forest cover (Platt and Schoennagel 2009).

A previous study using historical and contemporary air photos (1938 to 1999) in the montane zone of the NFR also identified greater increases in forest cover at low elevations in the montane zone than in the mid-upper montane (Platt and Schoennagel 2009). Yet there were important differences between our study and that of Platt and Schoennagel (2009). While this prior study identified no increases in forest cover in stands above 2,432 m, we documented substantial increases in forest cover for some areas in the upper montane and subalpine zones. In addition, the 4% overall increase in forest cover identified by Platt and Schoennagel (2009) is generally lower than that presented in this study (7.8% increase). These differences could be attributed to several factors. Classification scheme, spatial extents of image coverage, and dates

of contemporary imagery differed between these studies, which could have affected final outcomes. Specific percentage estimates of forest cover change using historical air photos are imperfect due to the various limitations of these data (Platt and Schoennagel 2009, Lydersen and Collins 2018). These limitations make direct comparisons between studies difficult and further highlight the importance of methods that account for potential error and uncertainty in change detection.

The pronounced increases in forest cover through the subalpine zone tell a complex story that may be linked to a combination of logging activities, widespread fires in the 1800s, and slow forest recovery from these events. In a portion of Rocky Mountain National Park (the study area of Sibold et al. 2006), we noted that forest cover increases were generally higher for stands that burned 1850-1938 than within stands originating prior to 1850. This rough classification of stands by age masks some of the ecological variability inherent to subalpine forests in the NFR, where rates and trajectories of forest succession vary strongly by site and with species composition (Veblen 1986, Rebertus et al. 1991, Donnegan and Rebertus 1999, Coop et al. 2010). Still, it is notable that subalpine stands originating following abundant fire activity in the mid-late 1800s (Buechling and Baker 2004, Sibold and Veblen 2006, Sibold et al. 2006) showed much greater increases in forest cover than did older stands. Unlike sites in the lower montane zone, the direct impacts of organized fire suppression in subalpine forests are likely quite minimal given that these forests typically burn in extreme events during which suppression activities are difficult and that the period of active fire suppression is much shorter than a typical subalpine fire interval (Schoennagel et al. 2004, Naficy et al. 2016). While a small portion of the subalpine forests in the NFR had a history of frequent surface fire (e.g. 1-3%; Sibold et al. 2006) and tree invasion into subalpine meadows could have resulted from fire exclusion at these sites,

the thinning effects of surface fires in subalpine forests were relatively minor across the NFR landscape (Sibold et al. 2007). Thus, we conclude that forest cover in the subalpine zone in the NFR increased from 1938-2015 primarily as a result of continued recovery from fire, logging, and mining disturbances c. 1850-1938 rather than as a result of 20th century fire suppression.

2.5.3 Contemporary Fire Activity Drove Observed Declines In Forest Cover

Recent (1978-2015) fire activity was the largest single driver of forest change in our Random Forests analysis. Indeed, while forest cover increased throughout the study area 1938-2015, areas within fire perimeters showed substantial declines. Recent wildfires have driven rapid and broad-scale changes in landscapes of the NFR, but these changes should be considered within the context of multiple management goals. On one hand, these past fires, considered in combination with poor post-fire recovery in severely burned areas (e.g., Chambers et al. 2016, Rother and Veblen 2016), portend a decline in forest cover into the future. Changes in fire activity and forest cover may also alter important ecosystem services (Rocca et al. 2014). However, severe wildfires can benefit many wildlife species (Hutto et al. 2016) and may moderate subsequent fire activity (Parks et al. 2014, Coop et al. 2016, Holsinger et al. 2016), thus acting as effective fuel treatments in a region with a high density of homes in fire prone areas (Platt et al. 2011). These are important considerations as climate warming is expected to lead to continued increases in wildfire activity throughout the Rocky Mountains (Spracklen et al. 2009, Westerling et al. 2011, Liu et al. 2013).

2.6 Study Limitations

Forest cover, the focus of this study, is not necessarily indicative of forest structure and composition. For example, a 250 m grid cell with 30% forest cover could encompass a wide range of stand densities, species compositions, and fine-scale spatial patterns, all of which are

ecologically meaningful and influence myriad ecosystem processes. Though temporal variability in climate probably played an important role in the observed changes in forest cover in the NFR through the 20th century, we did not directly quantify the influences of interannual and interdecadal climate variability on changes in forest cover. These analyses were not feasible given that we used only two sets of imagery spanning a broad time period. Instead, a review and synthesis of potential influences of climate on tree establishment, disturbance activity, and tree growth is provided in Fig. 2.2 and Appendix A. We addressed spatial variability in climate by including elevation and heat load index in our analyses. These variables are strong proxies for climate in the NFR.

The seasonal timing of image acquisition has the potential to influence our results, as many quaking aspen and other broad-leafed deciduous trees at higher elevations in the study area likely had no leaves during the collection of 1938 imagery (collected primarily in late October after leaf abscission). Aspen is a fairly minor component of forests of the NFR (Peet 1981), and currently occupies only c. 7% of our study area in fragmented locations throughout the montane and subalpine zones (Veblen and Donnegan 2005, Rollins 2009). Still, some of the observed increases in forest cover in the upper montane and subalpine zones could reflect conversions of post-disturbance aspen cohorts in 1938 to conifer-dominated systems in 2015, rather than a conversion of non-forest to forest cover.

Shadows cast by individual trees and topography likely led to variability in our estimates of forest cover across the NFR. Recognized by previous studies (e.g., Platt and Schoennagel 2009, Lydersen and Collins 2018), shadows can influence the results of classification in greyscale imagery. For example, large shadows often appear to be dense homogenous stands of forest, while shadows from individual trees appear as extensions of the tree crowns. We

addressed these problems by removing large shadows and water bodies from the forest classification through post-classification correction, by using site-specific uncertainty thresholds to identify areas in which forest change exceeded classification error and uncertainty, and by manually correcting this classification when necessary. In most cases, aerial photos in 1938 and 2015 appeared to have been collected under similar lighting conditions (mid-late morning near the spring or fall equinox), which permits a reasonable comparison through time.

The classification of standing dead trees can also be problematic in greyscale imagery without spectral information in the red and near-infrared wavelengths. Our initial accuracy assessment indicated that misclassification of standing dead trees was an important source of classification error in 2015 imagery. For this reason, we corrected 2015 forest classifications within known burn perimeters using systematic photointerpretation (Appendix A). Though scattered tree mortality due to insects has occurred throughout much of the NFR c. 1996-2015 (USFS 2015), widespread insect outbreaks (i.e., near-total mortality of large stands) are primarily confined to the northwest corner of the study area. We estimate these outbreaks influenced < 5% of the total study area based on manual photointerpretation and comparison with aerial detection survey data (USFS 2015). Insect outbreaks during the late 20th and 21st centuries have been generally much less widespread and of lower severity in our study area than in other regions in Colorado. Furthermore, forest recovery following insect mortality in the overstory can be relatively rapid due to post-outbreak release of advance regeneration as well as new tree establishment (Veblen et al. 1991, Hadley and Veblen 1993, Collins et al. 2011), thus conversion to non-forest is not the typical result of recent insect outbreaks in the NFR. Still, we acknowledge that the misclassification of standing dead trees in areas recently affected by insect mortality is a potential cause of error.

One additional source of error that could not be fully accounted for was the degradation of original imagery in portions of the study area, particularly for the 1938-1940 imagery. Some scenes were well-preserved, yet others had evidence of fading and creases that may have led to local error in forest cover estimates. We addressed these problems by removing the outer edges of each scene prior to mosaicking (showing the greatest likelihood of fading and distortion), and by manually removing a small number of areas in which imagery was visibly degraded. Image degradation is an important consideration when working with historical aerial imagery in a GIS; automatic detection and removal of degraded areas in imagery may lead to improved results in the future.

2.7 Conclusion

Our study highlights that forest cover change is rarely the result of a single causative mechanism. Observed forest cover gains in the northern Front Range 1938-2015 were related to a complex combination of effects of elevation, heat load index, historical fire activity, and 19th century mining activity. The effects of fire history varied along the elevation gradient, with subalpine forests showing the greatest increases in cover in part due to recovery from fire activity in 1850-1938. In the montane zone, fire-excluded stands with a history of frequent, low-severity surface fire showed a greater increase in cover than did stands with a history of mixed-severity fire (15.7% vs 11.7%). No single driver of forest gain applied across the entirety of the study area. In contrast, forest loss was primarily driven by recent fire activity in the montane zone. Late 20th and early 21st century silvicultural treatments (e.g., forest thinning and prescribed fire), exurban development, and road construction have also played important roles in forest loss or in limiting gains in some areas. Changes in forest cover in the NFR c. 1938-2015 are a reflection of short-term (e.g., development, recent wildfire) and long-term (e.g., pulses of

historical fire activity, fire quiescence, climatic influences on tree establishment, and 1800s mining and logging) landscape legacies which are then overlaid upon variability in the abiotic environment.

CHAPTER 3

LIMITATIONS TO RECOVERY FOLLOWING WILDFIRE IN DRY FORESTS OF SOUTHERN COLORADO AND NORTHERN NEW MEXICO, USA

3.1 Introduction

Over the past several decades, global-scale climate warming and extreme drought events have promoted increases in wildfire activity across a range of forest ecosystem types (Kasischke and Turetsky 2006, Brando et al. 2014, Singleton et al. 2018). Wildfire activity, in combination with the effects of warmer and drier conditions on tree regeneration processes, is increasing the potential for widespread forest losses (Enright et al. 2015, Stevens-Rumann et al. 2018). The rate of forest recovery following wildfire is a crucial parameter that controls the susceptibility of forests to type conversion (Tepley et al. 2018) and in dry coniferous forests of the western U.S. (i.e., lower-elevation forests with a dominant component of ponderosa pine [*Pinus ponderosa*]), early post-fire recovery differs drastically across biophysical gradients (Chambers et al. 2016, Rother and Veblen 2016, Kemp et al. 2019). Thus, forest resilience to wildfire (*sensu* Holling 1973) is also likely to vary across complex mountainous landscapes. Spatially-explicit predictions of post-fire forest recovery (e.g., Tepley et al. 2017, Haffey et al. 2018, Shive et al. 2018) can provide insight into relative differences in forest resilience across gradients in fire severity and in the physical environment.

The empirical assessment of specific processes involved in regeneration (e.g., seed cone production, seedling germination, site suitability) will help to identify key bottlenecks to forest

persistence in a warmer, drier future (Enright et al. 2015, Davis et al. 2018b). For the successful establishment of seed-obligate conifers (i.e., those incapable of vegetative reproduction) following wildfire, seed must be produced and transported to a suitable site for germination and survival. Together, these processes define the regeneration niche (*sensu* Grubb 1977), which has a tremendous influence on the distribution of forests. Following recent wildfires throughout the western US, it has been noted that conifer seedling abundance is typically highest near surviving mature trees (Haire and McGarigal 2010, Chambers et al. 2016, Kemp et al. 2016, Tepley et al. 2017) due, in part, to greater seed availability. While seed dispersal is influenced by tree height, seed characteristics, wind speed, and animal dispersal, seed availability is typically much higher in areas adjacent to mature trees (McCaughey et al. 1986). This spatial component is well-documented, yet temporal variability in seed cone production of many conifers is poorly characterized and is critical for a comprehensive examination of seed availability in post-fire landscapes. Interannual variability in seed cone production is difficult to quantify (requiring either long-term monitoring or reconstruction based on persistent reproductive structures), and only a small number of studies have characterized annual seed cone production for a limited number of conifer species in the Southern Rocky Mountains (e.g., Shepperd et al. 2006, Mooney et al. 2011, Redmond et al. 2012, Buechling et al. 2016).

Overstory forest cover and post-fire vegetation also have the potential to influence conifer establishment, growth, and survival through biotic interactions and microclimate modification. In mixed-species systems in which conifers coexist with resprouting angiosperm species, the cover of resprouting vegetation (shrubs and trees) typically increases with fire severity (Welch et al. 2016). Competing vegetation can reduce the growth rates of some conifers (Tepley et al. 2017) and may also inhibit seedling establishment, particularly for species such as

ponderosa pine (*Pinus ponderosa*) that regenerate well on bare mineral soil (Pearson 1942, Schubert 1976). Overstory canopy cover moderates the understory environment by reducing daily maximum temperatures and diurnal fluctuations (Davis et al. 2018a). These dampening effects have the potential to reduce the influence of climate variability on seedlings, particularly for more shade-tolerant tree species capable of establishing and surviving within densely forested, climatically-buffered sites (Dobrowski et al. 2015).

In dry forests of the U.S. West, post-fire conifer seedling abundance is typically higher on more mesic sites such as north-facing slopes and higher elevations (Dodson and Root 2013, Rother and Veblen 2016, Tepley et al. 2017, Haffey et al. 2018, Shive et al. 2018, Kemp et al. 2019). Post-fire recovery in conifer forests is also influenced by interdecadal trends in climate and by interannual climate variability. For example, recovery is less likely in fires that are followed by abnormally dry periods (Stevens-Rumann et al. 2018). One plausible mechanism is that seedling establishment for some montane conifer species is more likely in infrequent years with above-average moisture (Savage et al. 1996, League and Veblen 2006, Rother and Veblen 2017, Davis et al. 2019). Douglas-fir (*Pseudotsuga menziesii*) and ponderosa pine seedling survival is also greater under cool and moist conditions (Rother et al. 2015), with extreme drought years of particular importance to regeneration failure (Young et al. 2019).

An improved understanding of the potential limitations to post-fire conifer regeneration requires a synthetic approach that considers seed cone production, seedling establishment, and site suitability (Davis et al. 2018b). At 15 recent (1988 to 2010) fire events, we characterized annual seed cone production, resprouting of angiosperm trees, and conifer seedling establishment. We then combined these data with surveys of post-fire abundance for seedlings of two dominant coniferous tree species (Douglas-fir and ponderosa pine) and investigated the

influence of key biophysical factors in predicting seedling abundance across the 15 fire events. Finally, we used these data to develop spatial models of predicted seedling abundances within each fire to better infer landscape-scale patterns of conifer forest resilience to wildfire. Specifically, we asked: 1) *How do seed cone production, conifer seedling establishment, and angiosperm resprouting vary following each fire?* 2) *Which factors best predict plot-level variability in post-fire conifer seedling abundance?* 3) *What percentage of each fire and of total burned area has recovered to meet tree density thresholds consistent with historical tree densities? 4) What is the proportion of fire area that is limited primarily by post-fire canopy cover rather than by site suitability?*

3.2 Methods

3.2.1 Study Area and Site Selection

Our study sites include 15 recent (1988-2010) wildfires occurring in dry forests of southern Colorado and northern New Mexico, USA (Fig. 3.1, Table 3.1). We selected these fires as a subset of all large (> 404 ha) wildland fires in this region occurring 1984-2010 (Eidenshink et al. 2007). We limited fire selection using the following criteria: 1) vegetation type – fires must have occurred in areas with dominant components of pine-oak, ponderosa pine, or dry mixed-conifer vegetation types (Rollins 2009) and 2) accessibility – fires must have occurred on accessible public land, or on large private parcels for which we were permitted access. Fire severity, area burned, pre-fire vegetation (Table 3.1), and average climate vary across fires. Within fire perimeters, January minimum temperatures range -14.9 to -6.8 C° and July maximums range 18.1 to 30.2 C°. Annual precipitation ranges 35.1 to 104.9 cm, with a pronounced dry period in early summer (June and early July) in each fire site. Late-summer monsoons (mid-July to September) vary in importance across the study area and account for 30-

45% of average annual precipitation, with increasing monsoonal contributions to the south and east (1981-2010 normals from the Parameter-Elevation Regression on Independent Slopes Model; PRISM 2018).

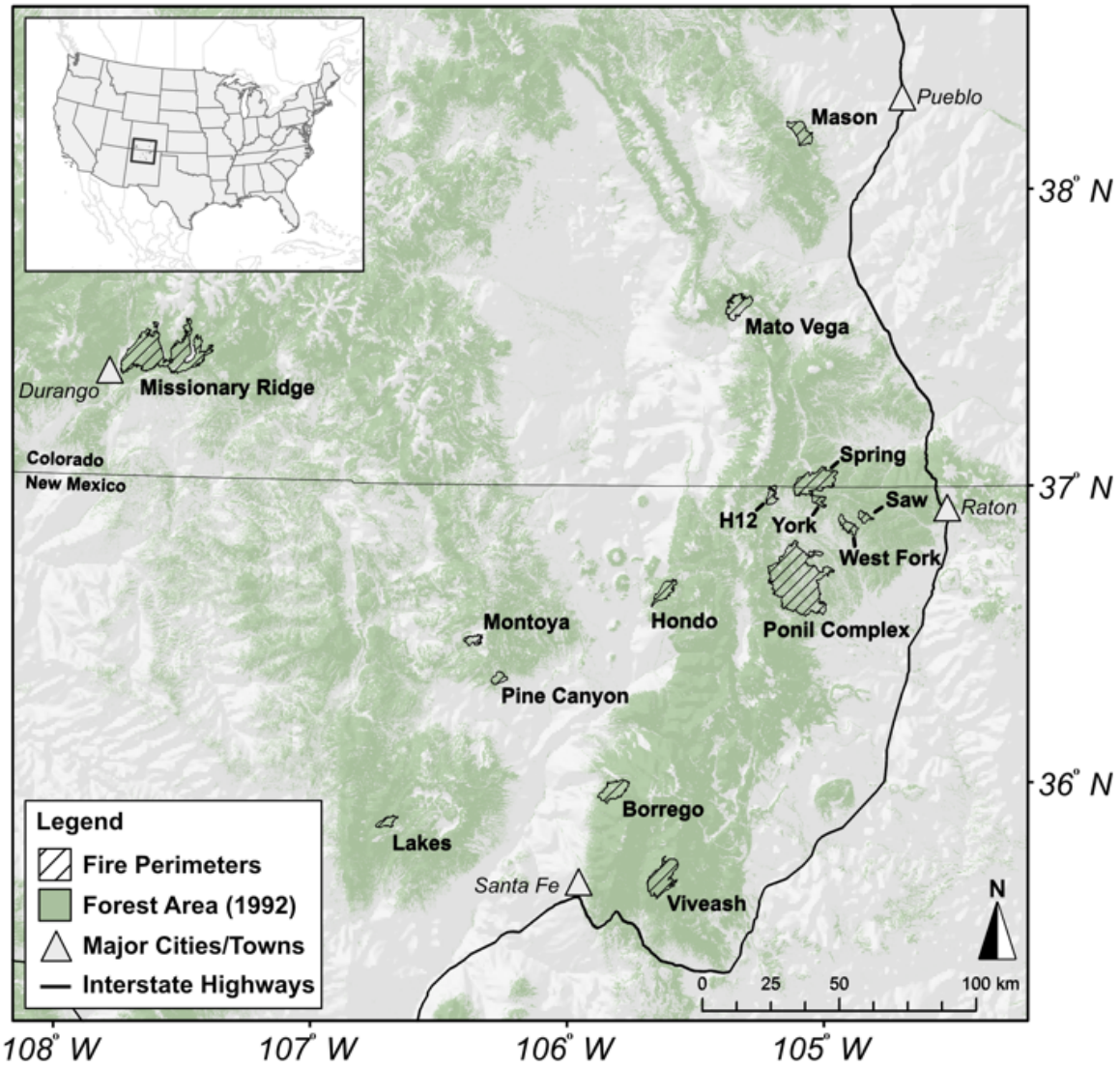

Fig. 3.1. Map of the study area in southern Colorado and northern New Mexico, USA, showing the 15 fires surveyed for post-fire conifer abundance. Green shading shows the distribution of forests based on the 1992 National Land Cover Dataset (NLCD), which preceded most of the fires surveyed.

Table 3.1. Descriptions of the 15 surveyed fires in s. Colorado and n. New Mexico, USA. "Area" is the areal extent of mapped fire perimeters from the Monitoring Trends in Burn Severity program (Eidenshink et al. 2007). "High severity (%)" is the percentage of each fire that burned at high severity (total canopy mortality) based on satellite-derived burn severity thresholding with field validation. Pre-fire species composition is given for the three most prevalent species across sites (Douglas-fir, Gambel oak, and ponderosa pine), and represents the percentage of pre-fire basal area belonging to a given species across all field plots in a given fire.

Fire Summary Information					**Pre-Fire Species Composition**			**Plots**
Name	**Area (ha)**	**High Severity (%)**	**Year**	**Elevation (m)**	**Douglas-Fir (% BA)**	**Gambel Oak (% BA)**	**Ponderosa Pine (% BA)**	**n**
Borrego	5211.1	20.6	2002	2163-3111	11.2	0.2	71.8	40
H12	1777.7	9.5	2010	2497-2964	18.2	2.2	77.4	40
Hondo	3338.8	69.2	1996	2261-3605	10.9	0.8	59.1	31
Lakes	1742.4	36.8	2002	2290-2673	43.1	0.3	38.8	40
Mason	4461.0	70.2	2005	1861-2494	13.6	1.3	78.1	37
Mato Vega	5311.8	60.9	2006	2568-3235	45.2	0	17.8	36
Missionary Ridge	27890.5	34.4	2002	2010-3560	31.8	0.3	22.7	33
Montoya	1665.5	45.4	2002	2437-2870	0	12.5	41.6	37
Pine Canyon	1656.1	21.0	2005	2214-2645	0	3	70.3	36
Ponil Complex	36050.8	31.7	2002	2027-2842	9.8	0.5	85.9	33
Saw	1258.7	0	1988	2262-2485	11.8	9.7	82.4	38
Spring	9730.3	48.6	2002	2316-2867	29.3	1.1	59.9	45
Viveash	9093.4	62.7	2000	2418-3539	48.5	0.1	28.6	29
West Fork	2199.8	14.8	2008	2196-2569	4.3	1.1	60.1	40
York	1313.8	9.0	2001	2389-2800	5.8	2.7	85.3	40
All Fires	**Total: 112701.6**	**Total: 38.7**	**Range: 1988-2010**	**Range: 1861-3605**	**Total: 23.0**	**Total: 1.7**	**Total: 55.7**	**Total: 555**

3.2.2 Cone Production, Conifer Seedling Establishment, and Angiosperm Resprouting

To characterize interannual variability in ponderosa pine seed cone production, we used the cone abscission scar method (Forcella 1981, Redmond et al. 2016). We performed these surveys within 8 of the 15 fires, a subset that was selected to span the geographic and climatic range of our sites. Within each of these eight fires, we surveyed at least two stands (27 stands total) and 4-6 trees/stand (n = 154 total trees) for seed cone production. Most stands were located in close proximity (< 1 km) to post-fire regeneration plots (i.e., *Regeneration Surveys*), either in

unburned areas or fire refugia within burn perimeters. At the tree level, seed cone years were defined as years in which at least 25 cones were produced. At the fire level, years of widespread seed cone production were defined as years in which at least 50% of trees produced more than 25 cones. To better understand synchrony in cone production, we also calculated pairwise Spearman rank correlation coefficients (of seed cone counts across years) between all trees surveyed for seed cone production (following Mooney et al. 2011). We then calculated the mean pairwise correlations of seed cone production for all trees (regional level), for trees within each fire (fire level), and trees within each stand (stand level) to better understand spatial scales of synchrony.

To describe temporal variability in conifer establishment and angiosperm resprouting following each fire, we collected up to two destructive samples of post-fire stems in each field plot (total n = 695 successfully dated; field plot site selection and layout described in *Regeneration Surveys*). If present, Douglas-fir, ponderosa pine, or lodgepole pine seedlings were excavated below soil level. If fewer than two post-fire individuals of these species were present on a plot, we then harvested angiosperm (i.e., aspen, Gambel oak) stems below the soil level. Lab methods used to identify the establishment year of conifer samples follow the protocols of Telewski (1993) and Rother and Veblen (2017). For angiosperm stems, we determined the year of stem initiation from a single cross section near ground level. This likely approximates annual resolution given the rapid growth of these stems in the first few years following stem initiation. Following sample processing, we identified significant pulses of establishment for ponderosa pine and Douglas-fir with CharAnalysis (Higuera et al. 2010, Tepley and Veblen 2015), using a five-year window width and a 90th percentile probability threshold. We then qualitatively compared pulses of establishment with interannual climate variables believed to influence tree establishment. Because moisture during the growing season may benefit conifer seedling

establishment (Rother and Veblen 2017), we calculated values of climatic water deficit (CWD; Appendix B) at a 30 m resolution across all fires for April-September of each year (1981-2015). We then calculated the area-weighted mean CWD (across all sites combined) for each year and scaled annual values through time using z-score transformation. Similarly, El Niño events (i.e., the warm phase of the El Niño Southern Oscillation) have been associated with episodic conifer establishment in the Southern Rocky Mountains (League and Veblen 2006), perhaps because of increases in winter precipitation during these years (Kurtzman and Scanlon 2007). Therefore, we also obtained a Multivariate ENSO Index (MEI; Wolter and Timlin 2011) for the two month period of January-February (following League and Veblen 2006).

3.2.3 Regeneration Surveys – Field Methods

Within each fire, we established 8-12 transects for surveys of post-fire seedling abundance, densities of resprouting angiosperms, and potential biophysical factors influencing post-fire recovery. Seedlings were defined as all conifers establishing following fire, but we did not survey first-year germinants because of the high mortality rates for these individuals. We stratified transect selection by dNBR(differenced Normalized Burn Ratio)-derived fire severity class (Eidenshink et al. 2007) and excluded any areas with post-fire reforestation activities. On each transect, we then established 4 plots (but in 18% of cases as few as 2 or as many as 6) with a 60 m systematic spacing and random offsets (10 m at a random azimuth). At each plot center (n = 555), we recorded the Euclidean distance to the closest mature conifer using a laser rangefinder. If these distances exceeded 500 m (the distance limitation of the instrument) or if live seed trees were not visible from plot center, we measured the distance from plot center to the closest mature conifer using 2014 or 2015 aerial imagery (USFS 2015). Following Harvey et al. (2016), we used a variable-sized plot design to survey post-fire abundances of conifer seedlings

and resprouting angiosperms. Plot sizes were species-specific and based on initial surveys of abundance. For tree species with fewer than 25 post-fire stems within the full 15 m radius circular plot (707 m^2), we surveyed all stems. If more than 25 stems of a species were present in the full plot, sampling areas were reduced to the following: 25-100 stems - 120 m^2, 101-500 stems - 30 m^2, > 500 stems - 10 m^2. In low- and moderate-severity areas, we used bud scar counts (*sensu* Urza and Sibold 2013) or ring counts from increment cores to exclude seedlings and saplings that may have originated prior to the fire. To develop field-derived estimates of fire severity and to quantify pre- and post-fire forest structure, we also surveyed live and dead overstory trees (> 10 cm for conifers and > 5 cm for angiosperms) that likely pre-dated each fire (Table 3.2). Lastly, we quantified ground cover on each plot using four 1 m^2 quadrats and noted any evidence of grazing or browse damage by cattle or other ungulates (Table 3.2).

Table 3.2. Descriptions of predictor variables included in statistical models of post-fire seedling abundance for ponderosa pine and Douglas-fir across 15 fires in southern Colorado and northern New Mexico. Expected relationships of each variable with ponderosa pine (PIPO) and Douglas-fir (PSME) abundances are shown with +/- signs, and variables that could be included in landscape models (used to spatially model seedling abundance) are denoted with (x).

Category	Variable Name	Description	PIPO	PSME	Landscape Model?
Average Climate	30-Year Average AET (Actual Evapotranspiration)	Average AET (evaporative loss constrained by moisture availability) in the calendar year each 30 m cell based on downscaled monthly PRISM climate normals from 1981-2010 (PRISM 2018) and a modified Thornthwaite water balance model. High AET is typical on warm sites with little moisture limitation. Low values are typical on dry sites or on cool sites with low evaporative demand.	+	+ or -	**x**
	30-Year Average CWD (Climatic Water Deficit)	Average CWD (the difference between potential and actual evapotranspiration) in	-	-	**x**

		the calendar year in each 30 m area based on downscaled monthly PRISM normals from 1981-2010 (PRISM 2018) and a modified Thornthwaite water balance model. Higher values are common on sites experiencing strong moisture limitation (warm and dry). Low values are common on sites with little moisture limitation (i.e., cool/wet sites, or warmer sites with high available moisture).			
Post-Fire Climate	Three-Year Post-Fire AET	Estimated AET in each 30m cell (in mm) based on downscaled monthly PRISM data in the three years after each fire (PRISM 2018) and a modified Thornthwaite water balance model.	+	+ or -	**x**
	Three-Year Post-Fire CWD	Estimated CWD in each 30m cell (in mm) based on downscaled monthly PRISM data in the three years after each fire (PRISM 2018) and a modified Thornthwaite water balance model.	-	-	**x**
	Post-Fire AET Deviation	The percent deviation between three-year post-fire AET and 30-year average AET. An index of relative post-fire AET specific to each 30 m cell.	+	+ or -	**x**
	Post-Fire CWD Deviation	The percent deviation between three-year post-fire CWD and 30-year average CWD. An index of relative post-fire CWD specific to each 30 m cell.	-	-	**x**
Tree Canopy	Canopy Cover	The percent of total area radii of varying distances (30-600 m in 30m increments) from plot center classified as mature conifer cover.	+ or -	+	**x**

	Distance to Seed Tree	Euclidean distance (m) from plot-center to nearest surviving conifer.	-	-	
Topography/ Terrain	Topographic Position Index	Index describing relative topographic position of each site. High values for ridgetops and low values for valley bottoms.	+ or -	-	**x**
	Landform Classification	Categorical variable combining topographic position, aspect, and soils at 30 m resolution. From Theobald et al. (2015)	+ on intermediate slopes	+ on cool/wet slopes	x
Biotic Interactions	Grazing/Browsing	Binary variable (presence/absence) of cattle grazing or ungulate browse damage on each plot	-	-	
	Douglas-Fir Seedling Density – Post-Fire	Density (seedlings/ha) of post-fire Douglas-fir establishment. Used only as predictor of ponderosa pine abundance.	+	N/A	
	Gambel Oak Sprout Density – Post-Fire	Density (stems/ha) of post-fire Gambel oak resprouting.	+ or -	+	
	Other Conifer Seedling Density – Post-Fire	Density (stems/ha) of post-fire conifers of other species, specifically fir, spruce, lodgepole pine, pinyon pine, and juniper.	-	-	
Fire Severity	Percent BA Mortality	Field-derived percent of pre-fire basal area killed during event. 100% indicates high-severity (canopy replacing) disturbance.	+ or -	-	
	RdNBR	Landsat-derived fire severity index using imagery pre- and post-fire. Higher values indicate higher vegetation mortality in a 30 m cell. From MTBS (Eidenshink et al. 2007) or calculated following standard protocol when striping present in original file.	+ or -	-	**x**
Pre-Fire Forest Structure	Pre-Fire BA	Combined basal area of live and dead overstory trees of all species in a given plot. Higher values	+	+	

		are indicative of higher site productivity and greater stand age.			
Groundcover/Seedbed	Bare Ground	Percent cover of bare ground in 1 m^2 quadrats.	+	-	
	Percent Coarse Wood	Percent cover of coarse wood in 1 m^2 quadrats.	+	+	
	Percent Forb Cover	Percent cover of forbs in 1 m^2 quadrats.	+	+	
	Percent Grass Cover	Percent cover of graminoids in 1 m^2 quadrats.	-	+ or -	
	Percent Litter Cover	Percent cover of litter in 1 m^2 quadrats.	-	+	
	Percent Rock Cover	Percent cover of rock in 1 m^2 quadrats.	-	-	
	Percent Shrub Cover	Percent cover of low (< 1.4 m in height) shrubs in 1 m^2 quadrats	+ or -	+	

3.2.4 Analytical Methods—Statistical Models of Post-fire Seedling Abundance

To develop statistical models of post-fire seedling abundances for ponderosa pine and Douglas-fir, we used generalized linear mixed models (GLMMs; *sensu* Bolker et al. 2009) in the "glmmTMB" package (Brooks et al. 2017) in R (R Core Team 2018). These statistical models included data from the 555 regeneration plots across the 15 surveyed fires. Because of the hierarchical structure of data collection, we used nested random intercepts (transect within fire) to account for spatial dependence of plot data within each transect and across each fire. Semivariogram analysis showed very little spatial dependence of model residuals with this random effect structure (nugget:sill ratio near 1; Bivand et al. 2013). To account for differences in sampling area across plots (due to the variable-sized subplots used in this study), we also included an offset term of "log(subplot area)" for each species on each plot (Zuur et al. 2009). Following the development of initial zero-inflated GLMMs with a Poisson error structure, we used simulation-based tests of model residuals in the "DHARMa" package (Hartig 2018) in R to

examine issues of dispersion. Our initial models were underdispersed and we therefore used a generalized Poisson error structure - a preferred distribution in these cases (Hilbe 2014).

Potential predictors in each GLMM included factors related to 30-year average climate, 3-year post-fire climate, seed tree distance and percent cover, topography, biotic interactions, fire severity, pre-fire forest structure, and post-fire groundcover (Table 3.2). All spatially explicit predictors were obtained or created at a 30 m resolution. To quantify 30-year average and 3-year post-fire climate, we first performed a statistical downscaling (following Nalder and Wein 1998) of gridded climate data from PRISM (PRISM 2018), and next modeled potential evapotranspiration (PET), actual evapotranspiration (AET), and climatic water deficit (CWD) using monthly water balance models (Appendix B; Lutz et al. 2010). We quantified post-fire canopy cover using image processing (following Rodman et al. 2019) and classification of 1 m 2014 and 2015 aerial photography from the National Agriculture Imagery Progam (USFS 2015; Appendix B). Overall accuracy for this classification was 90.2% at the level of a 1 m pixel (Table B1). We then aggregated the 1 m thematic maps to a 30 m resolution by extracting the percent cover of mature conifers in different neighborhood sizes (30-600 m radii in 30 m increments) surrounding the center of each field plot. We scaled and centered (z-score transformed) all continuous predictors prior to model fitting to facilitate direct comparison of standardized model coefficients and to improve model stability.

We performed variable selection for our GLMMs of post-fire seedling abundance using an information-theoretic approach (Burnham and Anderson 2002). First, we fit initial models by developing GLMMs that included all potential predictors (Table 3.2) with the exception of those in highly correlated groups (e.g., groundcover, canopy cover in different radii). We then independently added predictors from each correlated group and used AIC (Akaike Information

Criterion) to identify specific predictors in each group with the greatest explanatory power. After including these predictors, we then performed variable selection for final GLMMs by minimizing AIC while also balancing parsimony - in the case of two models with relatively similar AIC (i.e., $\Delta AIC < 2$), we selected the simpler model. To assess final model fit, we used a k-fold cross-validation procedure in which each GLMM was iteratively fit with the majority of the data, while plots from a single transect were withheld as the test set. We repeated this process with each transect (143 folds). We were interested in the ability of models to correctly predict abundances that exceeded different density thresholds (see *Analytical Methods – Spatial Modeling*) and therefore used balanced classification accuracy to assess model fit in cross-validation. For this, correct classification on a given plot indicates that model predictions were in agreement with observed seedling densities – where both exceeded or were below a given threshold.

3.2.5 Analytical Methods—Spatial Modeling

We developed an additional set of GLMMs to make spatially-explicit predictions of ponderosa pine and Douglas-fir seedling abundance at a 30 m resolution (hereafter "grid cells") throughout each surveyed fire. This was done by conducting GLMM analyses similar to above that used only predictors that were characterized at a 30 m resolution over the entire area of each fire (hereafter "landscape models"), and thus excluded groundcover, pre-fire forest structure, local vegetation characteristics, and field-derived distances to seed trees (Table 3.2). These landscape models were then used with spatially continuous datasets (Table 3.2) to predict post-fire seedling abundances in each grid cell throughout each fire (hereafter "spatial models"). Because Douglas-fir was only a minor component (< 10% basal area) of pre-fire basal area in five fires (Table 3.1), we excluded these fires from spatial modeling for this species. We present

spatial model results for each fire, the total fire area (summed across all fires), and the total high-severity area (38.7% of total fire area). To identify these high-severity areas (i.e., grid cells with total canopy mortality), we used field-derived fire severity (percent basal area mortality) and Landsat-derived RdNBR (relative differenced normalized burn ratio; Miller et al. 2009) to develop GLMMs (binomial family with logit-link) of the probability of total canopy mortality in each grid cell within each fire. We classified high-severity areas as grid cells exceeding a predicted probability of 0.628 (the threshold that maximized Youden's J statistic). Balanced classification accuracy of field plots with total canopy mortality was 84.4%.

Following spatial model development, we quantified the percentage of each fire, of total fire area, and of total high-severity area that exceeded density thresholds of 25 ponderosa pine seedlings ha^{-1} and 10 Douglas-fir seedlings ha^{-1}. These values correspond to some of the lowest reported stand densities in historical reconstructions of ponderosa pine and dry mixed-conifer forests throughout southern Colorado and the Southwest (Reynolds et al. 2013, Rodman et al. 2017). Because historical reconstructions in dry forests of the Southwest generally predict lower forest densities than those of contemporary forests, these thresholds indicate whether initial post-fire recovery in a grid cell reaches the lowest extent of what would be considered a ponderosa pine or dry mixed-conifer forest in this region. We also tested the sensitivity of model results and classification accuracies to different tree density thresholds; the 25 and10 seedlings ha^{-1} thresholds, for ponderosa pine and Douglas-fir, respectively, yielded the highest balanced accuracies of those tested (Table B2, Table B3). Therefore, we primarily discuss results from these 25 and 10 density thresholds as an indicator of landscape variation in post-fire recovery. In spatial models, grid cells with predicted seedling densities below these thresholds were classified as "low regeneration". To describe potential drivers of fire-level variability in these models, we

also calculated Spearman rank correlation coefficients between the percentage of each fire exceeding density thresholds and fire-level variables of: 1) percentage of each fire with total canopy mortality, 2) percentage of pre-fire basal area belonging to ponderosa pine or Douglas-fir, and 3) mean 30-year CWD throughout the fire.

Finally, to identify areas in which post-fire seedling abundances of Douglas-fir and ponderosa pine were limited by a lack of overstory trees following fire, we spatially modeled seedling abundances throughout each fire while assuming abundant canopy cover and holding all other predictor variables constant. Grid cells were then defined as "canopy limited" if they were predicted to have low regeneration in initial spatial models (with observed canopy cover), but exceeded density thresholds given modeled abundant canopy cover. Grid cells with low regeneration in both sets of spatial models were then interpreted to be limited by the other predictors (e.g., AET, CWD) in the landscape models and/or fire-level random effects.

3.3 Results

3.3.1 How Do Seed Cone Production, Conifer Seedling Establishment, and Angiosperm Resprouting Vary Following Each Fire?

While the frequency and abundance of ponderosa pine cone production varied by fire, we estimate that ponderosa pine seed was widely available in most areas with surviving mature trees (Fig. 3.2). From 2003-2017 (the range of years that could be adequately assessed), 74% of all surveyed trees had at least two seed cone years and 40% had at least five seed cone years (Fig. 3.2a). Each fire surveyed using the cone abscission scar method (n = 8) had multiple years of widespread seed cone availability following fire occurrence (Fig. 3.2b). These events occurred, on average, every 2-8 years at the fire-level. Seed cone production was asynchronous across fires (mean pairwise Spearman correlation; $\rho = 0.09$), though regionally important years occurred in

2006, 2009, 2012, 2015, and 2017 (Fig. 3.2c). Seed cone production was relatively synchronous within fires (mean $\rho = 0.25$, range = 0.08-0.40) and most synchronous within individual stands (mean $\rho = 0.38$, range = 0.02-0.64). Because of this widespread and relatively frequent seed cone production at the tree- and fire-level, we used spatial variability in canopy cover as a proxy for post-fire seed availability.

Lodgepole pine (which often have fire-adapted canopy seedbanks), as well as Gambel oak and aspen (which can re-sprout from established root systems following wildfire), showed abundant establishment immediately following individual fire events (Fig. 3.3). Specifically, 96% of lodgepole pine samples and 54% of oak and aspen stems were dated within three years of fire occurrence. Still, stems of resprouting angiosperms continued to initiate for many years after some fires (Fig. 3.3). Only 23% of ponderosa pine and Douglas-fir establishment occurred within three years of fire occurrence. CharAnalysis of seedling establishment dates aggregated across the 15 fires identified significant regional pulses of ponderosa pine and Douglas-fir seedling establishment in 1995, 1998, 2007, 2010, and 2014 (Fig. 3.4a). Three of the five pulses (1995, 1998, and 2007) occurred during years with below-average CWD during the growing season (Fig. 3.4b), and four of the five pulses (1995, 1998, 2007, and 2010) were associated with El Niño events (i.e., a positive MEI in January and February; Fig. 3.4c). No strong temporal associations were evident between ponderosa pine seed cone production and seedling establishment at broad scales (Fig. 3.4d).

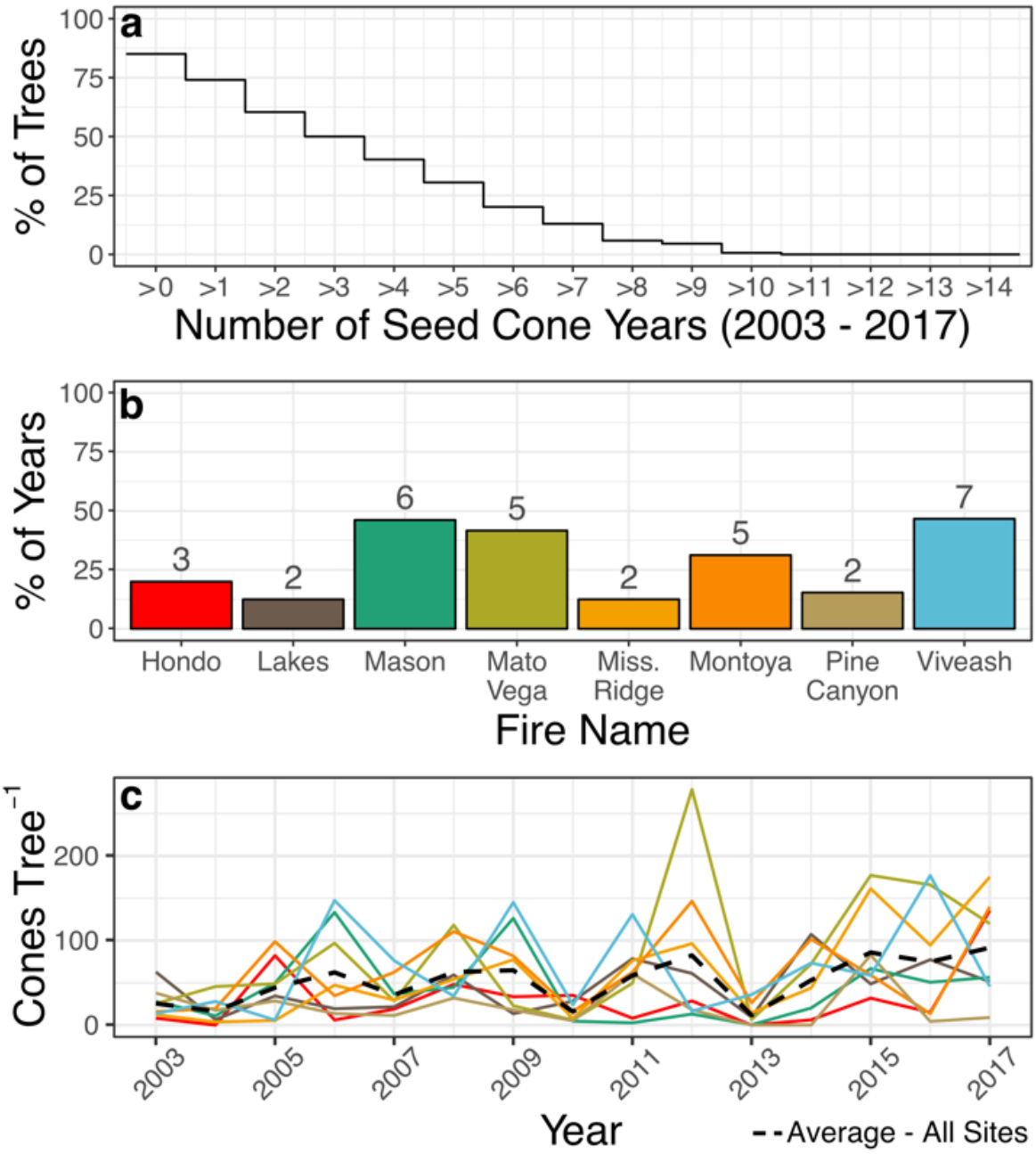

Fig. 3.2. A summary of (a) tree- and (b, c) fire-level ponderosa pine seed cone production across 8 of the 15 surveyed fires in southern Colorado and northern New Mexico (sites for which cone production data were collected using the cone abscission scar method). Tree-level cone production gives (a) the percentage of trees (across all sites; n = 154) exceeding different numbers of individual seed years (2003-2017), where seed years were defined as individual years with at least 25 cones produced by a given tree. Fire-level cone production gives (b) the proportion (bar heights) and number of post-fire years (numbers above each bar) with widespread cone production (> 25 cones produced on at least 50% of surveyed trees within a fire in a given year), as well as (c) the annual average cone production within each fire. Bar colors and fire names in (b) match lines in (c). Cone production prior to 2003 could not be reliably quantified using the cone abscission scar method.

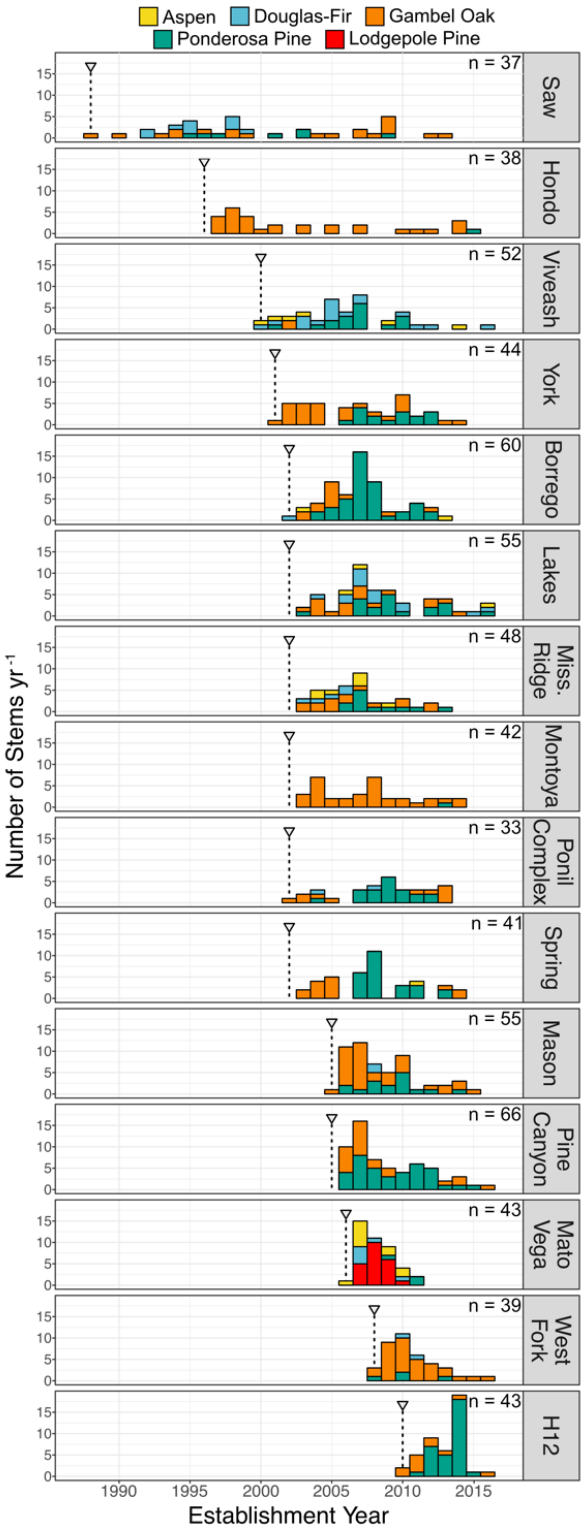

Fig. 3.3. Annual patterns of conifer seedling establishment (for Douglas-fir, ponderosa pine, and lodgepole pine) and timing of resprouting (for aspen and Gambel oak) across each of the 15 surveyed fires in southern Colorado and northern New Mexico. Counts are derived from destructive samples collected throughout each fire. Years of fire occurrence are shown with a and dashed line. The total number of seedlings and stems aged in each fire is given by n.

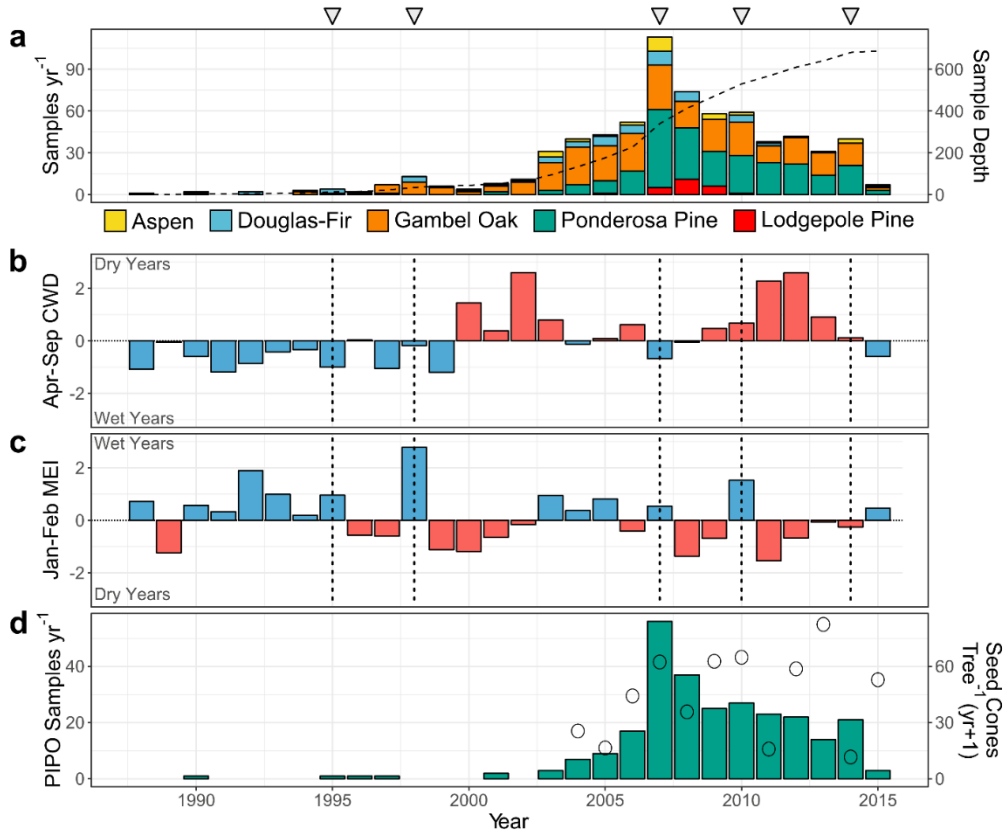

Fig. 3.4. A summary of conifer establishment, angiosperm resprouting, interannual climate variability (1988-2015), and ponderosa pine seed cone production across surveyed fires in southern Colorado and northern New Mexico. Destructively sampled seedlings (conifers) and stems (angiosperms) were collected throughout each fire and (a) dated with annual resolution. Bar colors correspond to each of the five sampled species, and bar heights correspond to the number of samples dated to each year. Triangles and vertical dashed lines show significant pulses of ponderosa pine and Douglas-fir establishment (1995, 1998, 2007, 2010, and 2014) based on CharAnalysis. Interannual climate variability was characterized with (b) CWD (climatic water deficit) during the growing season (April-September) and (c) the multivariate ENSO (El Niño Southern Oscillation) index (MEI). Lastly, (d) ponderosa pine establishment across all sites (green bars) is overlaid with mean seed cone production (from 27 stands throughout the region) in the year prior to seedling establishment (hollow circles).

3.3.2 Which Factors Best Predict Plot-Level and Landscape-Level Variability in Conifer Seedling Abundance Following Wildfire?

In the full ponderosa pine model (with both field-derived and landscape variables included), 30-year average AET, 30-year average CWD, distance to seed source, percent basal

area mortality, post-fire vegetation, and pre-fire basal area were all included in the final models of post-fire seedling abundance (Fig. 3.5a). Abundance was highest in sites with low 30-year average CWD and high 30-year average AET, together indicative of productive areas with abundant moisture (Fig. 3.5a). Interestingly, 30-year averages of CWD and AET were better predictors of seedling abundance than were 3-year post-fire AET and CWD. Including these post-fire climate variables did not improve predictive accuracy. Plots that were adjacent to seed trees but also burned at higher severity (i.e., greater percent basal area mortality) had higher abundances of ponderosa pine (Fig. 3.5a). Grass cover and Gambel oak sprouting density were negatively related to ponderosa pine abundance, while pre-fire basal area and post-fire Douglas-fir seedling density were positively related to ponderosa pine abundance (Fig. 3.5a). The full Douglas-fir model did not improve upon the landscape model (in terms of AIC), thus we only present the landscape model for Douglas-fir.

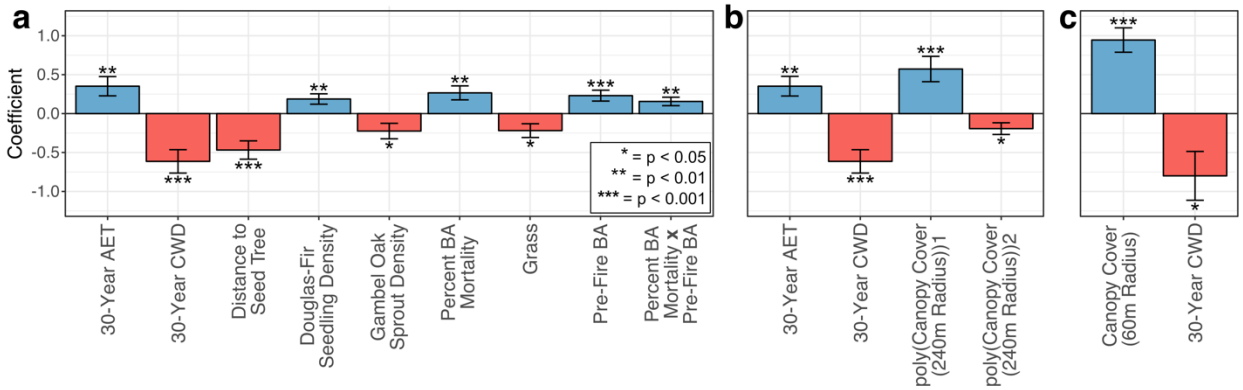

Fig. 3.5. Standardized coefficients and significance levels for each of the predictors included in final generalized linear mixed models for predicting postfire conifer abundance. Error bars are ± one standard error of the coefficient estimate. Models were developed for ponderosa pine seedling abundance from (a) all potential predictors (both field-derived and the landscape variables), (b) ponderosa pine seedling abundance from landscape-level predictors only (for later use in spatial modeling) and (c) Douglas-fir seedling abundance from landscape-level predictors. We did not develop a model for Douglas-fir seedling abundance from field-based predictors because the landscape-level model outperformed all other competing models. Coefficients given are for the conditional models only and do not include zero-inflation terms or intercept coefficients. Orthogonal polynomial terms (non-linear predictors) are given with the variable name preceded by "poly" and variable interactions are given by linking two variable names with "x".

Landscape models including only variables that were characterized at a 30 m resolution across each fire were relatively similar for each species, but also had some important differences (Fig. 3.5b, 3.5c; Fig. 3.6). The ponderosa pine landscape model included 30-year average CWD, 30-year average AET, and canopy cover within 240 m, with average CWD being the most important predictor. Low 30-year average CWD and high 30-year average AET were again associated with higher ponderosa pine abundance (Fig. 3.5b, Fig. 3.6b, Fig. 3.6c). The Douglas-fir landscape model was relatively simple and included only 30-year average CWD and canopy cover within a 60m radius. Canopy cover was more important than was 30-year average CWD for Douglas-fir (Fig. 3.5c). Similar to ponderosa pine, low 30-year average CWD was associated with high Douglas-fir abundance (Fig. 3.6e). The most notable difference between the two species was the relationship with canopy cover. Ponderosa pine abundance was highest in areas with intermediate (46%) canopy cover and the most influential neighborhood size was relatively broad - 240 m (Fig. 3.5b, Fig. 3.6a). A non-linear term for canopy cover led to a slightly improved model fit (ΔAIC = 1.8) and a more ecologically realistic response given the shade-intolerant nature of ponderosa pine. In contrast, Douglas-fir abundance was highest in dense stands (100% cover) and a 60 m neighborhood size was most influential (Fig. 3.5c, Fig. 3.6d), consistent with overstory microclimatic buffering and the higher shade tolerance of this species.

While the full model (i.e. field-derived and landscape variables) of ponderosa pine abundance had an improved fit when compared to the landscape model (ΔAIC = 11.8), the differences in classification accuracy from cross-validation were relatively minor (71.8% balanced accuracy for the full model vs. 70.6% for the landscape model; Table B1). In addition, 30-year average AET, 30-year average CWD, and distance to seed tree were the three best predictors in the full ponderosa pine model (highest absolute values of standardized coefficients;

Fig. 3.5a), and field derived distance to seed tree was strongly related to canopy cover in a 240 m radius (ρ = -0.68). For Douglas-fir, the landscape model outperformed any full models and had a balanced classification accuracy of 77.3% (Table B2). Therefore, landscape models for ponderosa pine and Douglas-fir are useful to broadly generalize and predict post-fire seedling abundances throughout each fire.

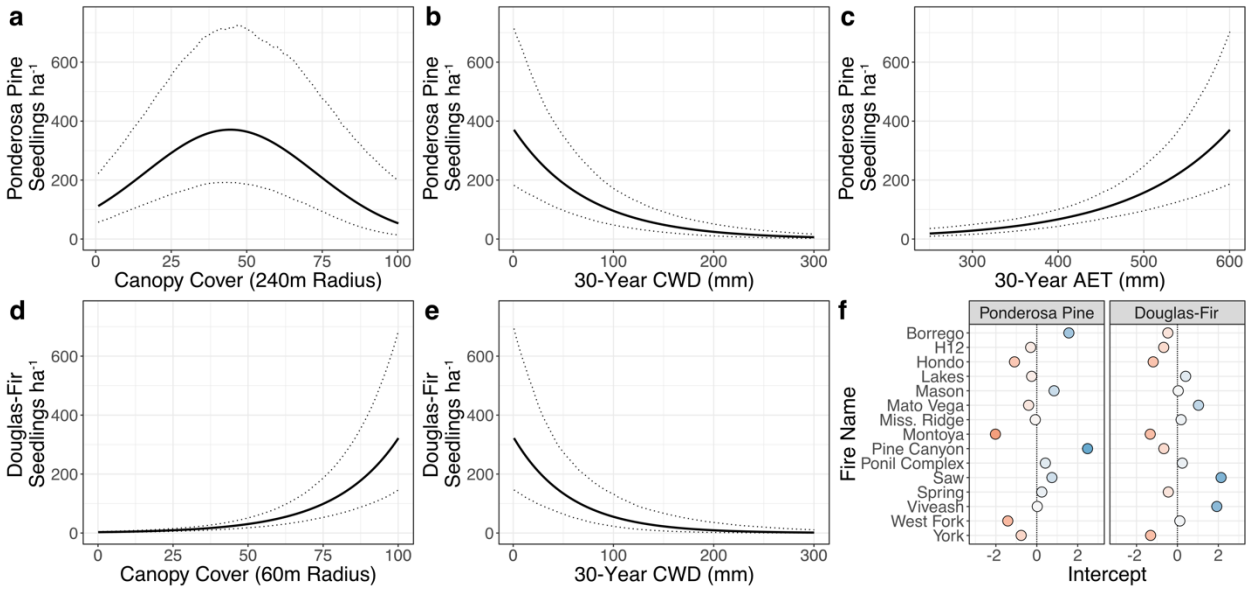

Fig. 3.6. Results of generalized linear mixed models that were used to predict post-fire seedling abundance of ponderosa pine and Douglas-fir across each of the surveyed fires in southern Colorado and northern New Mexico, USA. Predicted values (solid lines) represent the marginal effects of each predictor when assuming optimal values for the other predictors and mean values of random effects. Dotted lines are ± one standard error of prediction. Variables include (a, d) canopy cover - the percent surface area of mature conifers within a given radius, (b, e) 30-year average CWD (climatic water deficit) and (c) 30-year average AET (actual evapotranspiration) – measures of unmet evaporative demand and evaporation constrained by moisture availability, respectively. Variation among fires is shown with (f) random intercept coefficients for each species, where colors indicate positive (blue) or negative (red) deviations from the mean value across all sites.

3.3.3 What Percentage of Each Fire and of Total Burned Area Has Recovered to Meet Tree Density Thresholds Consistent With Historical Ranges for Ponderosa Pine and Douglas-Fir?

Spatial models of post-fire seedling abundance for each species (developed from predictions using landscape models described above; Fig. 3.7, Fig. 3.8) indicated that a substantial percentage of the total burned area was unlikely to exceed density thresholds of 25 ponderosa pine or 10 Douglas-fir seedlings ha^{-1}. Across the fires studied, 41.8% and 68.5% of total fire area had ponderosa pine regeneration and Douglas-regeneration below the 25 and 10 thresholds, respectively. In the portions of these fires with total canopy mortality (i.e., high-severity), abundances were lower. We predicted that 57.3% and 79.4% of the total high-severity area did not exceed the 25 and 10 tree density thresholds for ponderosa pine and Douglas-fir, respectively (Table B1, Table B2).

Recovery also varied substantially among fires. For example, the Montoya Fire had 0% of total fire area exceeding density thresholds for each species, while the Saw Fire had 100% (ponderosa pine) and 97.6% (Douglas-fir) of fire area exceeding density thresholds (Fig. 3.7, Fig. 3.8; ponderosa pine median = 70.7%, Douglas-fir median = 27.2%). The differences among fires could be partially explained by pre-fire species dominance and other fire-level effects. For example, the percentage of fire area exceeding density thresholds was positively correlated with pre-fire basal area for each species at the fire-level ($\rho = 0.55$ for ponderosa pine, $\rho = 0.38$ for Douglas-fir) and negatively correlated with percentage of fire area with total canopy mortality ($\rho = -0.50$ for ponderosa pine, $\rho = -0.52$ for Douglas-fir). There were weaker relationships with 30-year average CWD at the fire level ($\rho = -0.15$ for ponderosa pine, $\rho = -0.25$ for Douglas-fir), likely because CWD varies substantially throughout each burned landscape.

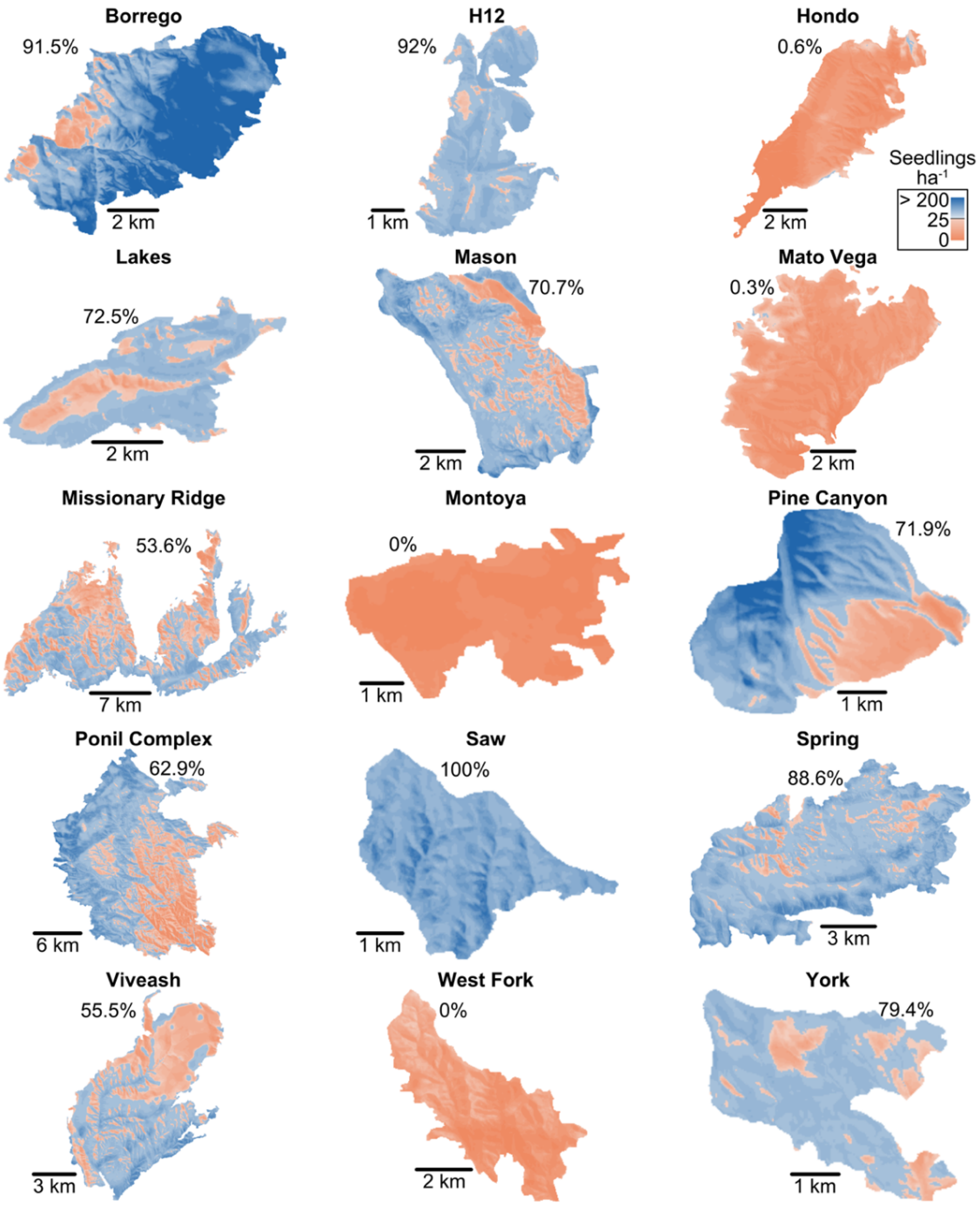

Fig. 3.7. Predicted ponderosa pine seedling abundances throughout each surveyed fire in southern Colorado and northern New Mexico based on the landscape GLMMs. The percentage values in each panel give the percentage of fire area exceeding a density threshold of 25 seedlings ha^{-1}, which corresponds to some of the lowest historically reported densities for this species in ponderosa-pine dominated forests of the Southern Rocky Mountains and Southwest (Rodman et al. 2017). Blue areas in each map exceed this threshold while red areas are below this threshold.

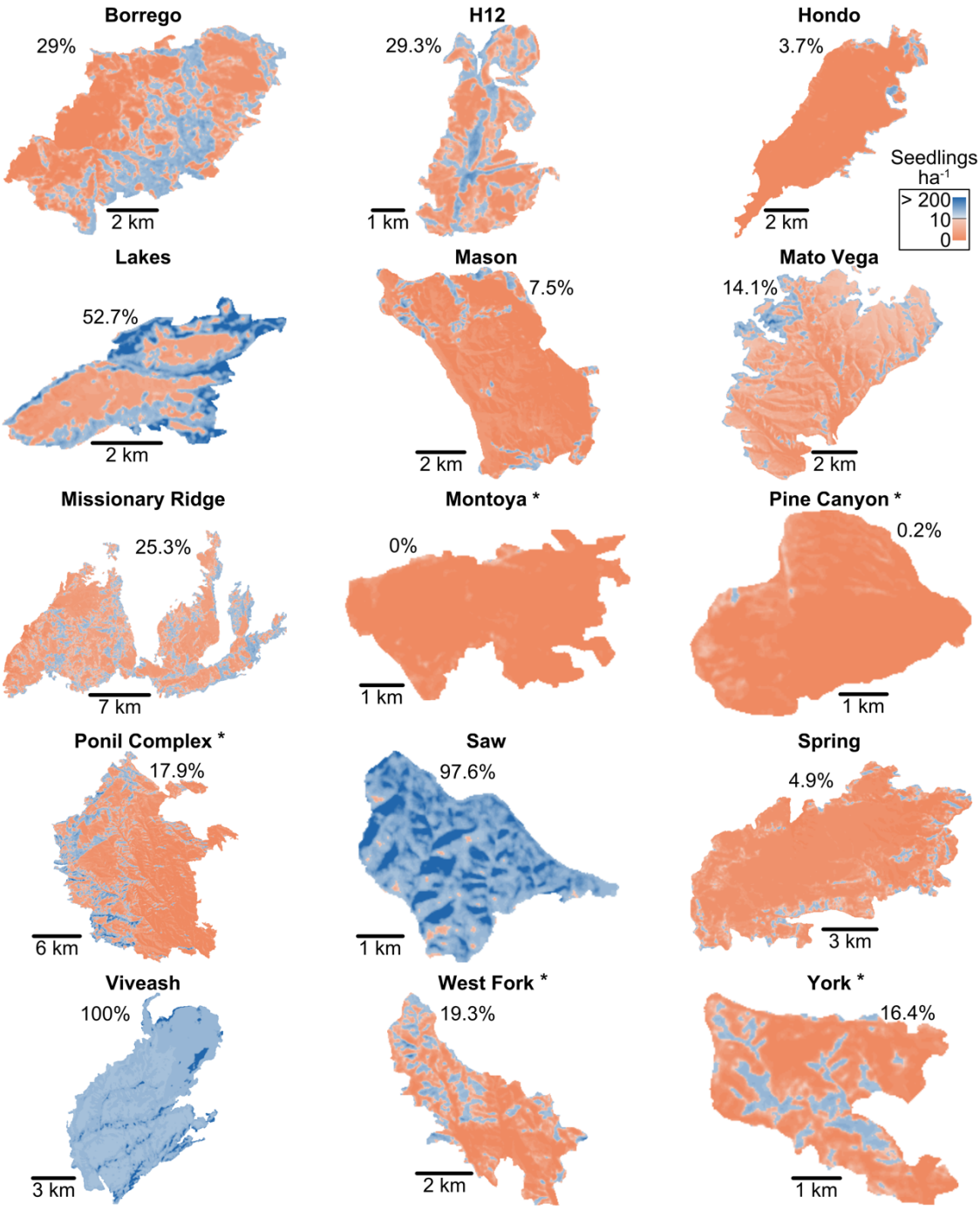

Fig. 3.8. Predicted Douglas-fir seedling abundances throughout each surveyed fire in southern Colorado and northern New Mexico based on the landscape GLMMs. The percentage values in each panel give the percentage of fire area exceeding a density threshold of 10 seedlings ha^{-1}, which corresponds to some of the lowest historically reported densities for this species in dry mixed-conifer forests of the Southern Rocky Mountains and Southwest (Rodman et al. 2017). Blue areas in each map exceed this threshold while red areas are below this threshold. Fire names followed by (*) are those in which Douglas-fir represented less than 10% of pre-fire basal area (i.e., a minor component of forests present prior to the fire) and were excluded from some analyses.

3.3.4 What Is the Proportion of Fire Area That Is Limited Primarily by Post-Fire Canopy Cover Rather Than by Site Suitability?

The drivers of limited conifer regeneration vary by species and throughout each site. While post-fire canopy cover is clearly an important predictor of ponderosa pine seedling abundance, not all areas were predicted to exceed conservative density thresholds even given optimal levels of canopy cover. When other variables were held constant, we found that 25.4% of total fire area (112,706 ha) was predicted to have low regeneration of ponderosa pine due primarily to seed source limitation (i.e., limited canopy cover; Table B1). An additional 16.4% of fire area had low ponderosa pine regeneration due to 30-year average AET, 30-year average CWD, and fire-level random effects (Table B1). In contrast, Douglas-fir may be more strongly influenced by canopy cover. For Douglas-fir, 67.6% of the total fire area (69,816 ha) was classified as canopy limited (Table B2).

3.4 Discussion

Limited recovery of seed-obligate conifers has been widely documented following recent wildfires throughout the western U.S. (e.g., Harvey et al. 2016, Rother and Veblen 2016, Shive et al. 2018, Stevens-Rumann et al. 2018, Davis et al. 2019, Kemp et al. 2019), yet the spatial and temporal variability in factors limiting forest resilience to wildfire are still poorly understood. Our surveys of seed cone production, seedling establishment, and post-fire conifer abundance show that variability in post-fire abundance relates to gradients in fire severity and in the physical environment. Douglas-fir and ponderosa pine post-fire seedling abundances are typically highest on more mesic sites and in close proximity to residual overstory trees. Seed cone production was not a major limitation to post-fire recovery of ponderosa pine. We also noted that at a regional scale the five peak years of seedling establishment coincided with above

average moisture availability. Together, the initial filter of seed availability (a combination of seed production and canopy cover) and the secondary filter of the physical environment limited conifer forest recovery across recent wildfires in southern Colorado and northern New Mexico, USA.

3.4.1 Spatial and Temporal Limitations to Seed Availability and Other Effects of Canopy Cover

Our findings pertinent to Question 1 indicate that the limited establishment of ponderosa pine following wildfires was not due to a lack of years of abundant seed cone production (i.e. mast years). Previous studies of seed cone production in ponderosa pine indicate that mast years may occur every 2-6 years or more (Maguire 1956, Krannitz and Duralia 2004, Shepperd et al. 2006, Mooney et al. 2011), similar to our estimates of 2-8 years at the fire-level. Seed cone production was also more frequent at the tree-level. These findings are important because they indicate two things. First, the time interval between the initial disturbance and the time of surveys was long enough to allow for at least one widespread ponderosa pine seed cone year in each fire. Second, given the relatively frequent cone production (at the tree- and fire-level) observed in this study, the patterns of surviving trees are a useful proxy for spatial variability in ponderosa pine seed availability throughout the landscape. Still, temporal variation in seed availability and alignment with climate conditions suitable for germination is a poorly understood component of post-fire recovery (Savage et al. 1996, 2013, Petrie et al. 2017) needing further research.

Canopy cover was among the factors best predicting post-fire Douglas-fir and ponderosa pine abundance, likely reflecting a combination of mechanisms. Most importantly, canopy cover influences spatial patterns in seed-availability, which is a necessary prerequisite for seedling germination and establishment. The overstory canopy also modifies temperature (Davis et al.

2018a), relative humidity (Paritsis et al. 2015), and light availability in the understory (Battaglia et al. 2002), all important to seedling survival harsh post-fire environments. While canopy moderation may benefit both ponderosa pine and Douglas-fir, Douglas-fir is better adapted to benefit from microclimatic buffering (*sensu* Dobrowski et al. 2015) given its greater ability to tolerate the shaded understories of densely forested areas (Bigelow et al. 2011). Related to this, we found that areas with high fire severity (high percent basal area mortality), but in close-proximity to seed trees had high post-fire ponderosa pine seedling abundances, likely due to fire-induced modifications of the seedbed and increased light availability on these sites (thus benefitting shade-intolerant ponderosa pine). Localized patches of high-severity fire may lead to abundant, aggregated establishment of ponderosa pine due to an adjacent seed source, the presence of a bare mineral seed bed, available light, and increased growing space (Sánchez Meador et al. 2009, Larson and Churchill 2012). Canopy cover, influencing seed availability and the understory environment, is one of the most important factors influencing recovery of seed-obligate conifers in post-fire environments.

3.4.2 Climate and Site Suitability as Constraints on Post-Fire Regeneration

Average climate (described by 30 year CWD and AET) was a strong predictor of post-fire abundance for both ponderosa pine and Douglas-fir. Consistent with the findings of other studies (e.g., Dodson and Root 2013, Chambers et al. 2016, Rother and Veblen 2016), we found that moisture-limited sites at low elevations and on southerly aspects typically had low conifer seedling abundances, even in areas adjacent to a seed source. Many previous studies have utilized individual climate variables such as precipitation and temperature or terrain variables such as aspect and elevation to analyze trends in post-fire conifer abundance. CWD and AET provide a more useful alternative because they effectively combine the influence of climate,

topography, and soils, and are functionally tied to the environmental conditions experienced by plants (Stephenson 1998, Dilts et al. 2015). While CWD provides an estimate of the intensity of drought stress because it estimates unmet atmospheric moisture demand, AET is an indicator of site productivity because high values are indicative of sites with high availability of moisture and energy (Dobrowski et al. 2015). When calculated at fine spatial resolutions that mirror the operational scales of post-fire recovery processes (as done in this study), AET and CWD are useful and complementary predictors of post-fire recovery in semi-arid landscapes and are helpful indicators of susceptibility to fire-driven conversions in vegetation.

Interestingly, three-year post-fire CWD and AET had little predictive power in our models of seedling abundance, yet post-fire climate has been noted as an influential driver of post-fire recovery in other studies (Harvey et al. 2016, Stevens-Rumann et al. 2018). During interdecadal periods of drought, such as the early 2000s in the western U.S., it is believed that post-fire climate may become a less important driver of recovery, because conditions become universally unfavorable for seedlings (Stevens-Rumann et al. 2018). Given that many of our fires occurred in the early-mid 2000s, this is one possible explanation for differences between our findings and those of previous studies in regards to average post-fire conditions. Another possible explanation for our results is the consideration of average conditions in the 3 years post-fire rather than individual extreme years. At an annual resolution, extreme drought years influence longer-term forest trajectories, likely by increasing seedling mortality (Young et al. 2019), while wetter years lead to increased conifer establishment (Rother and Veblen 2017, Davis et al. 2019). In our study, the 1995, 1998, 2007, 2010, and 2015 establishment pulses coincided with below-average drought stress during the growing season or with the positive phase of ENSO (which is associated with wet winters in the study area; Kurtzman and Scanlon

2007). Similar effects of interannual climatic variability are now well-documented in conifer forests throughout the Southern Rocky Mountains and Southwestern United States (Savage et al. 1996, League and Veblen 2006, Rother and Veblen 2017, Andrus et al. 2018, Davis et al. 2019). We also noted that establishment for ponderosa pine and Douglas-fir continued to occur for many years after fire occurrence. Taken together, these findings demonstrate that demographic models that tie interannual climate variability to specific components of the conifer reproductive cycle (e.g., Feddema et al. 2013, Savage et al. 2013, Petrie et al. 2017) may be more informative than 3-5 year post-fire climatic averages.

Additional factors that helped to predict post-fire seedling abundance included seedbed characteristics, biotic interactions, and pre-fire forest density. For example, our results indicated that grass cover and Gambel oak density both had negative relationships with ponderosa pine abundance at the plot-level. Bunch grasses (e.g., *Festuca arizonica*) may compete with ponderosa seedlings for soil moisture (Pearson 1942), potentially limiting seedling abundance (Flathers et al. 2016). In contrast to our findings, previous studies have noted that ponderosa pine may have weak (Owen et al. 2017) or even strong (Ziegler et al. 2017) positive spatial associations with resprouting angiosperm trees in post-fire environments. Gambel oak is believed to facilitate the establishment of another southwestern pine species (i.e., *Pinus edulis*; Floyd 1982) through microclimatic buffering and perhaps by attracting avian dispersers (such as corvids). Therefore, our finding of a negative relationship between Gambel oak density and ponderosa pine abundance may reflect the occupancy of different site types rather than competitive or inhibitory interactions between these species. We also noted that high pre-fire basal area and Douglas-fir post-fire seedling abundance were positively related to ponderosa seedling abundance, perhaps indicative of wetter sites with better growing conditions. Post-fire

seedling abundance is locally variable, likely reflecting variability in the seedbed, local vegetation, and growing conditions.

3.4.3 Landscape-Scale Variability in Resilience to Wildfire

Spatial variability in conifer abundance could be effectively predicted throughout each fire using statistical models developed from field data and broad-scale spatial datasets. Using these models, we determined that ponderosa pine and Douglas-fir regeneration was limited in large percentages (41.8% and 68.5%, respectively) of the total area burned throughout 15 recent wildfires in southern Colorado and northern New Mexico, USA. Importantly, there was also pronounced variability in post-fire recovery among fires, and individual fire events ranging widely in post-fire recovery (with both species ranging from 0-100% across fires), which makes broad generalizations about causal mechanisms difficult. Still, much of this limited regeneration could be attributed to post-fire canopy cover of mature conifers and variability in the physical environment (specifically 30-year average AET and CWD). Spatial models such as those developed in this study provide an effective means of scaling plot-level observations to spatially extensive post-fire landscapes (Tepley et al. 2017, Haffey et al. 2018, Shive et al. 2018), thus permitting broader inferences about susceptibility to post-fire vegetation type conversion.

Projections of future shifts from forest to non-forest vegetation types are inherently uncertain due to unknown future climatic variability as well as uncertainties about rates and specific drivers of vegetation change. Because our surveys were performed in relatively recent burn areas (1988-2010), it may be too early to suggest that transitions to non-forest vegetation types are permanent (Baker 2018). Still, the spatial variability in predicted abundances across our study area indicates that some site types (e.g., xeric sites and those in the interior of high-severity patches) are more vulnerable to vegetation type conversions than others. Forest response to

wildfire is often presented as a simplistic binary outcome of resilient versus non-resilient based on observations over periods of one to a few decades, yet a more nuanced approach to forest resilience considers rates of recovery, which can then create spatial gradients of "relative resilience" across the landscape (Tepley et al. 2017, 2018, Shive et al. 2018). Given the importance of canopy cover and 30-year average CWD in predicting abundances of both ponderosa pine and Douglas-fir, results from the current study imply that under continued warming and altered fire activity, some forested areas in the southwestern United States are likely to undergo fire-driven conversions to non-forested vegetation.

3.5 Adaptation and Management Implications

Continued climate warming will increase the vulnerability of many low-elevation forests to conversion to non-forest vegetation types (Parks et al. 2019), and this presents complex challenges to land managers. Adequately addressing these challenges requires consideration of societal values and forest ecosystem services, as well as the best possible technical understanding of the potential for success of a variety of possible management interventions. Potential management options include actions that attempt to forestall change through enhanced ecosystem resistance to fire effects, interventions aimed at improving post-fire resilience, and actions such as assisted migration aimed at facilitating transitions to ecosystems that are more compatible with a changing climate (Millar et al. 2007, Halofsky et al. 2014). All management interventions have considerable risk due to the uncertainties in predicting the rate and pattern of future climate change and the complexity of climate impacts on ecosystem dynamics. Therefore, a diverse range of approaches to adaptation and management should be considered (Millar et al. 2007, Baker 2018). Currently, reforestation is one of the most common management responses to large severe fires in the western United States (North et al. 2019), and the effectiveness of post-

fire planting can vary widely (e.g., 0-70% survival in fires throughout the Southwest; Ouzts et al. 2015); seedling survival may be particularly sensitive to moisture availability and hydraulic stress (Rother et al. 2015, Simeone et al. 2019). The potential for successful reforestation can benefit from the type of site-specific research on regeneration processes presented in the current study. If reforestation of recently-burned areas remains an important goal, planting should be prioritized for sites where available seed sources are too distant to be sufficient and seedling survival is likely to be highest, now and into the future (i.e., relatively cool/wet sites). Our results are also important in informing discussions among stakeholders of the likelihood of future changes in the extent of forest cover, the probable changes in forest ecosystem services, and the costs and benefits of a range of adaptation strategies.

3.6 Conclusion

The factors limiting forest recovery to wildfire vary by species and across gradients in fire severity and the physical environment. Because seed cone production was relatively widespread and frequent across our sites, the canopy cover of surviving mature conifers is a reliable proxy for seed availability and may be one of the most important factors driving post-fire recovery. Thirty-year averages of actual evapotranspiration and climatic water deficit were also strong predictors of post-fire conifer abundance in our study area. Statistical models using surviving canopy cover and water balance metrics indicated that the factors that most strongly predicted post-fire seedling abundance differed by species, but that in general abundances were highest on wetter sites and near surviving trees. Anthropogenic climate change has led to increases in wildfire area burned throughout much of the western U.S. (Abatzoglou and Williams 2016) and these trends are likely to continue (Liu et al. 2013, Kitzberger et al. 2017), highlighting the importance of understanding the patterns of ecosystem recovery following these

events. Post-fire recovery in dry forests should be considered holistically, through an improved understanding of the factors defining a species' regeneration niche and driving conifer seedling regeneration: seed cone production, seedling establishment, biotic interactions, spatial patterns of overstory trees, and spatial and temporal variation in moisture availability.

CHAPTER 4

A CHANGING CLIMATE IS SNUFFING OUT POST-FIRE FOREST RECOVERY IN THE SOUTHERN ROCKY MOUNTAINS

4.1 Introduction

The impacts of climate change on plants are pervasive and widespread. Climate warming is driving changes in species phenologies (Cleland et al. 2007), increases in mortality rates (van Mantgem et al. 2009), altered interspecific interactions (Tylianakis et al. 2008), and shifts in species distributions (Parmesan and Yohe 2003, Chen et al. 2011). Given the tremendous importance of plant life to Earth's ecosystems and to humans, a better understanding of these effects is needed to facilitate adaptation and mitigation planning. Species distribution models (SDMs) and demographic models are two commonly-used approaches that aid in understanding and projecting the influence of climate on plant species ranges. SDMs relate georeferenced observations of the presence or abundance of a species with potential biophysical predictors using a range of statistical learning methods (Guisan and Zimmermann 2000, Franklin 2010). Demographic models (e.g., Enright et al. 2015, Conlisk et al. 2017, Petrie et al. 2017) take an alternative approach, focusing instead on processes or life stages that may be differentially constrained by climate. Key limitations of the SDM approach include the poor incorporation of species dispersal in limiting future projections, the lack of direct ties to species physiology, and potential disequilibrium between existing species distributions and climate (Pearson and Dawson 2003). In contrast, demographic models can target important bottlenecks to population

persistence that are directly tied to physiological and reproductive processes, but they may be poorly parameterized during the modeling process due to a lack of available data. While SDMs and demographic models offer obvious benefits and drawbacks, both can be improved by targeting the most climatically-sensitive life stages and situations in which a species is most prone to local extinction.

Wildfire is the dominant terrestrial disturbance (Bowman et al. 2009) and represents a crucial indirect pathway by which climate can affect plant communities. Wildfire activity has increased throughout the western United States since the 1980s, and a large percentage of these increases has been attributed to the influence of anthropogenic climate change (Abatzoglou and Williams 2016). A warming climate also hinders post-fire forest recovery, and high-severity fires that are followed by warm, dry periods are less likely to recover to a pre-fire forested state (Harvey et al. 2016, Stevens-Rumann et al. 2018). In the absence of disturbance, many forested ecosystems have the potential for resilience to climate warming (*sensu* Holling 1973) through system inertia. Tree species are sensitive to the environmental conditions present during early stages of their life cycle (Grubb 1977), yet they are capable of tolerating a relatively wide range of conditions in mature life stages (Dobrowski et al. 2015), well-outside of their climatic optimum. Microclimatic buffering (Davis et al. 2018a) and localized species dominance (i.e., legacy effects) are two potential mechanisms by which species could persist in their current range and continue to establish under a warming climate. High-severity wildfire, in combination with a changing climate, "breaks the legacy lock" (*sensu* Johnstone et al. 2010) of the prior system state and can drive rapid shifts in local vegetation. The integration of fire activity and post-fire recovery into projections of future vegetation dynamics is therefore crucial to effectively predict changes in forested ecosystems throughout the western United States.

In this study, we identified species-specific responses to wildfire and climate variability in the climatically-sensitive seedling stage for two widely distributed conifers (Douglas-fir – *Pseudotsuga menziesii* var. *glauca*, and ponderosa pine – *Pinus ponderosa* var. *scopulorum*), and modeled spatiotemporal trends in post-fire establishment and abundance. We did this using two complementary and spatially-extensive datasets that span the Southern Rocky Mountains, USA. Specifically, we asked the following questions: *1) How do annual patterns of post-fire tree seedling establishment relate to interannual climate variability, and what biophysical factors are most strongly associated with post-fire seedling abundance in recent fires? 2) What proportion of the Southern Rocky Mountains Ecoregion has exceeded estimated climatic thresholds for seedling establishment in the recent (1981-2015) period and how might this change under a range of climate projections and emission scenarios? 3) What sites in the Southern Rocky Mountains are most susceptible to regeneration failure in the 21st century due to increases in drought stress?*

4.2 Methods

4.2.1 Study Area

This study focuses on the montane zone of the Southern Rocky Mountains Ecoregion (SRME; EPA Level III Ecoregion 21; Omernik and Griffith 2014). The SRME spans 144,462 km² of topographically-complex terrain in southern Wyoming, Colorado, and northern New Mexico, USA. Forested landscapes cover 56.3% of the SRME (Homer et al. 2015), and the montane zone makes up 77.3% of the forested area (Fig. 4.1). Here, we define the montane zone using 12 cover types in the 2014 LANDFIRE environmental site potential (ESP) dataset (Rollins 2009; Table C1). ESP represents neither the current or historical vegetation type, but rather the potential vegetation that could be supported on a site given the current biophysical environment.

This provides a useful means of identifying the montane zone through time because the area does not change throughout the historical period of analysis and provides a consistent baseline of comparison for future changes. Climate in the montane zone of the SRME is widely variable. Average annual precipitation ranges 236 to 1562 mm, January minimum temperature ranges -20.3 to -5.4 C, and June maximum temperature ranges 13.85 to 30.5 C (PRISM 2018). Dominant tree species in the montane zone include ponderosa pine, Douglas-fir, white fir (*Abies concolor* var. *concolor*), lodgepole pine (*Pinus contorta* var. *latifolia*), quaking aspen (*Populus tremuloides*), Gambel oak (*Quercus gambelii*), and blue spruce (*Picea pungens*). The montane zone also include other species in the genera *Abies*, *Juniperus*, *Picea*, *Pinus*, and *Populus* that vary in importance throughout the region.

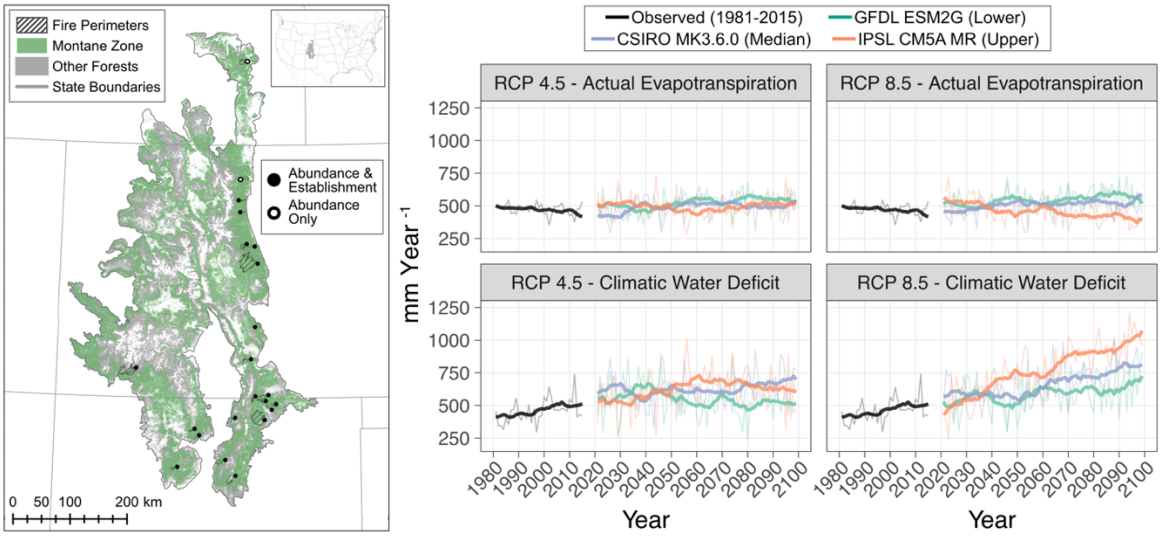

Fig. 4.1. Site map showing the locations of the 22 surveyed fires, as well as a summary of past climate and future climate scenarios in the Southern Rocky Mountains Ecoregion. In the site map, montane forests are shown in green, while other forests are shown in grey. Non-forest vegetation and other land cover types within the region are shown in white. Solid circles identify fires in which post-fire seedling abundance and seedling establishment data were collected, while open circles identify fires with only post-fire abundance surveys. Line graphs show observed (1981-2015) and projected future (2021-2099) trends in annual actual evapotranspiration (AET; evaporation constrained by moisture availability) and climatic water deficit (CWD; unmet evaporative demand) across the region. Transparent lines give annual values, while solid lines give 10-year running means. Future trends are based on three coupled atmosphere-ocean general circulation models (GCMs) and two representative concentration pathways (RCPs) spanning a range of potential 21st-century trajectories.

4.2.2 Field Data

We combined data from five prior studies that described annual patterns of conifer seedling (i.e., all juvenile trees originating following fire) establishment or post-fire seedling abundance (Ouzts et al. 2015, Chambers et al. 2016, Rother and Veblen 2016, 2017, Rodman et al. *In Review*) to develop a regionally extensive database of post-fire recovery in the montane zone of the SRME. Specifically, we focused on two widespread conifers (i.e., Douglas-fir and ponderosa pine) that vary in shade-, drought-, and fire-tolerance (Burns and Honkala 1990). In total, this dataset is comprised of 723 destructively-sampled seedlings (Douglas-fir n = 98; ponderosa pine n = 625) spanning sites in 20 fires, and 1301 field plots used to survey post-fire abundance in 22 fires (Fig. 4.1, Fig. C1, Table C2). Destructively-sampled seedlings were dated at an annual resolution following the protocol described by Telewski (1993) and Rother and Veblen (2017). Field surveys of post-fire conifer abundance differed slightly among studies, but similar data were collected in each of the 1301 field plots. Specifically, each study recorded georeferenced observations of post-fire abundance by species and field-derived distance to nearest seed tree. When not recorded in the field, distance to seed source was quantified using aerial photo interpretation (n = 48; e.g. Rodman et al. *In Review*).

4.2.3 Spatial Data

We acquired or developed spatial datasets describing topography/terrain, soils, fire severity, and climate to be used as predictors in statistical models (Appendix C). We calculated topographic position index (TPI; Weiss 2001) and heat load index (HLI; McCune and Keon 2002) using 1 arc-second (c. 30 m) digital elevation models from the National Elevation Dataset. We also acquired data describing soil texture (percent clay content), soil pH, and available water capacity from POLARIS (Chaney et al. 2016). Finally, we acquired satellite-derived data

describing fire severity (the relative differenced Normalized Burn Ratio) for each fire from the Monitoring Trends in Burn Severity program (Eidenshink et al. 2007). Following acquisition or calculation, all topographic, soils, and fire severity data were projected to UTM Zone 13N, resampled to a 60 m resolution (to permit comparisons with field data), and aligned to the same grid.

We obtained gridded climate data from GridMET (Abatzoglou 2013) and MACA (Abatzoglou and Brown 2012) for each year of the historical (1981-2015) and future climate periods (2006-2099) (Appendix C). Future projections were derived from 19 coupled atmosphere-ocean general circulation models (GCMs) from the fifth Coupled Model Intercomparison Project (CMIP5) that had been bias-corrected and downscaled to 2.5 arc-minute resolution using GridMET (c. 4 km; Abatzoglou and Brown 2012). We used two different RCPs (representative concentration pathways) for each GCM. RCPs estimate changes in radiative forcing (Δ W/m^2) at the tropopause from 1750-2100. RCP 4.5 assumes moderate increases in emissions through 2040, followed by declines. RCP 8.5 assumes substantial increases in emissions through 2100 (Riahi et al. 2011).

We developed annual layers of three climate variables from GridMET and MACA data. These were AET (actual evapotranspiration), annual CWD (climatic water deficit), and total precipitation during the April-September growing season. AET is an indicator of site productivity because it identifies areas with the simultaneous availability of energy and moisture, key limitations to plant growth; CWD is the difference between potential and actual evapotranspiration and is an indicator of drought stress experienced by plants (Stephenson 1998, Lutz et al. 2010). Growing season precipitation may be beneficial to seedling establishment across a broad elevational range in the SRME (Rother and Veblen 2017, Andrus et al. 2018).

After the initial development of these layers at a 4 km resolution, we selected three GCMs that span the range of projected changes in CWD over the 2006-2099 period (Appendix C). Following this, we statistically downscaled historical climate variables and future projections (i.e., three GCMs with two RCPs) to a spatial resolution of 250 m using gradient and inverse distance squared (GIDS) interpolation (Nalder and Wein 1998, Flint and Flint 2012). The development and statistical downscaling of gridded climate data are further described in Appendix C. As an exploratory analysis, we analyzed trends in historical and future AET and CWD across the SRME using Mann-Kendall trend tests with the variance correction approach of Hamed and Rao (1998) to address serial autocorrelation in each time series.

4.2.4 Statistical Analysis – Annual Seedling Establishment

To quantify the importance of interannual climate variability in the establishment of ponderosa pine and Douglas-fir, we used annual establishment dates from the 723 destructively-sampled seedlings spanning 20 fires. First, we aggregated counts of establishing seedlings (by year and by species) to the level of individual fires because of differences between the plot designs of Rodman et al. (*In Review*) and Rother and Veblen (2017). As potential predictors of annual seedling establishment, we extracted CWD, AET, and precipitation during the April-September growing season in each year (1981-2015) in each fire perimeter. Following this, we scaled and centered these values on zero in each fire (using z-score transformation) based on historical baseline period of 1981-2015, thus identifying relative differences between the climate of each year in each fire and the historical average. Lastly, we created a variable of "time since fire", representing the number of years between fire occurrence and seedling establishment.

We modeled counts of establishing seedlings in each year in each fire we using boosted regression trees (BRTs) with a Poisson loss function. In addition to annual climate variables and

time since fire, we also included "fire ID" as a categorical term in the model to account for differences in sample design and number of total samples in each fire site. We used the "gbm.step" function in the "dismo" package (Hijmans et al. 2017) in R (R-Core-Team 2018) to select the optimal number of trees in each BRT model. We used a learning rate of 0.001, a step size of 5 for each species, and a complexity parameter of 2 (allowing for two-way variable interactions; Elith et al. 2008). The final number of trees in each model was 545 for ponderosa pine and 825 for Douglas-fir. We assessed the accuracy of BRTs by comparing observed and predicted abundances, both for the entire dataset and with 10-fold cross-validation.

4.2.5 Statistical Analysis – Post-Fire Abundance Surveys

We also developed statistical models to predict post-fire conifer seedling abundances for each species using 1301 field plots throughout the 22 fires. For this, we used both generalized linear mixed models (GLMMs; Bolker et al. 2009) and BRTs. GLMMs were developed using the "glmmTMB" package (Brooks et al. 2017) in R (R-Core-Team 2018). We used zero-inflated models with a generalized Poisson error structure and random intercepts by fire. We used seedling count in each field plot as the response variable with an offset term for "log(plot area)" to account for differences in sampling areas. We then selected variables for the final GLMMs using a spatially stratified cross-validation, in which models were fit using data from 21/22 fires and the remaining fire was withheld as a test set (i.e., 22 folds). Variables were selected for inclusion in the final GLMMs if they improved cross-validated accuracy and also predicted ecologically-realistic relationships that matched prior understanding in the published literature. For BRTs, we used a modified version of the "gbm.simplify" function in the "dismo" package (Hijmans et al. 2017) in R (R-Core-Team 2018) to automatically select the subset of variables that led to the greatest predictive accuracy using the same spatially stratified cross-validation

approach applied to GLMMs. For the assessment of accuracy and variable selection in cross-validation, we used square root transformations of both predicted and observed seedling densities to minimize the influence of extreme outliers. GLMMs outperformed BRTs and ensemble models for the prediction of post-fire abundance (Table C7). Therefore, we present only the results of GLMMs for post-fire abundance models.

4.2.6 Historical Reconstruction and Future Projection Using Annual Establishment Models

Because BRTs of annual establishment data identified non-linear thresholds for the establishment of each species, we built a simple GIS model to identify 250 m grid cells in each year of the historical period, as well as each year in future GCMs, that exceeded establishment thresholds for AET, CWD, and growing season precipitation. For this GIS model, we developed maps of establishment suitability for each year in the historical period (1981-2015), and each future year (2021-2099) in each GCM and RCP combination. For each map, we identified areas with climatic conditions suitable for establishment as 250 m grid cells in the montane zone of the SRME with 1) above-average growing season precipitation, 2) above-average AET, and 3) below-average CWD relative to 1981-2015 historical averages in each cell. We summarized establishment suitability across the region in each year as the percent surface area of the montane zone in the SRME exceeding each of the three climatic thresholds. Thus, high values in a given year indicate climatic conditions beneficial to seedling establishment for each species across much of the montane zone, while low values indicate the opposite. We then analyzed temporal trends in model projections for the 1981-2015 historical period and 2021-2099 GCMs using Mann-Kendall trend tests with variance correction.

4.2.7 Historical Reconstruction and Future Projection Using Post-Fire Abundance Models

We used fitted GLMMs to make projections for post-fire ponderosa pine and Douglas-fir seedling abundance at a 60 m resolution across the montane zone for each historical year (1981-2010) and for each future GCM and RCP combination (2021-2080). We restricted this analysis to these years to allow for three 30-year periods (i.e., 1981-2010, 2021-2050, 2051-2080) that could be directly compared. Terrain variables used in statistical models were held constant across years in projections. Minimum distance to seed tree was set at a constant value of 10 m in all 60 m cells in each year to focus the analysis on the limitations of the biophysical environment while assuming the availability of a nearby seed source. Similarly, we assumed that models were predicting seedling density for each species five years following fire. In the historical period (1981-2010), 30-year average climate variables were based on cell-specific averages in the 1981-2010 period, and thus average climate did not vary by year during the historical period. For future scenarios, we used a 30-year moving average (centered around the focal year) of each climate variable in each cell in each year. Maximum post-fire CWD was the highest z-score value (based on cell-specific historical values) of CWD in the five years following the focal year.

We assessed the adequacy of post-fire seedling abundance in each year using minimum historical tree density thresholds of 20 ponderosa pine ha^{-1}, and 5 Douglas-fir ha^{-1}. To develop these thresholds, we compiled data from three published studies that reconstructed 1800s forest density and species composition in the Southern Rocky Mountains Ecoregion (Fulé et al. 2009, Rodman et al. 2017, Battaglia et al. 2018). We then used the 5^{th} percentile of species-specific 1800s densities for plots that had ponderosa pine or Douglas-fir presence, respectively. Using these low historical densities assesses whether post-fire seedling densities could be expected to reach the lowest extent of what would be considered a montane forest in this region. See Appendix C for a further discussion of density thresholds. Using these thresholds, we then

quantified the number of years in each 30-year period (1981-2010, 2021-2050, 2051-2080) in which a 60 m cell was projected to have seedling densities exceeding these historical tree density thresholds. In future projections, this was done for each GCM, and values in each 60 m cell were taken as the mean value across GCMs, within a given RCP.

4.3 Results

4.3.1 Historical Trends and Projected Future Changes in AET and CWD

In the 1981-2015 historical period, annual CWD increased (Kendall's correlation τ = 0.30, $p < 0.01$) and annual AET showed slight declines (τ = -0.14, $p = 0.24$) across the SRME (Fig. 4.1). Future climate scenarios exhibited similar trends through time. Of the 19 GCMs initially studied, 18 predict 21st-century increases in annual CWD in RCP 4.5, and all predict increases in annual CWD in RCP 8.5 (Table C4). Future trends in annual AET were more muted (Table C3), likely because AET is predicted to increase at upper elevations and decrease at lower elevations, which is not captured when analyzing regional averages. Still, 17 of 19 GCMs predicted moderate increases in annual AET in both RCP 4.5 and 8.5. The selected CMIP5 GCMs that were used for further analysis were GFDL ESM2G (Dunne et al. 2012; hereafter "GFDL"), CSIRO MK3.6.0 (Jeffrey et al. 2013; hereafter "CSIRO"), and IPSL CM5A MR (Dufresne et al. 2013; hereafter "IPSL"). These GCMs span the range of 21st century climate projections in the region (Table C3, Table C4). From 2021-2099, GFDL and CSIRO predict increases in AET in both RCP 4.5 and 8.5. IPSL predicts no trends in AET in RCP 4.5 and predicts declines in AET in RCP 8.5. CWD is predicted to increase in all GCMs and RCPs, with the exception of GFDL in RCP 4.5 which predicts slight declines in CWD over the 2021-2099 period (Fig. 4.1; Table C5).

4.3.2 Annual Climatic Drivers of Post-Fire Seedling Establishment

Based on our analysis of annual establishment dates and interannual climate variability, we found that the relationship between climate and establishment was remarkably consistent between species (Fig. 4.2). Years with below-average CWD, above-average AET, and above-average precipitation during the April-September growing season were associated with increases in Douglas-fir and ponderosa pine seedling establishment. Annual CWD and AET were the most influential variables for each species, having higher variable importance than any other predictors in each boosted regression tree models. Unsurprisingly, BRT models performed better on training data than on independent test data, but observed and predicted values were still positively correlated in cross-validation. For the ponderosa pine model, the correlation of observed to predicted values with the training data was 0.60 and the cross-validated correlation was 0.18. For the Douglas-fir model, the correlation with the training data was 0.57 and the cross-validated correlation was 0.23.

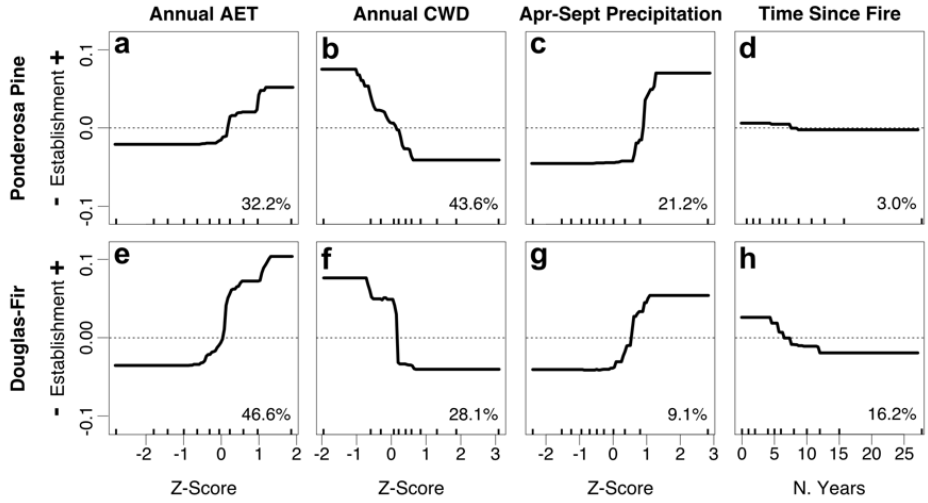

Fig. 4.2. The influence of interannual climate variability on post-fire establishment for Douglas-fir and ponderosa pine, two dominant coniferous species in the montane zone of the Southern Rockies. Derived from boosted regression tree analyses, each subfigure shows the marginal influence of a given predictor (y-axis) across the range of values observed in the data (x-axis). X-axis values at which a solid line is above zero (i.e., dotted lines) indicate a positive relationship between that variable and counts of establishing seedlings, while values at which the solid line is below zero indicate a negative relationship. Percentages in each subpanel give the relative importance of each variable for each species after excluding site-level effects. Tick marks at the bottom of each subfigure give decile values showing the ranges of observed data.

4.3.3 Factors Predicting Post-Fire Tree Seedling Abundance

For each species, wetter sites and those closest to seed trees had higher post-fire tree seedling abundances (Fig. 4.3). Thirty-year average CWD was an influential predictor of both ponderosa pine and Douglas-fir abundances, and lower values of 30-year CWD (common on higher, wetter sites) were associated with higher post-fire abundances (Fig. 4.3b, 4.3g). Abundances for each species were also higher when fires were not followed by an extreme drought year (low values of maximum post-fire CWD; Fig. 4.3c, 4.3h). Max post-fire CWD led to improved predictive accuracy of GLMMs when compared to individual wet years or 5-year averages (not shown). Terrain variables were also important for each species. Heat load was predictive of Douglas-fir abundance, where abundance was higher on northeasterly aspects with lower heat loads (Fig. 4.3i). Similarly, valley bottoms (low values of topographic position in a 15 x 15 cell neighborhood) had higher abundances of Douglas-fir (Fig. 4.3j). We also identified an interaction between precipitation and topographic position for ponderosa pine, where valley bottoms had higher seedling abundances on sites with lower average growing season precipitation, and ridgetops had higher abundances on sites with average growing season precipitation exceeding 450 mm (Fig. 4.3e). GLMMs for ponderosa pine had a correlation of 0.46 between observed and predicted values in the training data and 0.22 in spatially stratified cross-validation. The Douglas-fir model performed slightly better. GLMMs for Douglas-fir and had a correlation of 0.61 between observed and predicted values in the training data and 0.25 in cross-validation.

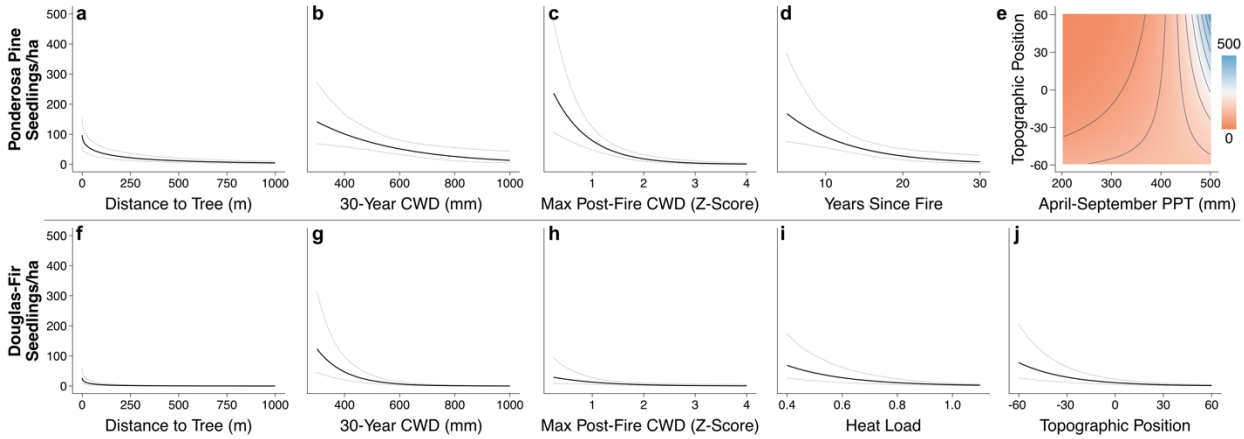

Fig. 4.3. Predicted values of post-fire abundance for Douglas-fir and ponderosa pine based on generalized linear mixed models of 1301 field plots in 22 wildfires in the Southern Rocky Mountains Ecoregion. Black lines give predicted abundances for each value of a predictor when assuming the mean value of random effects and of other predictors. Dotted lines give 95% prediction intervals surrounding each predicted value. The colored contour plot (e) shows the interaction between topographic position and precipitation for ponderosa pine, where the effect of topographic position is dependent upon average precipitation; the colored scale indicates seedlings/ha.

4.3.4 Past and Future Trends in Annual Suitability for Conifer Seedling Establishment

The percent surface area of the montane zone considered suitable for establishment (i.e., exceeding annual establishment thresholds for AET, CWD, and April-September precipitation) varied through time. Historically, the early 1980s, 1998, and 2014-2015 were the years in which climatic conditions were most suitable to widespread establishment throughout the region, while 2000-2003 had no areas that exceeded these thresholds in the montane zone. Much of the 2000s had low values, with slight increases from 2005-2008 (Fig. 4.4). Despite recent increases in 2014 and 2015, there were overall declines in establishment suitability over the 1981-2015 period (τ = -0.29, p = 0.062). Future trends in annual establishment suitability varied by GCM and emissions scenario. In RCP 4.5, the moderate emissions scenario, one of the three GCMs predicted 2021-2099 declines in annual establishment suitability (IPSL: τ = -0.14, p = 0.055), while two of the three predicted levels generally consistent with the 1981-2015 historical average (GFDL: τ = 0.09, p = 0.215; CSIRO: τ = -0.02, p = 0.762). In RCP 8.5, one GCM predicted little change in

the area of the montane zone with suitable climate (GFDL: τ = -0.08, p = 0.217), while the other two predicted substantial declines (CSIRO: τ = -0.23, p = 0.023; IPSL: τ = -0.36, p = 0.016). Notably, in RCP 8.5, the number of years with any area considered suitable for establishment declines drastically after 2040 in IPSL and 2075 in CSIRO.

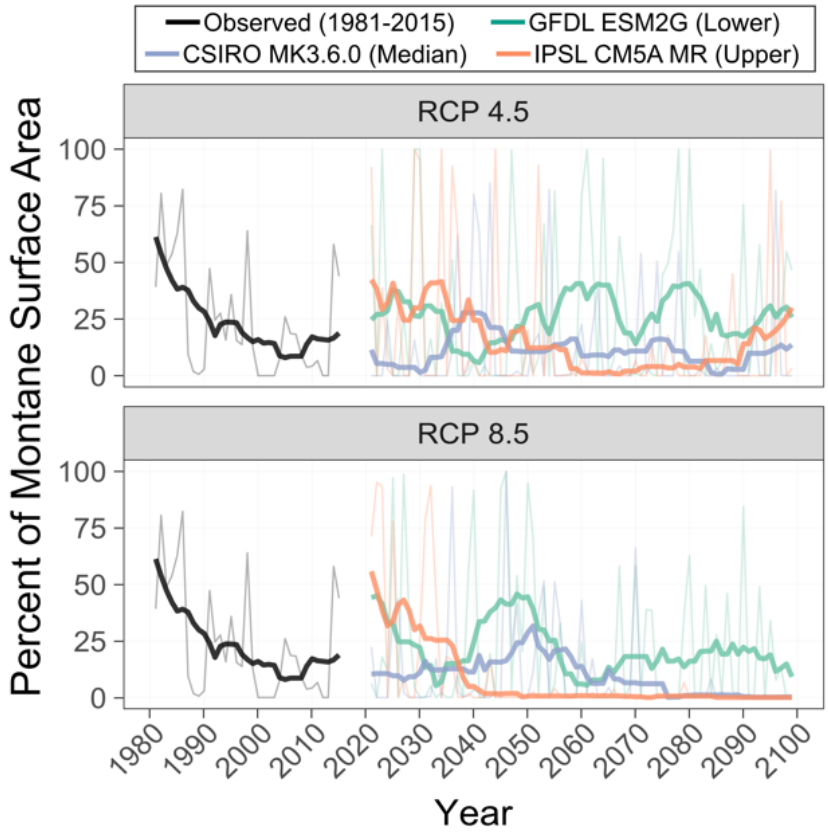

Fig. 4.4. The percent surface area of the montane zone in the Southern Rocky Mountains Ecoregion with above-average actual evapotranspiration, below-average climatic water deficit, and above average precipitation in the April-September growing season in each year. These annual climatic establishment thresholds were identified in boosted regression tree analyses. Observed values (1981-2015) are derived from GridMET. Future trends (2021-2099) are based on three coupled atmosphere-ocean general circulation models (GCMs) and two representative concentration pathways (RCPs) initiated in 2006 and spanning a range of potential trajectories. Transparent lines give annual values, while solid lines give 10-year running means to show trends through time.

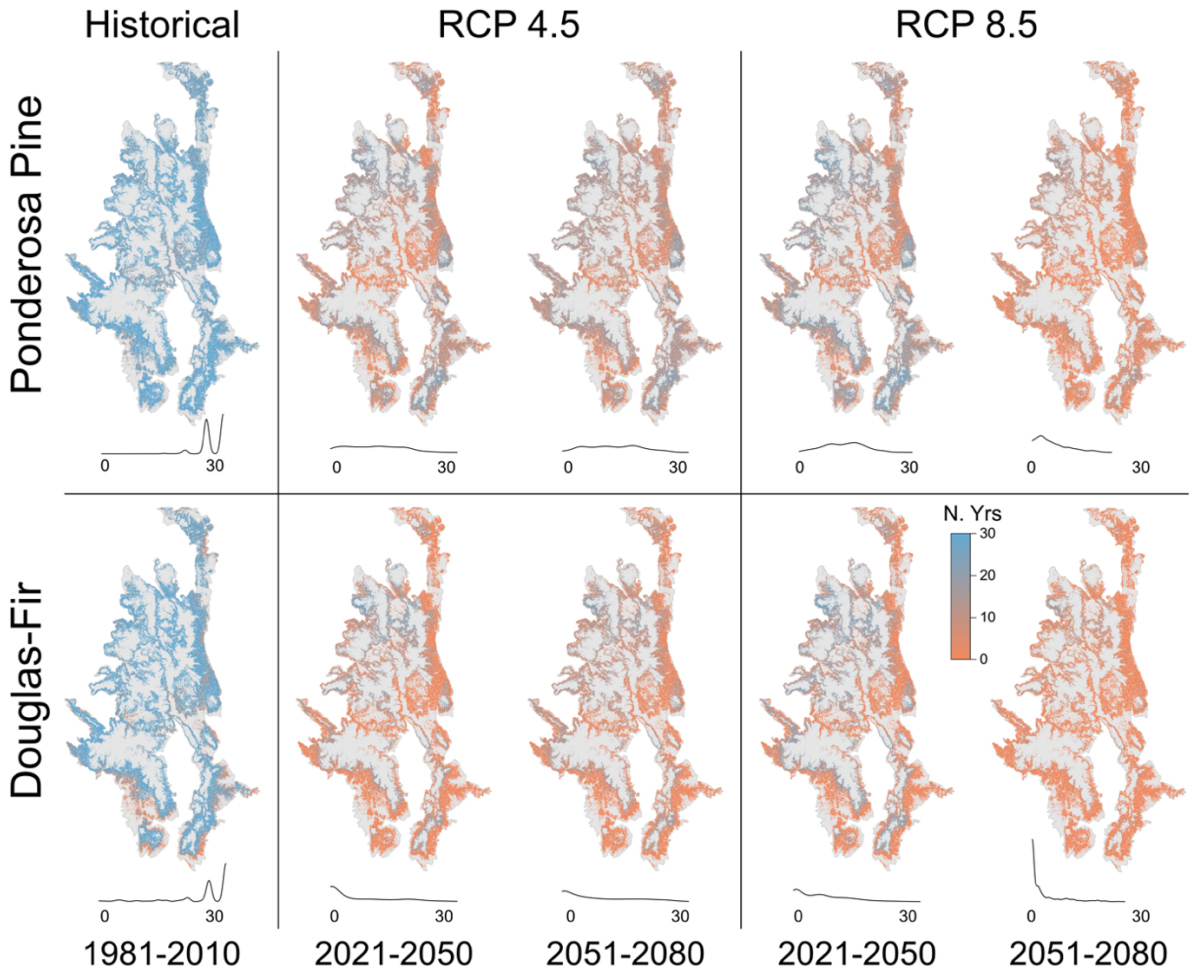

Fig. 4.5. Summary of spatial models predicting post-fire tree seedling abundance across the montane zone of the Southern Rocky Mountains Ecoregion in 1981-2010 (historical), and 2021-2080 (potential climate scenarios from three coupled atmosphere-ocean general circulation models [GCMs] and two representative concentration pathways [RCPs 4.5 and 8.5]). We used generalized linear mixed models to predict post-fire abundance across the region at a 60 m resolution in each year 1981-2010 (i.e., historical) based on average climate, interannual climate variability, and topography. We also projected seedling abundances in each year from 2021-2080. Map colors and density plots (below each map) show the number of years in which each 60 m cell was predicted to exceed historical density thresholds (20 ponderosa pine/ha and 5 Douglas-fir/ha) in each 30-year time period.

4.3.5 Spatiotemporal Models of Susceptibility to Regeneration Failure in the 21st Century

We projected broad declines in post-fire seedling abundances for Douglas-fir and ponderosa pine across the SRME from 2021-2080. While the majority of the montane zone was predicted to have seedling abundances exceeding historical density thresholds of 20 ponderosa pine ha^{-1} and 5 Douglas-fir ha^{-1} in theoretical fires occurring in each year of the 1981-2010

period, the number of years in which most 60 m cells were projected to exceed these thresholds was lower under the three GCMs. Future projections of post-fire seedling abundance indicate that there would be declines in the early portion of the 21st century (2021-2050) under RCP 4.5, but these declines would generally stabilize in the 2051-2080 period. In contrast, GCMs using RCP 8.5 (the high emissions scenario) showed continued and drastic declines in predicted post-fire abundances throughout the 21st century (Fig. 4.5). Under RCP 8.5, sites at the highest elevations in the montane zone are the only areas predicted to have post-fire recovery that consistently exceeds historical density thresholds. Increases in 30-year average CWD and max post-fire CWD were the primary reasons for these projected changes in the future.

4.4 Discussion and Conclusion

Increasing wildfire activity, in combination with poor post-fire recovery, has the potential to drive widespread conversions from forested to non-forested vegetation types across the western United States. To assess spatial and temporal variation in post-fire recovery, we used demographic models of post-fire tree seedling establishment and correlative SDMs of post-fire seedling abundance for two widely-distributed conifers in the Southern Rocky Mountains Ecoregion (SRME). Both sets of models were developed using extensive field datasets and high-resolution climate surfaces. Using these methods, we confirmed the expectations that 1) forest resilience to wildfire has experienced climate-driven declines in the Southern Rocky Mountains Ecoregion (SRME) over the 1981-2015 period, and 2) further declines in resilience across the SRME are likely, with some sites being more susceptible to declines in resilience than others.

We found that ponderosa pine and Douglas-fir seedling establishment was greater in years with above-average AET, below-average CWD, and above-average precipitation during the April-September growing season. Years most beneficial to the establishment of each species

were those in which moisture and energy were widely available and drought stress was minimal. These types of climate conditions became increasingly infrequent throughout the 1981-2015 period. Because seedlings are sensitive to climate conditions early in life, the seedling stage is a crucial bottleneck to population persistence (Grubb 1977, Dobrowski et al. 2015). Our findings align with those of the few studies that have related annual patterns of conifer seedling establishment to interannual climate variability in the western U.S. (Savage et al. 1996, League and Veblen 2006, Rother and Veblen 2017, Andrus et al. 2018, Davis et al. 2019, Rodman et al. *In Review*). Infrequent years with climate conditions conducive to seedling germination and survival may have critical implications for subsequent forest trajectories (Davis et al. 2016). In this sense, stage-structured demographic models that predict seedling establishment and survival based on interannual climate variability (e.g., Feddema et al. 2013, Petrie et al. 2017) are a useful approach to assessing forest sensitivity to a warming climate. These models can be further improved with the incorporation of site-specific empirical data as was done in the present study.

Correlative models developed using an SDM approach provided additional insight into the factors that influence spatial and temporal variability in post-fire seedling abundance. We found that distance to seed source, average climate (i.e., 30-year average CWD and 30-year average precipitation), individual drought years (i.e., max post-fire CWD), aspect-driven heat load, and topographic position all influenced landscape-scale variability in post-fire abundance. These findings are in agreement with the results of prior studies in the western U.S. that illustrate the importance of seed availability (Haire and McGarigal 2010), average climate (Tepley et al. 2017), post-fire climate (Harvey et al. 2016, Stevens-Rumann et al. 2018), and terrain (Welch et al. 2016) to the post-fire recovery of conifer forests. The overlaid patterns of each these biotic

and abiotic factors create complex responses to wildfire across heterogeneous landscapes, throughout which recovery differs substantially in abundance and rate.

Across a range of GCMs and emissions scenarios, we projected that further declines in establishment suitability and post-fire abundance are likely across the SRME. Considering the importance of altered recovery trajectories in a warmer and increasingly fire-prone future, it is surprising that a relative paucity of prior research has projected trends in post-fire recovery of conifer forests based on future climate scenarios (e.g., Feddema et al. 2013, Tepley et al. 2017, Kemp et al. 2019). It has been suggested that warming is likely to lead to overall declines in post-fire conifer seedling establishment and abundance, but that increasing temperatures could benefit regeneration at some sites, particularly those near the cold end of the species range (Feddema et al. 2013, Petrie et al. 2017, Kemp et al. 2019). Still, other research has indicated near-universal declines in future post-fire seedling abundances due to increasing CWD (Tepley et al. 2017). While there is potential that fire and a warming climate may facilitate range shifts at the leading edge of a species' distribution, the combined effects of pre-fire species dominance and extreme drought events may constrain the potential for range shifts (Young et al. 2019). Our study indicated that increases in average CWD and post-fire drought stress (i.e., max post-fire CWD) were likely to drive future declines in establishment and abundance across much of the region. Importantly, shifts in average climate are likely to drive increases in the frequency of years that are considered extreme relative to the historical record in a given area (McCullough et al. 2016). This has critical implications for the establishment of tree species that are sensitive to interannual climate variability (F. Davis et al. 2016, Andrus et al. 2018, K. Davis et al. 2019).

Future climate velocity is likely to exceed the dispersal capabilities and capacities for genetic adaptation of many plant species (Quintero and Wiens 2013, Batllori et al. 2017).

Therefore, we primarily focused on questions of resilience and *in-situ* population persistence following wildfire, and made no assumptions about dispersal into new habitat in higher-elevation areas or about species' ability to adapt to rapid environmental change. Species that are most likely to successfully migrate to newly suitable sites are those with light, wind-borne seeds capable of travelling broad distances (Normand et al. 2011), and both ponderosa pine and Douglas-fir have relatively heavy seeds that are unlikely to disperse across broad distances based solely on wind or water (McCaughey et al. 1986). Both species are also relatively long-lived, and rates of genetic adaptation are relatively slow for long-lived plant species. However, localized genetic differences already present in a population (Beckman and Mitton 1984, Jump and Peñuelas 2005) as well as phenotypic plasticity (Nicotra et al. 2010), may foster resistance and resilience to drought. Likewise, avian- and mammal-mediated dispersal (Vander Wall 2008) offer hope for the migration of ponderosa pine and Douglas-fir into newly suitable sites.

One additional factor that was not considered in this study but is relevant to the question of post-fire resilience, is the influence of climate warming on area burned, fire size, and fire severity. While warm, dry years are strongly tied to area burned in the western U.S. (Littell et al. 2009, 2016), the influence of warming on fire severity is less clear (Abatzoglou et al. 2017). In addition to the influences of fire weather, severity is also driven by a complex combination of fuels characteristics and topography (Holden et al. 2009, Dillon et al. 2011, Krawchuk et al. 2016). Still, some studies have documented increases in fire severity in recent years (Miller et al. 2009b, Singleton et al. 2018). Severity is a crucial parameter that influences post-fire seedling abundance by influencing the availability of seed sources for dispersal into recently burned areas. Full canopy removal would also lead to increased daytime temperatures and greater diurnal fluctuations (Davis et al. 2018a), likely contributing to increases in seedling mortality. In our

analyses, we attempted to isolate the influence of climate on post-fire recovery by assuming that a nearby seed source was available in any given fire event. If climate warming increases fire size and severity, in addition to reducing climatic suitability for establishment, dramatic declines in post-fire resilience are likely in many coniferous forests (Savage et al. 2013, Parks et al. 2019).

One of our most striking findings was the difference in future projections of post-fire recovery between RCP 4.5 and RCP 8.5. While RCP 4.5 assumes moderate growth in emissions through 2040, followed by declines, RCP 8.5 assumes rapid increases in emissions that continue through 2100 (Riahi et al. 2011). Models of annual establishment suitability and post-fire seedling abundance indicated similar trends in RCP 4.5 and 8.5 through mid-century, but showed strong divergence beyond that point. These findings echo those of two prior studies that demonstrate the importance of emissions scenario to projected effects on regeneration processes and on post-fire abundances (Petrie et al. 2017, Tepley et al. 2017). While committed warming is likely to lead to increases in wildfire activity and declines in post-fire resilience throughout the Southern Rocky Mountains, there may be the potential to mitigate the most extreme climate impacts through emissions reductions in the next two decades. The magnitude of ecological and societal impacts of a changing climate is dependent upon future emissions trajectories (IPCC 2014, USGCRP 2017).

CHAPTER 5

SUMMARY AND CONCLUSIONS

5.1 Changes in Forest Extent and the Important Role of Wildfire

The distribution of forested ecosystems is influenced by historical dynamics as well as contemporary processes. The goals of this dissertation were to assess the extent to which forests have changed throughout the 20th century due to human land use and wildfire activity, to quantify the factors limiting post-fire conifer forest recovery in recently-burned areas, and to project future trends in post-fire recovery throughout the region. To accomplish these goals, we combined geospatial approaches, tree-ring analyses, field ecology, and statistical modeling in study areas spanning the Southern Rocky Mountains Ecoregion in southern Wyoming, Colorado, and northern New Mexico.

To quantify forest cover change across of forests in the northern Front Range of Colorado (NFR), we used supervised classifications of 1938 and 2015 aerial imagery across a landscape with a complex history of disturbance and human land use (Chapter 2; Rodman et al. 2019). There are many approaches to reconstructing historical forest change, including tree-ring methods (Fulé et al. 1997, Battaglia et al. 2018), historical forest inventories (Moore et al. 2004), repeat photographs (Veblen and Lorenz 1991), and general land office surveys (Williams and Baker 2012b). While our approach using historical air photos is more temporally-limited than some other methods, it offers the advantages of high spatial resolution (c. 1 m) and seamless spatial coverage across broad areas. Using these data, we found that slow recovery from 19th

century fires was a key driver of observed increases in forest cover at upper elevations, and the exclusion of formerly frequent fire was a contributor to increases in forest cover at lower elevations. Historical logging and mining activity also appeared to play an important role in observed changes. Recent fire activity was the largest single driver of forest loss. Our findings can contribute to discussions surrounding local land management issues because forest restoration and fire mitigation based on historical conditions are common goals in the NFR (Dickinson et al. 2014, Addington et al. 2018), and an understanding of historical changes and causative mechanisms of change helps to inform these management activities (Veblen et al. 2012). In addition, this research contributes to the broader ecological literature through novel methods of image processing, uncertainty analysis, change-detection, and by combining remotely sensed data with extensive fire history records. This research also provides an example workflow that may be repeated in other regions in which historical aerial photography collections are available.

For conifer seedlings to establish following fire, seed must be produced and transported to a suitable site for germination and longer-term survival. These characteristics of the post-fire environment – seed availability and site suitability – vary across both space and time. While the factors limiting conifer regeneration in recent wildfires throughout the western U.S. are widely discussed in the literature, few studies have empirically assessed each of these drivers in a single area to identify key bottlenecks to post-fire recovery. Throughout 15 wildfires in southern Colorado and northern New Mexico, USA, we performed field surveys of post-fire seedling abundance and recent seed cone production, and used tree-ring methods to quantify temporal variation in seedling establishment, and resprouting. We then used classification of 1 m aerial imagery, downscaled climate surfaces, and monthly water balance models, to quantify spatial

variability in post-fire canopy cover and site suitability. We found that temporal variation in seed cone production was not a key bottleneck to post-fire recovery, but that seedling germination and establishment were more likely in wet years. In addition, post-fire seedling abundances were highest on mesic sites and adjacent to surviving trees, though they were relatively low across a substantial proportion of the total fire area. This study is the first of its kind to use site-specific data to assess the potential limitation of seed cone production on post-fire forest recovery. In addition, this is one of just a small number of studies in the western U.S. that have dated tree establishment at an annual resolution (e.g., Savage et al. 1996, League and Veblen 2006, Rother and Veblen 2017, Andrus et al. 2018, Davis et al. 2019), which is key when assessing the effects of interannual climate variability on forest recovery to disturbance.

It is now recognized that a warming climate is inhibiting post-fire recovery across conifer forests in the western U.S. (e.g., Stevens-Rumann et al. 2018, Davis et al. 2019). To address these ideas in pine-oak, ponderosa pine, and mixed-conifer forests in the Southern Rocky Mountains, we combined field data collected in five prior studies (Ouzts et al. 2015, Chambers et al. 2016, Rother and Veblen 2016, 2017, Rodman et al. *In Review*) and used these data to develop two sets of statistical models. For these models, we incorporated terrain variables, average climate, and interannual climate variability (i.e., annual AET, CWD, growing season precipitation, and post-fire drought) throughout the region to predict post-fire seedling establishment and abundance. Key in this process was the development of high-resolution (c. 250 m) climate surfaces for the historical (1981-2015) and future (2006-2099) periods. Climate futures were based on three coupled atmosphere-ocean general circulation models (GCMs) and two representative concentration pathways (RCPs) spanning a range of potential 21st century trajectories. We then reconstructed past trends and made future projections of post-fire conifer

forest recovery. Our models of past trends suggested that climate suitability for establishment declined throughout the 1981-2015 period as interannual climate became increasingly unsuitable for establishment. However, during this same historical period, post-fire abundances were predicted to exceed minimum historical tree densities in most sites during most fire years, given an available seed source. However, models using future climate scenarios project additional declines in establishment suitability and post-fire abundance throughout much of the region. Because results strongly differed by RCP, the ecological effects of climate warming appear dependent on emissions scenario. The combination of demographic modeling and species distribution modeling (SDM) is a novel approach to the problem of predicting climate impacts on forested ecosystems. Because years of above average moisture availability are important to seedling establishment across broad geographic and elevational gradients (Andrus et al. 2018, Davis et al. 2019), the better incorporation of interannual climate variability into is a particularly important contribution of this study. In addition, few studies have incorporated GCMs into projections of future post-fire recovery in the western U.S. (Feddema et al. 2013, Tepley et al. 2017, Hansen et al. 2018, Kemp et al. 2019).

Together, the individual chapters in this dissertation reveal some of the key climate-related and non-climatic mechanisms that explain 20th-21st century changes in forest cover in the northern Front Range of Colorado and in the Southern Rocky Mountains. Episodes of increased fire activity as well as periods of fire quiescence both act as agents of change in these forests, and historical fire activity influenced observed patterns of forest gain c. 1938-2015. Contemporary fire activity and slow forest recovery were the primary drivers of forest loss in this same time period. Forest recovery has been limited throughout recent fires, likely due the combination of inadequate seed availability in high-severity patches as well as increasingly

unsuitable climate for seedling establishment and recovery. There is substantial uncertainty in projecting future trends in these processes. Still, with further warming, fire activity is likely to increase throughout the western U.S. and the potential for recovery following these events is likely to decline. The consideration of past trends in forest cover, as well as contemporary processes, will improve our ability to understand and predict the potential for future changes in western U.S. forests.

5.2 Implications to Management

There is broad interest in using a knowledge of the how past landscape conditions reflect climate-dependent and climate-independent processes in the context of understanding of potential future climate impacts on forests and forest management in the western United States (Hayward et al. 2012). Management for "historical fidelity", based on historical reference conditions, is a broadly-used approach (Hobbs et al. 2010). However, biological invasions and a warming climate are likely to lead to novel ecosystem assemblages and processes throughout the western U.S., calling into question the idea of using the natural ranges of variability (*sensu* Landres et al. 1999, Keane et al. 2009) and historical reference conditions as a sole basis for management (Hayward et al. 2012). Given the uncertainty of future trends and trajectories, managers can benefit from using a range of approaches informed by the best available science (Millar et al. 2007, Millar and Stephenson 2015). Following the classification of Millar et al. (2007), these approaches can broadly be categorized into 1) management activities that attempt to forestall change and increase ecosystem resistance to disturbance, 2) management activities that foster resilience and improve the ability of ecosystems to return to a prior state following disturbance, and 3) actions that facilitate transitions to ecosystem types that are more capable of tolerating current or future climate and disturbance. Importantly, each of these types of

approaches can range from aggressive human intervention to “no action”, and all potential approaches may be appropriate under certain circumstances (Hobbs et al. 2010). The research in this dissertation helps to inform multiple management strategies throughout forested landscapes in the Southern Rocky Mountains.

Forest restoration and fuels reduction are common practices in forests throughout the western United States and could best be categorized as management activities that attempt to foster resistance to disturbance and improve historical fidelity (Millar et al. 2007, Hobbs et al. 2010) . Our quantification of 21st century forest change in the northern Front Range of Colorado, in combination with a knowledge of fire history, have the potential to improve the site-specificity of these types of treatments in the region; we have made these data publicly available. Identifying areas in which forests increased in extent and density primarily due to the exclusion of previously frequent, low-severity fire regimes, helps to identify sites in which the goals of restoration (i.e., improving historical fidelity) and fuels reduction (i.e., reducing fire hazard) are most congruent (Platt et al. 2006). Importantly, the initial time period used in this study (c. 1938) did not capture a natural landscape. At this point, the NFR had already been highly altered by mining, logging, and other factors, and therefore our findings must also be supplemented with a historical knowledge of place. In addition, changes in forest cover are just one piece of an integrative management framework that must also incorporate a range of social and cultural values. In the Colorado Front Range, an area with high densities of homes and valuable water resources in fire-prone areas (Theobald and Romme 2007, Platt et al. 2011, Calkin et al. 2014), protection of these resources should likely take precedent over strict adherence to the natural ranges of variability.

Resilience to disturbance is a widely-discussed topic in theoretical ecology (Holling 1973, Carpenter et al. 2001, Scheffer et al. 2012), and in forest management (Derose and Long 2014). The work in this dissertation helps to identify the scenarios under which forests are most resilient to wildfire (i.e., mesic sites adjacent to surviving trees), and when transitions to alternative vegetation types are likely (i.e., the interior of high-severity patches and xeric sites). Reforestation is an example of a management approach involving aggressive human intervention to foster resilience. Reforestation treatments should not be required within 200 m of a surviving forest, assuming that seed will be available for natural regeneration in these areas (North et al. 2019), though the threshold distance also depends on seed size and dispersal characteristics (McCaughey et al. 1986). Beyond this distance, reforestation may be an appropriate goal in more mesic sites, where seedling survival is likely to be highest. These more mesic sites can be identified using the types of high-resolution climate surfaces we have developed in each of the 15 studied fires. "No action" can also be an appropriate management approach to resilience in some areas, particularly those in which natural regeneration is most likely. Though site preparation and shrub control may increase the ease of planting and subsequent seedling survival (Lanini and Radosevich 1986), heavy equipment use may lead to soil erosion and compaction, and the loss of coarse wood in activities such as salvage logging may also inhibit natural regeneration (Donato et al. 2006).

Given the potential for rapid changes in climate, response options that facilitate transitions to new, better-adapted ecosystem types are appropriate in many places. Relaxation of seed-transfer zones, a component of current reforestation practices in national forests of the United States that restrict seed used for reforestation to relatively local provenances, is one such approach. More flexible seed transfer zones (*sensu* Mckenney et al. 2009, Potter and Hargrove

2012) would allow for the use of more drought-adapted genotypes of pre-fire species in post-fire reforestation activities. A more aggressive approach would be to experiment with assisted migration, in which tree species, generally from lower latitudes and elevations, would be used as a component of post-fire reforestation (Williams and Dumroese 2013). For example, in fires in low or mid-elevation sites in the Colorado Front Range, piñon pine and juniper species are likely more suited to future climate than are ponderosa pine or Douglas-fir, even in locations in which piñon and juniper were not present prior to the fire. Lastly, "no action" can be a suitable management approach to facilitate transitions. Gambel oak and other resprouting shrubs are becoming increasingly dominant in recently burned sites in northern New Mexico and southern Colorado. These species may be quite resilient to future climate (Rehfeldt et al. 2006) and to future fire activity (Coop et al. 2016). So, while attempts to reforest these types of sites (i.e. persistent shrublands) through aggressive management actions such as brush control and planting may return some areas to forested cover, alternative states of vegetation may be more appropriate in a warmer, increasingly fire-prone future. All management approaches should be accompanied with an appropriate sense of humility (Hobbs et al. 2010) and the recognition that we have an incomplete scientific understanding of forested ecosystems and of the magnitude of future changes in climate.

5.3 Broader Applicability and Future Research Directions

While our analyses were constrained to sites in the Southern Rocky Mountains, the concepts, methods, and analytical approaches used in this dissertation may also be useful in other regions. Beginning c. 1930, aerial photographs were collected for the purpose of natural resource inventory throughout the United States and many other nations. These data provide a high resolution and spatially continuous record of land cover in the early 1900s that can be used to

quantify changes in natural ecosystems and the impacts of human activity across broad landscapes. The methods described in Chapter 2 provide a means by which ancillary data (e.g., fire history and records of land use) and uncertainty in change detection can be better incorporated into these types of studies. Similarly, while Chapters 3 and 4 focus on specific forest types within the Southern Rocky Mountains, wildfire and successional processes occur in nearly every terrestrial ecosystem. A multi-scaled approach that identifies specific spatial and temporal constraints to post-fire recovery (as described in Chapters 3 and 4) may help to identify sites that are most likely to convert to alternative states of vegetation in other fire-prone ecosystems and regions throughout the world.

This dissertation focused on historical dynamics of forest cover, recent fire activity, and post-fire recovery in the Southern Rocky Mountains. Related to these ideas and, more broadly, to the changing dynamics of forest ecosystems, there remain many important questions to be answered. Relevant to historical forest change and the natural ranges of variability, forest managers are increasingly trying to incorporate a knowledge of fine-scale and broad-scale spatial patterns into silvicultural treatments. I am currently working with Teresa Chapman on a project to quantify landscape-scale spatial patterns in the 1938 aerial images used in Chapter 2. There is also the potential to combine these data with other historical datasets in the region such as tree-ring reconstructions (Battaglia et al. 2018) and General Land Office records (Williams and Baker 2012a) to quantify changes in forests of the NFR at a range of spatial and temporal scales.

Chapters 3 and 4 in this dissertation focused on potential limitations to post-fire recovery and projected future trends in post-fire recovery due to a warming climate. Though we considered the influence of interannual climate variability on tree seedling establishment, a more robust demographic framework (*sensu* Enright et al. 2015, Davis et al. 2018b) that incorporates

climatic influences on multiple components of tree regeneration (i.e., seed cone production, seedling establishment, and seedling survival) would be a fruitful area for future research. Previous studies of this kind have primarily relied on literature review to parameterize models, often relying on studies performed in very localized areas to characterize the importance of interannual climate variability on the processes of seed cone production by mature trees, seedling establishment, and seedling survival (Feddema et al. 2013, Petrie et al. 2017). Site-specific data on seed cone production and seedling establishment, such as those presented in Chapter 3, may be used to develop data-driven demographic models that could then be used to model the influence of climate on tree regeneration. I am currently involved in two projects that are related to this. First, I will be collecting additional data on seed cone production this summer and continuing collaborations with Miranda Redmond and Andreas Wion at Colorado State University to better characterize climatic influences on seed cone production. Second, I am involved in a collaborative international research project with Neal Enright and Joe Fontaine at Murdoch University in Perth, Australia, as well as Brian Harvey at the University of Washington, to describe and model the influence of demographic processes on post-fire tree regeneration.

Animal dispersal is a key area for future research in fire ecology and in climate change impacts on plants. Because ponderosa pine, Douglas-fir, and many other conifers have relatively large, heavy seeds, animal-mediated seed dispersal may be the best hope for seedling establishment in the interior of large patches of high-severity fire, and in new areas outside of existing species ranges. Plant species that have been best able to track previous changes in climate are those with light, wind-borne propagules capable of traveling broad distances (e.g., ferns, Normand et al. 2011). However, many conifers are known to be dispersed by avian and

mammal species (Ligon 1978, Hutchins and Lanner 1982, Vander Wall 2008), and animal-mediated dispersal likely facilitated the migration of large-seeded tree species at the end of the Pleistocene (Johnson and Webb 1989). The extent to which animal-mediated dispersal will be able to aid tree species in establishing in large, high-severity fire patches, and in tracking changes in climate, will have important implications for future species distributions.

If species are unable to migrate, in-situ adaptation will become crucial to avoid extinction (Jump and Peñuelas 2005). Adaptation can potentially involve many components, including the genotypic and phenotypic diversity already present in a population and the capacity of a population to rapidly evolve or to change phenotypic expression through plasticity (Nicotra et al. 2010). Both of these components of adaptation are typically discussed with respect to the ability of a plant population to tolerate novel climatic conditions and to endure drought. However, the ability to survive disturbance is also an important driver of local population persistence. Individuals and populations in certain portions of the landscape – refugia – are more likely to survive disturbances such as wildfire (Krawchuk et al. 2016, Meigs and Krawchuk 2018). Similarly, some species and local populations may be more resistant to disturbances than others, and traits such as bark thickness can help to identify variation in fire resistance (Pausas 2015, Pellegrini et al. 2017). During summer 2019, we plan to collect data on bark thickness and other demographic traits that promote resistance to wildfire.

REFERENCES

Abatzoglou, J. T. 2013. Development of Gridded Surface Meteorological Data for Ecological Applications and Modelling. International Journal of Climatology 33:121–131.

Abatzoglou, J. T., and T. J. Brown. 2012. A Comparison of Statistical Downscaling Methods Suited for Wildfire Applications. International Journal of Climatology 32:772–780.

Abatzoglou, J. T., C. A. Kolden, A. P. Williams, J. A. Lutz, and A. M. S. Smith. 2017. Climatic Influences on Interannual Variability in Regional Burn Severity Across Western US Forests. International Journal of Wildland Fire 26:269–275.

Abatzoglou, J. T., and A. P. Williams. 2016. The Impact of Anthropogenic Climate Change on Wildfire Across Western US Forests. Proceedings of the National Academy of Sciences 113:11770–11775.

Abella, S. R., and P. Z. Fulé. 2008. Fire Effects on Gambel Oak in Southwestern Ponderosa Pine-Oak Forests. RMRS-RN-34. Fort Collins, CO.

Addington, R. N., G. H. Aplet, M. A. Battaglia, J. S. Briggs, P. M. Brown, A. S. Cheng, Y. Dickinson, J. A. Feinstein, K. A. Pelz, C. M. Regan, J. Thinnes, R. Truex, J. Paula, B. Gannon, C. W. Julian, J. L. Underhill, and B. Wolk. 2018. Principles and Practices for the Restoration of Ponderosa Pine and Dry Mixed-Conifer Forests of the Colorado Front Range. RMRS GTR-373. USDA Forest Service, Rocky Mountain Research Station, Fort Collins, CO.

Andrus, R. A., B. J. Harvey, K. C. Rodman, S. J. Hart, and T. T. Veblen. 2018. Moisture Availability Limits Subalpine Tree Establishment. Ecology 99:567–575.

Aplet, G. H., R. D. Laven, and F. W. Smith. 1988. Patterns of Community Dynamics in Colorado Engelmann Spruce-Subalpine Fir Forests. Ecology 69:312–319.

ArcGIS v. 10.4.1. 2016. ESRI, Redlands, CA.

Asner, G. P., S. Archer, R. F. Hughes, R. J. Ansley, and C. A. Wessman. 2003. Net Changes in Regional Woody Vegetation Cover and Carbon Storage in Texas Drylands, 1937-1999. Global Change Biology 9:316–335.

Baddeley, A., and R. Turner. 2005. spatstat: An R Package for Analyzing Spatial Point Patterns. Journal of Statistical Software 12:1–42.

Baker, W. L., W. H. Romme, D. Binkley, and T. Cheng. 2017. The Landscapes They Are A-Changin ' - Severe 19th-Century Fires, Spatial Complexity, and Natural Recovery in Historical Landscapes on the Uncompahgre Plateau. Colorado Forest Restoration Institute, Fort Collins, CO.

Baker, W. L. 2009. Fire Ecology in Rocky Mountain Landscapes. Island Press, Washington, D.C.

Baker, W. L. 2018. Transitioning Western U.S. Dry Forests to Limited Committed Warming with Bet-Hedging and Natural Disturbances. Ecosphere 9:e02288.

Baker, W. L., and D. J. Shinneman. 2004. Fire and Restoration of Piñon-Juniper Woodlands in the Western United States: W Review. Forest Ecology and Management 189:1–21.

Batllori, E., C. Miller, P. Sean, and A. P. Max. 2017. Potential Relocation of Climatic Environments Suggests High Rates of Climate Displacement Within the North American Protection Network. Global Change Biology 23:3219–3230.

Battaglia, M. A., B. Gannon, P. M. Brown, P. J. Fornwalt, A. S. Cheng, and L. S. Huckaby. 2018. Changes in Forest Structure Since 1860 in Ponderosa Pine Dominated Forests in the Colorado and Wyoming Front Range, USA. Forest Ecology and Management 422:147–160.

Battaglia, M. A., P. Mou, B. Palik, and R. J. Mitchell. 2002. The Effect of Spatially Variable Overstory on the Understory Light Environment of an Open-Canopied Longleaf Pine Forest. Canadian Journal of Forest Research 32:1984–1991.

Beckman, J. S., and J. B. Mitton. 1984. Peroxidase Allozyme Differentiation Among Successional Stands of Ponderosa Pine. The American Midland Naturalist 112:43–49.

Bigelow, S. W., M. P. North, and C. F. Salk. 2011. Using Light to Predict Fuels-Reduction and Group-Selection Effects on Succession in Sierran Mixed-Conifer Forest. Canadian Journal of Forest Research 41:2051–2063.

Bigler, C., D. G. Gavin, C. Gunning, and T. T. Veblen. 2007. Drought Induces Lagged Tree Mortality in a Subalpine Forest in the Rocky Mountains. Oikos 116:1983–1994.

Bischl, B., M. Lang, L. Kotthoff, J. Schiffner, J. Richter, E. Studerus, G. Casalicchio, and Z. Jones. 2016. mlr: Machine Learning in R. Journal of Machine Learning Research 17:1–5.

Bivand, R. S., E. Pebesma, and V. Gómez-Rubio. 2013. Applied Spatial Data Analysis with R. Springer, New York.

Black, A. E., P. Morgan, and P. E. Hessburg. 2003. Social and Biophysical Correlates of Change in Forest Landscapes of the Interior Columbia Basin, USA. Ecological Applications 13:51–67.

Blaschke, T. 2010. Object Based Image Analysis for Remote Sensing. ISPRS Journal of Photogrammetry and Remote Sensing 65:2–16.

Bolker, B. M., M. E. Brooks, C. J. Clark, S. W. Geange, J. R. Poulsen, M. H. H. Stevens, and J.-S. S. White. 2009. Generalized Linear Mixed Models: A Practical Guide for Ecology and Evolution. Trends in Ecology & Evolution 24:127–135.

Bonan, G. B. 2008. Forests and Climate Change: Forcings, Feedbacks, and the Climate Benefits of Forests. Science 320:1444–1449.

Bond, W. J., F. I. Woodward, and G. F. Midgley. 2005. The Global Distribution of Ecosystems in a World Without Fire. New Phytologist 165:525–538.

Bonnet, V. H., A. W. Schoettle, and W. D. Shepperd. 2005. Postfire Environmental Conditions Influence the Spatial Pattern of Regeneration for Pinus ponderosa. Canadian Journal of Forest Research 35:37–47.

Bowman, D. M. J. S., J. K. Balch, P. Artaxo, W. J. Bond, J. M. Carlson, M. A. Cochrane, C. M. D'Antonio, R. S. DeFries, J. C. Doyle, S. P. Harrison, and others. 2009. Fire in the Earth System. Science 324:481–484.

Boyden, S., D. Binkley, and W. Shepperd. 2005. Spatial and Temporal Patterns in Structure, Regeneration, and Mortality of an Old-Growth Ponderosa Pine forest in the Colorado Front Range. Forest Ecology and Management 219:43–55.

Brando, P. M., J. K. Balch, D. C. Nepstad, D. C. Morton, F. E. Putz, M. T. Coe, D. Silverio, M. N. Macedo, E. A. Davidson, C. C. Nobrega, A. Alencar, and B. S. Soares-Filho. 2014. Abrupt Increases in Amazonian Tree Mortality Due to Drought-Fire Interactions. Proceedings of the National Academy of Sciences 111:6347–6352.

Breshears, D. D., N. S. Cobb, P. M. Rich, K. P. Price, C. D. Allen, R. G. Balice, W. H. Romme, J. H. Kastens, M. L. Floyd, J. Belnap, J. J. Anderson, O. B. Myers, and C. W. Meyer. 2005. Regional Vegetation Die-off in Response to Global-Change-Type Drought. Proceedings of the National Academy of Sciences 102:15144–15148.

Brooks, M. E., K. Kristensen, K. J. van Benthem, A. Magnusson, C. W. Berg, A. Nielsen, H. J. Skaug, M. Maechler, and B. M. Bolker. 2017. glmmTMB Balances Speed and Flexibility Among Packages for Zero-inflated Generalized Linear Mixed Modeling. The R Journal 9:378–400.

Brown, P. M., M. A. Battaglia, P. J. Fornwalt, B. Gannon, L. S. Huckaby, C. Julian, and A. S. Cheng. 2015. Historical (1860) Forest Structure in Ponderosa Pine Forests of the Northern Front Range, Colorado. Canadian Journal of Forest Research 1132:1121–1132.

Buechling, A., and W. L. Baker. 2004. A Fire History from Tree Rings in a High-Elevation Forest of Rocky Mountain National Park. Canadian Journal of Forest Research 34:1259–1273.

Buechling, A., P. H. Martin, C. D. Canham, W. D. Shepperd, M. A. Battaglia, and N. Rafferty. 2016. Climate Drivers of Seed Production in Picea engelmannii and Response to Warming Temperatures in the Southern Rocky Mountains. Journal of Ecology 104:1051–1062.

Bunn, A. G. 2008. A Dendrochronology Program in R (dplR). Dendrochronologia 26:115–124.

Burnham, K. P., and D. R. Anderson. 2002. Model Selection and Multimodel Inference: A Practical Information-Theoretic Approach. 2nd edition. Springer, New York.

Burns, R. M., and B. H. Honkala. 1990. Silvics of North America: Vol 1, Conifers. Agricultural Handbook 654. USDA Forest Service, Washington, D.C.

Caggiano, M. D. 2017. Front Range Round Table 2016 Interagency Fuel Treatment Database. Colorado Forest Restoration Institute, Fort Collins, CO.

Calkin, D. E., J. D. Cohen, M. A. Finney, and M. P. Thompson. 2014. How Risk Management Can Prevent Future Wildfire Disasters in the Wildland-Urban Interface. Proceedings of the National Academy of Sciences 111:746–751.

Carpenter, S., B. Walker, J. M. Anderies, and N. Abel. 2001. From Metaphor to Measurement: Resilience of What to What? Ecosystems 4:765–781.

Chambers, M. E., P. J. Fornwalt, S. L. Malone, and M. A. Battaglia. 2016. Patterns of Conifer Regeneration Following High Severity Wildfire in Ponderosa Pine – Dominated Forests of the Colorado Front Range. Forest Ecology and Management 378:57–67.

Chaney, N. W., E. F. Wood, A. B. McBratney, J. W. Hempel, T. W. Nauman, C. W. Brungard, and N. P. Odgers. 2016. POLARIS: A 30-Meter Probabilistic Soil Series Map of the Contiguous United States. Geoderma 274:54–67.

Chapman, T. B., T. T. Veblen, and T. Schoennagel. 2012. Spatiotemporal Patterns of Mountain Pine Beetle Activity in the Southern Rocky Mountains. Ecology 93:2175–2185.

Chen, D., G. Gao, C. Xu, J. Guo, and G. Ren. 2005. Comparison of the Thornthwaite Method and Pan Data with the Standard Penman-Monteith Estimates of Reference Evapotranspiration in China. Climate Research 28:123–132.

Chen, I. C., J. K. Hill, R. Ohlemüller, D. Roy, and C. D. Thomas. 2011. Rapid Range Shifts of Species Associated with High Levels of Climate Warming. Science 333:1024–1026.

Cleland, E. E., I. Chuine, A. Menzel, H. A. Mooney, and M. D. Schwartz. 2007. Shifting Plant Phenology in Response to Global Change. Trends in Ecology and Evolution 22:357–365.

Coburn, C. A., and A. C. B. Roberts. 2004. A Multiscale Texture Analysis Procedure for Improved Forest Stand Classification. International Journal of Remote Sensing 25:4287–4308.

Cocke, A. E., P. Z. Fulé, and J. E. Crouse. 2005. Forest Change on a Steep Mountain Gradient After Extended Fire Exclusion: San Francisco Peaks, Arizona, USA. Journal of Applied Ecology 42:814–823.

Collins, B. J., C. C. Rhoades, R. M. Hubbard, and M. A. Battaglia. 2011. Tree Regeneration and Future Stand Development After Bark Beetle Infestation and Harvesting in Colorado Lodgepole Pine Stands. Forest Ecology and Management 261:2168–2175.

Collins, B. M., D. L. Fry, J. M. Lydersen, R. G. Everett, and S. L. Stephens. 2017. Impacts of Different Land Management Histories on Forest Change. Ecological Applications 27:2475–2486.

Collins, B. M., P. N. Omi, and P. L. Chapman. 2006. Regional Relationships Between Climate and Wildfire-Burned Area in the Interior West, USA. Canadian Journal of Forest Research 36:699–709.

Colorado Ownership Management and Protection (COMaP), V8. 2010. <https://my.usgs.gov/eerma/data/index/4f4e483ce4b07f02db4f1ba3>

Congalton, R. G. 1991. A Review of Assessing the Accuracy of Classifications of Remotely Sensed Data. Remote Sensing of Environment 37:35–46.

Conlisk, E., C. Castanha, M. J. Germino, T. T. Veblen, J. M. Smith, and L. M. Kueppers. 2017. Declines in Low-Elevation Subalpine Tree Populations Outpace Growth in High-Elevation Populations with Warming. Journal of Ecology 105:1347–1357.

Cook, E., and R. L. Holmes. 1986. User's Manual for Program ARSTAN. Laboratory of Tree-Ring Research, Tuscon, AZ.

Coop, J. D., and T. J. Givnish. 2007. Spatial and Temporal Patterns of Recent Forest Encroachment in Montane Grasslands of the Valles Caldera, New Mexico, USA. Journal of Biogeography 34:914–927.

Coop, J. D., R. T. Massatti, and A. W. Schoettle. 2010. Subalpine Vegetation Pattern Three Decades After Stand-Replacing Fire: Effects of Landscape Context and Topography on Plant Community Composition, Tree Regeneration, and Diversity. Journal of Vegetation Science 21:472–487.

Coop, J. D., S. A. Parks, S. R. McClernan, and L. M. Holsinger. 2016. Influences of Prior Wildfires on Vegetation Response to Subsequent Fire in a Reburned Southwestern Landscape. Ecological Applications 26:346–354.

Costanza, R., R. D'Arge, R. de Groot, S. Farber, M. Grasso, B. Hannon, K. Limburg, S. Naeem, R. V. O'Neill, J. Paruelo, R. G. Raskin, P. Sutton, and M. van den Belt. 1997. The Value of the World's Ecosystem Services and Natural Capital. Nature 387:253–260.

Davis, F. W., L. C. Sweet, J. M. Serra-Diaz, J. Franklin, I. McCullough, A. Flint, L. Flint, J. R. Dingman, H. M. Regan, A. D. Syphard, L. Hannah, K. Redmond, and M. A. Moritz. 2016. Shrinking Windows of Opportunity for Oak Seedling Establishment in Southern California Mountains. Ecosphere 7:e01573.

Davis, K. T., S. Z. Dobrowski, P. E. Higuera, Z. A. Holden, T. T. Veblen, M. T. Rother, A. Sala, and M. P. Maneta. 2019. Wildfires and Climate Change Push Low-Elevation Forests Across a Critical Climate Threshold for Tree Regeneration. Proceedings of the National Academy of Sciences 116: 6193–6198.

Davis, K. T., S. Z. Dobrowski, Z. A. Holden, P. E. Higuera, and J. T. Abatzoglou. 2018a. Microclimatic Buffering in Forests of the Future: The Role of Local Water Balance. Ecography 42:1–11.

Davis, K. T., P. E. Higuera, and A. Sala. 2018b. Anticipating Fire-Mediated Impacts of Climate Change Using a Demographic Framework. Functional Ecology 32:1729–1745.

Dennison, P. E., S. C. Brewer, J. D. Arnold, and M. A. Moritz. 2014. Large Wildfire Trends in the Western United States, 1984-2011. Geophysical Research Letters 41:2928–2933.

Derose, R. J., and J. N. Long. 2014. Resistance and Resilience: A Conceptual Framework for Silviculture. Forest Science 60:1205–1212.

Dethier, D. P., W. B. Ouimet, S. F. Murphy, M. Kotikian, W. Wicherski, and R. M. Samuels. 2018. Anthropocene Landscape Change and the Legacy of Nineteenth- and Twentieth-Century Mining in the Fourmile Catchment, Colorado Front Range. Annals of the American Association of Geographers 4452:1–21.

Dickinson, Y. L., R. N. Addington, G. H. Aplet, M. Babler, M. A. Battaglia, P. M. Brown, A. S. Cheng, C. Cooley, R. Edwards, J. A. Feinstein, P. J. Fornwalt, H. Gibbs, M. S. Matonis, K. A. Pelz, and C. M. Regan. 2014. Desirable Forest Structures for a Restored Front Range. Colorado Forest Restoration Institute, Fort Collins, CO.

Dillon, G. K., Z. A. Holden, P. Morgan, M. A. Crimmins, E. K. Heyerdahl, and C. H. Luce. 2011. Both Topography and Climate Affected Forest and Woodland Burn Severity in Two Regions of the Western US, 1984 to 2006. Ecosphere 2:1–33.

Dilts, T. E., P. J. Weisberg, C. M. Dencker, and J. C. Chambers. 2015. Functionally Relevant Climate Variables for Arid Lands: A Climatic Water Deficit Approach for Modelling Desert Shrub Distributions. Journal of Biogeography 42:1986–1997.

Dobrowski, S. Z., J. Abatzoglou, and A. K. Swanson. 2013. The Climate Velocity of the Contiguous United States During the 20th Century. Global Change Biology 19:241–251.

Dobrowski, S. Z., A. K. Swanson, J. T. Abatzoglou, Z. A. Holden, H. D. Safford, M. K. Schwartz, and D. G. Gavin. 2015. Forest Structure and Species Traits Mediate Projected Recruitment Declines in Western US Tree Species. Global Ecology and Biogeography 24:917–927.

Dodson, E. K., and H. T. Root. 2013. Conifer Regeneration Following Stand-Replacing Wildfire Varies Along an Elevation Gradient in a Ponderosa Pine Forest, Oregon, USA. Forest Ecology and Management 302:163–170.

Donato, D. C., J. B. Fontaine, J. L. Campbell, W. D. Robinson, J. B. Kauffman, and B. E. Law. 2006. Post-Wildfire Logging Hinders Regeneration and Increases Fire Risk. Science 311:352.

Donato, D. C., J. B. Fontaine, J. L. Campbell, W. D. Robinson, J. B. Kauffman, and B. E. Law. 2009. Conifer Regeneration in Stand-Replacement Portions of a Large Mixed-Severity Wildfire in the Klamath – Siskiyou Mountains. Canadian Journal of Forest Research 39:823–838.

Donato, D. C., B. J. Harvey, and M. G. Turner. 2016. Regeneration of Montane Forests 24 Years After the 1988 Yellowstone Fires: A Fire-Catalyzed Shift in Lower Treelines? Ecosphere 7:e01410.

Donnegan, J. A., and A. J. Rebertus. 1999. Rates and Mechanisms of Subalpine Forest Succession along an Environmental Gradient. Ecology 80:1370–1384.

Dufresne, J.-L., M.-A. Foujols, S. Denvil, A. Caubel, O. Marti, O. Aumont, Y. Balkanski, S. Bekki, H. Bellenger, R. Benshila, S. Bony, L. Bopp, P. Braconnot, P. Brockmann, P. Cadule, F. Cheruy, L. Fairhead, T. Fichefet, F. Codron, A. Cozic, D. Cugnet, N. De Noblet, C. Ethe, S. Flavoni, P. Friedlingstein, L. Guez, E. Guilyardi, D. Hauglustaine, F. Hourdin, A. Idelkadi, J. Ghattas, S. Joussaume, M. Kageyama, G. Krinner, S. Labetoulle, A. Lahellec, F. Lefevre, C. Levy, Z. X. Li, J. Lloyd, F. Lott, G. Madec, M. Mancip, M. Marchand, S. Masson, Y. Meurdesoif, J. Mignot, I. Musat, S. Parouty, J. Polcher, C. Rio, M. Schulz, D. Swingedouw, S. Szopa, C. Talandier, P. Terray, N. Viovy, and N. Vuichard. 2013. Climate Change Projections Using the IPSL-CM5 Earth System Model: From CMIP3 to CMIP5. Climate Dynamics 40:2123–2165.

Dunne, J. P., J. G. John, A. J. Adcroft, S. M. Griffies, R. W. Hallberg, E. Shevliakova, R. J. Stouffer, W. Cooke, K. A. Dunne, M. J. Harrison, J. P. Krasting, S. L. Malyshev, P. C. D. Milly, P. J. Phillips, L. T. Sentman, B. L. Samuels, M. J. Spelman, M. Winton, A. T. Wittenberg, and N. Zadhe. 2012. GFDL's ESM2 Global Coupled Climate – Carbon Earth

System Models. Part I : Physical Formulation and Baseline Simulation Characteristics. Journal of Climate 25:6646–6665.

Easterday, K., P. Mcintyre, and M. Kelly. 2018. Land Ownership and 20th Century Changes to Forest Structure in California. Forest Ecology and Management 422:137–146.

Ehle, D. S., and W. L. Baker. 2003. Disturbance and Stand Dynamics in Ponderosa Pine Forests in Rocky Mountain National Park. Ecological Monographs 73:543–566.

Eidenshink, J., B. Schwind, K. Brewer, Z. Zhu, B. Quayle, S. Howard, S. Falls, and S. Falls. 2007. A Project for Monitoring Trends in Burn Severity. Fire Ecology 3:3–21.

Elith, J., J. R. Leathwick, and T. Hastie. 2008. A Working Guide to Boosted Regression Trees. Journal of Animal Ecology 77:802–813.

Enright, N. J., J. B. Fontaine, D. M. J. S. Bowman, R. A. Bradstock, and R. J. Williams. 2015. Interval Squeeze: Altered Fire Regimes and Demographic Responses Interact to Threaten Woody Species Persistence as Climate Changes. Frontiers in Ecology and the Environment 13:265–272.

Evans, J. S. 2017. spatialEco. R package version 0.0.1-7. <https://CRAN.R-project.org/package=spatialEco>

Evans, J. S., M. A. Murphy, Z. A. Holden, and S. A. Cushman. 2011. Modeling Species Distribution and Change Using Random Forests. Pages 139–159 in C. A. Drew, Y. F. Wiersma, and F. Huettmann, editors. Predictive Species and Habitat Modeling in Landscape Ecology: Concepts and Applications. Springer, New York.

Feddema, J. J., J. N. Mast, and M. Savage. 2013. Modeling High-Severity Fire, Drought and Climate Change Impacts on Ponderosa Pine Regeneration. Ecological Modelling 253:56–69.

Flathers, K. N., T. E. Kolb, J. B. Bradford, K. M. Waring, and W. K. Moser. 2016. Long-Term Thinning Alters Ponderosa Pine Reproduction in Northern Arizona. Forest Ecology and Management 374:154–165.

Flint, L. E., and A. L. Flint. 2012. Downscaling Future Climate Scenarios to Fine Scales for Hydrologic and Ecological Modeling and Analysis. Ecological Processes 1:1–15.

Floyd, M. E. 1982. The Interaction of Piñon Pine and Gambel Oak in Plant Succession Near Dolores, Colorado. The Southwestern Naturalist 27:143–147.

Food and Agriculture Organization of the United Nations. 2015. <http://www.fao.org/forestry/en/>

Forcella, F. 1981. Estimating Pinyon Cone Production in New Mexico and Western Oklahoma. Journal of Wildlife Management 45:553–557.

Franklin, J. 2010. Mapping Species Distributions: Spatial Inference and Prediction. Cambridge University Press, Cambridge, England.

Franklin, J., F. W. Davis, M. Ikegami, A. D. Syphard, L. E. Flint, A. L. Flint, and L. Hannah. 2013. Modeling Plant Species Distributions Under Future Climates: How Fine Scale Do Climate Projections Need to Be? Global Change Biology 19:473–483.

Fulé, P. Z., W. W. Covington, and Moore. 1997. Determining Reference Conditions for Ecosystem Management of Southwestern Ponderosa Pine Forests. Ecological Applications 7:895–908.

Fulé, P. Z., J. E. Korb, and R. Wu. 2009. Changes in Forest Structure of a Mixed Conifer Forest, Southwestern Colorado, USA. Forest Ecology and Management 258:1200–1210.

Gartner, M. H., T. T. Veblen, S. Leyk, and C. A. Wessman. 2015. Detection of Mountain Pine Beetle-Killed Ponderosa Pine in a Heterogeneous Landscape Using High-Resolution Aerial Imagery. International Journal of Remote Sensing 1161:1–20.

Gartner, M. H., T. T. Veblen, R. L. Sherriff, and T. L. Schoennagel. 2012. Proximity to Grasslands Influences Fire Frequency and Sensitivity to Climate Variability in Ponderosa Pine Forests of the Colorado Front Range. International Journal of Wildland Fire 21:562–571.

GDAL - Geospatial Data Abstraction Library. 2017. Open Source Geospatial Foundation.

Geils, B. B. W., K. E. Hummer, and R. S. Hunt. 2010. White Pines, Ribes, and Blister Rust: A Review and Synthesis. Forest Pathology 40:147–185.

Gorte, R. 2013. The Rising Cost of Wildfire Protection. Headwaters Economics, Bozeman, MT.

Grubb, P. J. 1977. The Maintenance of Species-Richness in Plant Communities: The Importance of the Regeneration Niche. Biological Reviews of the Cambridge Philosophical Society 52:107–145.

Gruell, G. E. 1983. Fire and Vegetative Trends in the Northern Rockies: Interpretations from 1871-1982 Photographs. GTR INT-158. USDA Forest Service, Intermountain Forest and Range Experiment Station, Ogden, Utah.

Gruell, G. E. 2001. Fire in Sierra Nevada Forests: A Photographic Interpretation of Ecological Change Since 1849. Mountain Press, Missoula, MT.

Guisan, A., and N. E. Zimmermann. 2000. Predictive Habitat Distribution Models in Ecology. Ecological Modelling 135:147–186.

Guiterman, C. H., E. Q. Margolis, C. D. Allen, D. A. Falk, and T. W. Swetnam. 2017. Long-Term Persistence and Fire Resilience of Oak Shrubfields in Dry Conifer Forests of Northern New Mexico. Ecosystems.

Hadley, K. S., and T. T. Veblen. 1993. Stand Response to Western Spruce Budworm and Douglas-Fir Bark Beetle Outbreaks, Colorado Front Range. Canadian Journal of Forest Research 23:479–491.

Haffey, C., T. D. Sisk, C. D. Allen, A. E. Thode, and E. Q. Margolis. 2018. Limits to Ponderosa Pine Regeneration Following Large High-Severity Forest Fires in the United States Southwest. Fire Ecology 14:143–162.

Haire, S. L., and K. McGarigal. 2010. Effects of Landscape Patterns of Fire Severity on Regenerating Ponderosa Pine Forests (Pinus ponderosa) in New Mexico and Arizona, USA. Landscape Ecology 25:1055–1069.

Halofsky, J. S., J. E. Halofsky, T. Burcsu, and M. A. Hemstrom. 2014. Dry Forest Resilience Varies Under Simulated Climate-Management Scenarios in a Central Oregon, USA Landscape. Ecological Applications 24:1908–1925.

Hamed, K. H., and A. R. Rao. 1998. A Modified Mann-Kendall Trend Test for Autocorrelated Data. Journal of Hydrology 204:182–196.

Hankin, L. E., P. E. Higuera, and S. Z. Dobrowski. 2019. Impacts of Growing-Season Climate on Tree Growth and Post-Fire Regeneration in Ponderosa Pine and Douglas-Fir Forests. Ecosphere 10:e02679.

Hansen, M. C., P. V Potapov, R. Moore, M. Hancher, S. A. Turubanova, A. Tyukavina, D. Thau, S. V Stehman, S. J. Goetz, T. R. Loveland, A. Kommareddy, A. Egorov, L. Chini, C. O. Justice, and J. R. G. Townshend. 2013. High-Resolution Global Maps of 21st-Century Forest Cover Change. Science 342:850–853.

Hansen, W. D., K. H. Braziunas, W. Rammer, R. Seidl, and M. G. Turner. 2018. It Takes a Few to Tango: Changing Climate and Fire Regimes Can Cause Regeneration Failure of Two Subalpine Conifers. Ecology 99:966–977.

Hart, S. J., T. T. Veblen, K. S. Eisenhart, D. Jarvis, and D. Kulakowski. 2014. Drought Induces Spruce Beetle (Dendroctonus rufipennis) Outbreaks Across Northwestern Colorado. Ecology 95:930–939.

Hart, S. J., T. T. Veblen, D. Schneider, and N. P. Molotch. 2017. Summer and Winter Drought Drive the Initiation and Spread of Spruce Beetle Outbreak. Ecology 98:2698–2707.

Hartig, F. 2018. DHARMa: Residual Diagnostics for Hierarchical (Mulit-Level/Mixed) Regression Models. R package version 0.1.6.2. <https://cran.r-project.org/web/packages/DHARMa/vignettes/DHARMa.html>

Harvey, B. J., D. C. Donato, W. H. Romme, and M. G. Turner. 2013. Influence of Recent Bark Beetle Outbreak on Fire Severity and Postfire Tree Regeneration in Montane Douglas-fir forests. Ecology 94:2475–2486.

Harvey, B. J., D. C. Donato, W. H. Romme, and M. G. Turner. 2014a. Fire Severity and Tree Regeneration Following Bark Beetle Outbreaks: The Role of Outbreak Stage and Burning Conditions. Ecological Applications 24:1608–1625.

Harvey, B. J., D. C. Donato, and M. G. Turner. 2014b. Recent Mountain Pine Beetle Outbreaks, Wildfire Severity, and Postfire Tree Regeneration in the US Northern Rockies. Proceedings of the National Academy of Sciences 111:15120–15125.

Harvey, B. J., D. C. Donato, and M. G. Turner. 2016. High and Dry: Postfire Drought and Large Stand-Replacing Burn Patches Reduce Postfire Tree Regeneration in Subalpine Forests. Global Ecology and Biogeography 25:655–669.

Hastie, T., R. Tibshirani, and J. Friedman. 2009. The Elements of Statistical Learning: Data Mining, Inference, and Prediction. 2nd edition. Springer, New York.

Hayward, G. D., T. T. Veblen, L. H. Suring, and B. Davis. 2012. Challenges in the Application of Historical Range of Cariation to Conservation and Land Management. Pages 32–45 *in* J. A. Wiens, G. D. Hayward, H. D. Safford, and C. Giffen, editors. Historical Environmental Variation in Conservation and Natural Resource Management. Wiley-Blackwell, Hoboken, NJ.

Hessburg, P. F., and J. K. Agee. 2003. An Environmental Narrative of Inland Northwest United States Forests, 1800-2000. Forest Ecology and Management 178:23–59.

Hessburg, P. F., J. K. Agee, and J. F. Franklin. 2005. Dry Forests and Wildland Fires of the Inland Northwest USA: Contrasting the Landscape Ecology of the Pre-Settlement and Modern Eras. Forest Ecology and Management 211:117–139.

Hessburg, P. F., B. G. Smith, S. D. Kreiter, C. A. Miller, R. B. Salter, C. H. McNicoll, and W. J. Hann. 1999. Historical and Current Forest and Range Landscapes in the Interior Columbia River Basin and Portions of the Klamath and Great Basins. PNW-GTR-458. USDA Forest Service, Pacific Northwest Research Station, Portland, OR.

Higuera, P. E., D. G. Gavin, P. J. Bartlein, and D. J. Hallett. 2010. Peak Detection in Sediment Charcoal Records: Impacts of Alternative Data Analysis Methods on Fire-History. International Journal of Wildland Fire 19:996–1014.

Hijmans, R. J. 2015. raster: Geographic Data Analysis and Modeling. R package version 2.7-15. <https://CRAN.R-project.org/package=raster>

Hijmans, R. J., S. Phillips, J. R. Leathwick, and J. Elith. 2017. dismo: Species Distribution Modeling. R Package version 1.1-4. < https://CRAN.R-project.org/package=dismo>

Hilbe, J. A. 2014. Modeling Count Data. Cambridge University Press, New York.

Hobbs, R. J., D. N. Cole, L. Yung, E. S. Zavaleta, G. H. Aplet, F. S. C. Iii, P. B. Landres, D. J. Parsons, N. L. Stephenson, P. S. White, D. M. Graber, E. S. Higgs, C. I. Millar, J. M. Randall, K. A. Tonnessen, and S. Woodley. 2010. Guiding Concepts for Park and Wilderness Stewardship in an Era of Global Environmental Change. Frontiers in Ecology and the Environment 8:483–390.

Holden, Z. A., P. Morgan, and J. S. Evans. 2009. A Predictive Model of Burn Severity Based on 20-Year Satellite-Inferred Burn Severity Data in a Large Southwestern US Wilderness Area. Forest Ecology and Management 258:2399–2406.

Holden, Z. A., A. Swanson, A. E. Klene, J. T. Abatzoglou, S. Z. Dobrowski, S. A. Cushman, J. Squires, G. G. Moisen, and J. W. Oyler. 2016. Development of High-Resolution (250 m) Historical Daily Gridded Air Temperature Data Using Reanalysis and Distributed Sensor Networks for the US Northern Rocky Mountains. International Journal of Climatology 36:3620–3632.

Holden, Z. A., A. Swanson, C. H. Luce, W. M. Jolly, M. Maneta, J. W. Oyler, D. A. Warren, R. Parsons, and D. Affleck. 2018. Decreasing Fire Season Precipitation Increased Recent Western US Forest Wildfire Activity. Proceedings of the National Academy of Sciences 115:E8349–E8357.

Holling, C. S. 1973. Resilience and Stability of Ecological Systems. Annual Review of Ecology and Systematics 4:1–23.

Holsinger, L., S. A. Parks, and C. Miller. 2016. Weather, Fuels, and Topography Impede Wildland Fire Spread in Western US Landscapes. Forest Ecology and Management 380:59–69.

Homer, C. G., J. A. Dewitz, L. Yang, S. Jin, P. Danielson, G. Xian, J. Coulston, N. D. Herold, J. D. Wickham, and K. Megown. 2015. Completion of the 2011 National Land Cover Database for the Conterminous United States - Representing a Decade of Land Cover Change Information. Photogrammetric Engineering and Remote Sensing 81:345–354.

Howard, J. L., and K. C. Jones. 2016. U.S. Timber Production, Trade, Consumption, and Price Statistics, 1965-2013. FPL-RP-679. USDA Forest Service, Forest Products Laboratory, Madison, WI.

Huckaby, L. S., M. R. Kaufmann, J. M. Stoker, and P. J. Fornwalt. 2001. Landscape Patterns of Montane Forest Age Structure Relative to Fire History at Cheesman Lake in the Colorado Front Range. Pages 19–27 in R. K. Vance, C. B. Edminster, W. W. Covington, and J. A. Blake, editors. Ponderosa Pine Ecosystems Restoration and Conservation: Steps Toward Stewardship. USDA Forest Service, Rocky Mountain Research Station, Flagstaff, AZ.

Hugunin, J. 1995. The Python Matrix Object: Extending Python for Computation. Proceedings of the Third Python Workshop. Reston, VA.

Hutchins, H. E., and R. M. Lanner. 1982. The Central Role of Clark's Nutcracker in the Dispersal and Establishment of Whitebark Pine. Oecologia 55:192–201.

Hutto, R. L., R. E. Keane, R. L. Sherriff, C. T. Rota, L. A. Eby, V. A. Saab, U. F. Service, and R. Mountain. 2016. Toward a More Ecologically Informed View of Severe Forest Fires. Ecosphere 7:1–13.

IPCC. 2014. Climate Change 2014: Synthesis Report. Contribution of Working Groups I, II and III to the Fifth Assessment Report of the Intergovernmental Panel on Climate Change. Geneva, Switzerland.

Jeffrey, S., L. Rotstayn, M. Collier, S. Dravitzki, C. Hamalainen, C. Moeseneder, K. Wong, and J. Syktus. 2013. Australia's CMIP5 Submission Using the CSIRO-Mk3.6 Model. Australian Meteorological and Oceanographic Journal 63:1–13.

Johnson, W. C., and T. Webb. 1989. The Role of Blue Jays (Cyanocitta cristata L.) in the Postglacial Dispersal of Fagaceous Trees in Eastern North America. Journal of Biogeography 16:561–571.

Johnston, J. D. 2017. Forest Succession Along a Productivity Gradient Following Fire Exclusion. Forest Ecology and Management 392:45–57.

Johnstone, J. F., T. N. Hollingsworth, F. S. Chapin, and M. C. Mack. 2010. Changes in Fire Regime Break the Legacy Lock on Successional Trajectories in Alaskan Boreal Forest. Global Change Biology 16:1281–1295.

Jolly, W. M., M. A. Cochrane, P. H. Freeborn, Z. A. Holden, T. J. Brown, G. J. Williamson, and D. M. J. S. Bowman. 2015. Climate-Induced Variations in Global Wildfire Danger from 1979 to 2013. Nature Communications:1–21.

Jump, A. S., and J. Peñuelas. 2005. Running to Stand Still: Adaptation and the Response of Plants to Rapid Climate Change. Ecology Letters 8:1010–1020.

Kasischke, E. S., and M. R. Turetsky. 2006. Recent Changes in the Fire Regime Across the North American Boreal Region - Spatial and Temporal Patterns of Burning Across Canada and Alaska. Geophysical Research Letters 33:1–5.

Kaufmann, M. R., D. W. Huisjen, S. Kitchen, M. Babler, S. R. Abella, S. Gardiner, D. Mcavoy, and J. Howie. 2016. Gambel Oak Ecology and Management in the Southern Rockies: The Status of Our Knowledge. Southern Rockies Fire Science Network, Fort Collins, CO.

Kaufmann, M. R., C. M. Regan, and P. M. Brown. 2000. Heterogeneity in Ponderosa Pine/Douglas-Fir Forests: Age and Size Structure in Unlogged and Logged Landscapes of Central Colorado. Canadian Journal of Forest Research 30:698–711.

Keane, R. E., P. F. Hessburg, P. B. Landres, and F. J. Swanson. 2009. The Use of Historical Range and Variability (HRV) in Landscape Management. Forest Ecology and Management 258:1025–1037.

Keenan, R. J., G. A. Reams, F. Achard, J. V. de Freitas, A. Grainger, and E. Lindquist. 2015. Dynamics of Global Forest Area: Results from the FAO Global Forest Resources Assessment 2015. Forest Ecology and Management 352:9–20.

Kemp, K. B., P. E. Higuera, and P. Morgan. 2016. Fire Legacies Impact Conifer Regeneration Across Environmental Gradients in the U.S. Northern Rockies. Landscape Ecology 31:619–635.

Kemp, K. B., P. E. Higuera, P. Morgan, and J. T. Abatzoglou. 2019. Climate Will Increasingly Determine Post-Fire Tree Regeneration Success in Low-Elevation Forests, Northern Rockies, USA. Ecosphere 10:e02568.

Keyser, T. L., L. B. Lentile, F. W. Smith, and W. D. Shepperd. 2008. Changes in Forest Structure After a Large, Mixed-Severity Wildfire in Ponderosa Pine Forests of the Black Hills, South Dakota, USA. Forest Science 54:328–338.

Kittel, T. G. F., M. W. Williams, K. Chowanski, M. Hartman, T. Ackerman, M. Losleben, and P. D. Blanken. 2015. Contrasting Long-Term Alpine and Subalpine Precipitation Trends in a Mid-Latitude North American Mountain System, Colorado Front Range, USA. Plant Ecology and Diversity 8:607–624.

Kitzberger, T., P. M. Brown, E. K. Heyerdahl, T. W. Swetnam, and T. T. Veblen. 2007. Contingent Pacific-Atlantic Ocean Influence on Multicentury Wildfire Synchrony Over Western North America. Proceedings of the National Academy of Sciences 104:543–548.

Kitzberger, T., D. A. Falk, A. L. Westerling, and T. W. Swetnam. 2017. Direct and Indirect Climate Controls Predict Heterogeneous Early-Mid 21st Century Wildfire Burned Area Across Western and Boreal North America. PLoS ONE 12:1–24.

Krannitz, P. G., and T. E. Duralia. 2004. Cone and Seed Production in Pinus ponderosa: A Review. Western North American Naturalist 64:208–218.

Krawchuk, M. A., S. L. Haire, J. Coop, M. A. Parisien, E. Whitman, G. Chong, and C. Miller. 2016. Topographic and Fire Weather Controls of Fire Refugia in Forested Ecosystems of Northwestern North America. Ecosphere 7:e01632.

Kuhn, M. 2008. Building Predictive Models in R Using the caret Package. Journal of Statistical Software 28:1–26.

Kurtzman, D., and B. R. Scanlon. 2007. El Niño-Southern Oscillation and Pacific Decadal Oscillation Impacts on Precipitation in the Southern and Central United States: Evaluation of Spatial Distribution and Predictions. Water Resources Research 43:1–12.

Landres, P. B., P. Morgan, F. J. Swanson, S. E. Applications, and N. Nov. 1999. Overview of the Use of Natural Variability Concepts in Managing Ecological Systems. Ecological Applications 9:1179–1188.

Lanini, W. T., and S. R. Radosevich. 1986. Response of Three Conifer Species to Site Preparation and Shrub Control. Forest Science 32:61–77.

Larson, A. J., and D. Churchill. 2012. Tree Spatial Patterns in Fire-Frequent Forests of Western North America, Including Mechanisms of Pattern Formation and Implications for Designing Fuel Reduction and Restoration Treatments. Forest Ecology and Management 267:74–92.

League, K., and T. Veblen. 2006. Climatic Variability and Episodic Pinus ponderosa Establishment Along the Forest-Grassland Ecotones of Colorado. Forest Ecology and Management 228:98–107.

Leyk, S., J. H. Uhl, D. Balk, and B. Jones. 2018. Assessing the Accuracy of Multi-Temporal Built-Up Land Layers Across Rural-Urban Trajectories in the United States. Remote Sensing of Environment 204:898–917.

Leyk, S., and N. E. Zimmermann. 2004. A Predictive Uncertainty Model for Field-Based Survey Maps Using Generalized Linear Models. Lecture Notes in Computer Science 3234:191–205.

Leyk, S., and N. E. Zimmermann. 2007. Improving Land Change Detection Based on Uncertain Survey Maps Using Fuzzy Sets. Landscape Ecology 22:257–272.

Liebmann, M. J., J. Farella, C. I. Roos, A. Stack, S. Martini, and T. W. Swetnam. 2016. Native American Depopulation, Reforestation, and Fire Regimes in the Southwest United States, 1492-1900 CE. Proceedings of the National Academy of Sciences 113:696–704.

Ligon, J. D. 1978. Reproductive Interdependence of Piñon Jays and Piñon Pines. Ecologial Monographs 48:111–126.

Littell, J. S., D. M. McKenzie, D. L. Peterson, and A. L. Westerling. 2009. Climate and Wildfire Area Burned in Western U.S. Ecoprovinces, 1916-2003. Ecological Applications 19:1003–1021.

Littell, J. S., D. L. Peterson, K. L. Riley, Y. Liu, and C. H. Luce. 2016. A Review of the Relationships Between Drought and Forest Fire in the United States. Global Change Biology 22:2353–2369.

Liu, Y., S. L. Goodrick, and J. A. Stanturf. 2013. Future U.S. Wildfire Potential Trends Projected Using a Dynamically Downscaled Climate Change Scenario. Forest Ecology and Management 294:120–135.

Lukas, J., J. Barsugli, N. Doesken, I. Rangwala, and K. Wolter. 2014. Climate Change in Colorado: A Synthesis to Support Water Resources Management and Adaptation. University of Colorado Press, Boulder, CO.

Lutz, J. A., J. W. van Wagtendonk, and J. F. Franklin. 2010. Climatic Water Deficit, Tree Species Ranges, and Climate Change in Yosemite National Park. Journal of Biogeography 37:936–950.

Lydersen, J. M., and B. M. Collins. 2018. Change in Vegetation Patterns Over a Large Forested Landscape Based on Historical and Contemporary Aerial Photography. Ecosystems 21:1348–1363.

Maguire, W. P. 1956. Are Ponderosa Pine Cone Crops Predictable? Journal of Forestry 54:778–779.

van Mantgem, P. J., N. L. Stephenson, J. C. Byrne, L. D. Daniels, J. F. Franklin, P. Z. Fulé, M. E. Harmon, A. J. Larson, J. M. Smith, A. H. Taylor, and T. T. Veblen. 2009. Widespread Increase of Tree Mortality Rates in the Western United States. Science 323:521–524.

Mast, J. N., T. T. Veblen, and M. E. Hodgson. 1997. Tree Invasion Within a Pine/Grassland Ecotone: An Approach with Historic Aerial Photography and GIS Modeling. Forest Ecology and Management 93:181–194.

Mast, J. N., T. T. Veblen, and Y. B. Linhart. 1998. Disturbance and Climatic Influences on Age Structure of Ponderosa Pine at the Pine/Grassland Ecotone, Colorado Front Range. Journal of Biogeography 25:743–755.

Matonis, M. S., D. Binkley, M. C. Tuten, and A. S. Cheng. 2014. The Forests They Are A - Changin ' - Ponderosa Pine and Mixed Conifer Forests on the Uncompahgre in 1875 and 2010-13. Colorado Forest Restoration Institute, Fort Collins, CO.

Matthews, L. E. 2005. Historical Imagery Holdings For The United States Department of Agriculture. United States Department of Agriculture Aerial Photography Field Office, Salt Lake City, UT.

McCaughey, W. W., W. C. Schmidt, and R. C. Shearer. 1986. Seed-Dispersal Characteristics of Conifers in the Inland Mountain West. Pages 50–62 in R. C. Shearer, editor. Conifer Tree Seed in the Inland Mountain West Symposium. Gen. Tech. Rep. INT-GTR-203. USDA Forest Service, Intermountain Research Station, Missoula, MT.

McCullough, I. M., F. W. Davis, J. R. Dingman, L. E. Flint, A. L. Flint, J. M. S. Alexandra, M. A. Moritz, L. Hannah, and J. Franklin. 2016. High and Dry: High Elevations Disproportionately Exposed to Regional Climate Change in Mediterranean-Climate Landscapes. Landscape Ecology 31:1063–1075.

McCune, B., and D. Keon. 2002. Equations for Potential Annual Direct Incident Radiation and Heat Load. Journal of Vegetation Science 13:603–606.

McKenney, D., J. Pedlar, and G. O. Neill. 2009. Climate Change and Forest Seed Zones: Past Trends, Future Prospects and Challenges to Ponder. The Forestry Chronicle 85:258–266.

Meigs, G. W., and M. A. Krawchuk. 2018. Composition and Structure of Forest Fire Refugia: What are the Ecosystem Legacies Across Burned Landscapes? Forests 9:243.

Merschel, A. G., T. A. Spies, and E. K. Heyerdahl. 2014. Mixed-Conifer Forests of Central Oregon: Effects of Logging and Fire Exclusion Vary with Environment. Ecological Applications 24:1670–1688.

Millar, C. I., and N. L. Stephenson. 2015. Temperate Forest Health in an Era of Emerging Megadisturbance. Science 349:823–826.

Millar, C. I., N. L. Stephenson, and S. L. Stephens. 2007. Climate Change and Forests of the Future: Managing in the Face of Uncertainty. Ecological Applications 17:2145–2151.

Miller, J. D., E. E. Knapp, C. H. Key, C. N. Skinner, C. J. Isbell, R. M. Creasy, and J. W. Sherlock. 2009a. Calibration and Validation of the Relative Differenced Normalized Burn Ratio (RdNBR) to Three Measures of Fire Severity in the Sierra Nevada and Klamath Mountains, California, USA. Remote Sensing of Environment 113:645–656.

Miller, J. D., H. D. Safford, M. A. Crimmins, and A. E. Thode. 2009b. Quantitative Evidence for Increasing Forest Fire Severity in the Sierra Nevada and Southern Cascade Mountains, California and Nevada, USA. Ecosystems 12:16–32.

Miller, J. D., and A. E. Thode. 2007. Quantifying Burn Severity in a Heterogeneous Landscape With A Relative Version of the Delta Normalized Burn Ratio (dNBR). Remote Sensing of Environment 109:66–80.

Mooney, K. A., Y. B. Linhart, and M. A. Snyder. 2011. Masting in Ponderosa Pine: Comparisons of Pollen and Seed Over Space and Time. Oecologia 165:651–661.

Moore, M. M., D. W. Huffman, J. D. Bakker, A. J. Sánchez Meador, D. M. Bell, P. Z. Fulé, P. F. Parysow, and W. W. Covington. 2004. Quantifying Forest Reference Conditions for Ecological Restoration: The Woolsey Plots. Final Report to the Ecological Restoration Institute for the Southwest Fire Initiative. Flagstaff, AZ.

Morgan, J. L., S. E. Gergel, and N. C. Coops. 2010. Aerial Photography: A Rapidly Evolving Tool for Ecological Management. BioScience 60:47–59.

Naficy, C. E., E. G. Keeling, P. Landres, P. F. Hessburg, T. T. Veblen, and A. Sala. 2016. Wilderness in the 21st Century: A Framework for Testing Assumptions about Ecological Intervention in Wilderness Using a Case Study of Fire Ecology in the Rocky Mountains. Journal of Forestry 114:384–395.

Naficy, C. E., A. Sala, E. G. Keeling, J. Graham, and T. H. DeLuca. 2010. Interactive Effects of Historical Logging and Fire Exclusion on Ponderosa Pine Forest Structure in the Northern Rockies. Ecological Applications 20:1851–1864.

Nalder, I. A., and R. W. Wein. 1998. Spatial Interpolation of Climatic Normals: Test of a New Method in the Canadian Boreal Forest. Agricultural and Forest Meteorology 92:211–225.

Natural Resources Conservation Service, University Camp Snow Course. 2016. <https://wcc.sc.egov.usda.gov/nwcc/rgrpt?report=snowcourse&state=CO>

Nicotra, A. B., O. K. Atkin, S. P. Bonser, A. M. Davidson, E. J. Finnegan, U. Mathesius, P. Poot, M. D. Purugganan, C. L. Richards, F. Valladares, and M. van Kleunen. 2010. Plant Phenotypic Plasticity in a Changing Climate. Trends in Plant Science 15:684–692.

Normand, S., R. E. Ricklefs, F. Skov, J. Bladt, O. Tackenberg, and J. C. Svenning. 2011. Postglacial Migration Supplements Climate in Determining Plant Species Ranges in Europe. Proceedings of the Royal Society B: Biological Sciences 278:3644–3653.

North, M. P., J. T. Stevens, D. F. Greene, M. Coppoletta, E. E. Knapp, A. M. Latimer, C. M. Restaino, R. E. Tompkins, K. R. Welch, R. A. York, D. J. N. Young, J. N. Axelson, T. N. Buckley, B. L. Estes, R. N. Hager, J. W. Long, M. D. Meyer, S. M. Ostoja, H. D. Safford, K. L. Shive, C. L. Tubbesing, H. Vice, D. Walsh, C. M. Werner, and P. Wyrsch. 2019. Tamm Review: Reforestation for Resilience in Dry Western U.S. Forests. Forest Ecology and Management 432:209–224.

Oliphant, T. E. 2007. Python for Scientific Computing. Computing in Science and Engineering 9:10–20.

Olofsson, P., G. M. Foody, M. Herold, S. V. Stehman, C. E. Woodcock, and M. A. Wulder. 2014. Good Practices for Estimating Area and Assessing Accuracy of Land Change. Remote Sensing of Environment 148:42–57.

Omernik, J. M., and G. E. Griffith. 2014. Ecoregions of the Conterminous United States: Evolution of a Hierarchical Spatial Framework. Environmental Management 54:1249–1266.

Ouzts, J., T. Kolb, D. Huffman, and A. Sánchez Meador. 2015. Post-Fire Ponderosa Pine Regeneration With and Without Planting in Arizona and New Mexico. Forest Ecology and Management 354:281–290.

Owen, S. M., C. H. Sieg, A. J. Sánchez Meador, P. Z. Fulé, J. M. Iniguez, L. S. Baggett, P. J. Fornwalt, and M. A. Battaglia. 2017. Spatial Patterns of Ponderosa Pine Regeneration in High-Severity Burn Patches. Forest Ecology and Management 405:134–149.

Paritsis, J., T. T. Veblen, and A. Holz. 2015. Positive Fire Feedbacks Contribute to Shifts from Nothofagus pumilio Forests to Fire-Prone Shrublands in Patagonia. Journal of Vegetation Science 26:89–101.

Parks, S. A., S. Z. Dobrowski, J. D. Shaw, and C. Miller. 2019. Living on the Edge: Trailing Edge Forests at Risk of Fire-Facilitated Conversion to Non-Forest. Ecosphere 10:e02651.

Parks, S. A., C. Miller, C. R. Nelson, and Z. A. Holden. 2014. Previous Fires Moderate Burn Severity of Subsequent Wildland Fires in Two Large Western US Wilderness Areas. Ecosystems 17:29–42.

Parmesan, C., and G. Yohe. 2003. A Globally Coherent Fingerprint of Climate Change Impacts Across Natural Systems. Nature 421:37–42.

Pausas, J. G. 2015. Bark Thickness and Fire Regime. Functional Ecology 29:315–327.

Pearson, G. A. 1942. Herbaceous Vegetation a Factor in Natural Regeneration of Ponderosa Pine in the Southwest. Ecological Monographs 12:315–338.

Pearson, R. G., and T. P. Dawson. 2003. Predicting the Impacts of Climate Change on the Distribution of Species: Are Bioclimate Envelope Models Useful? Global Ecology and Biogeography 12:361–371.

Peet, R. 1981. Forest Vegetation of the Colorado Front Range. Vegetatio 45:3–75.

Pellegrini, A. F. A., W. R. L. Anderegg, C. E. T. Paine, W. A. Hoffmann, T. Kartzinel, S. S. Rabin, D. Sheil, A. C. Franco, and S. W. Pacala. 2017. Convergence of Bark Investment According to Fire and Climate Structures Ecosystem Vulnerability to Future Change. Ecology Letters 20:307–316.

Petrie, M. D., J. B. Bradford, R. M. Hubbard, W. K. Lauenroth, C. M. Andrews, and D. R. Schlaepfer. 2017. Climate Change May Restrict Dryland Forest Regeneration in the 21st Century. Ecology 98:1548–1559.

Picotte, J. J., B. Peterson, G. Meier, and S. M. Howard. 2016. 1984–2010 Trends in Fire Burn Severity and Area for the Conterminous US. International Journal of Wildland Fire 25:413–420.

Platt, R. V., and T. Schoennagel. 2009. An Object-Oriented Approach to Assessing Changes in Tree Cover in the Colorado Front Range 1938-1999. Forest Ecology and Management 258:1342–1349.

Platt, R. V., T. Schoennagel, T. T. Veblen, and R. L. Sherriff. 2011. Modeling Wildfire Potential in Residential Parcels: A Case Study of the North-Central Colorado Front Range. Landscape and Urban Planning 102:117–126.

Platt, R. V, T. T. Veblen, and R. L. Sherriff. 2006. Are Wildfire Mitigation and Restoration of Historic Forest Structure Compatible? A Spatial Modeling Assessment. Annals of the Association of American Geographers 96:455–470.

Potter, K. M., and W. W. Hargrove. 2012. Determining Suitable Locations For Seed Transfer Under Climate Change: A Global Quantitative Method. New Forests 43:581–599.

PRISM Climate Group, Oregon State University. 2018. <http://prism.oregonstate.edu>

Puhlick, J. J., D. C. Laughlin, and M. M. Moore. 2012. Factors Influencing Ponderosa Pine Regeneration in the Southwestern USA. Forest Ecology and Management 264:10–19.

Quintero, I., and J. A. Wiens. 2013. Rates of Projected Climate Change Dramatically Exceed Past Rates of Climatic Niche Evolution Among Vertebrate Species. Ecology Letters 16:1095–1103.

R Core Team. 2018. R: A Language and Environment for Statistical Computing. R Foundation for Statistical Computing, Vienna, Austria.

Radeloff, V. C., R. B. Hammer, and S. I. Stewart. 2005. Rural and Suburban Sprawl in the U.S. Midwest from 1940 to 2000 and Its Relation to Forest Fragmentation. Conservation Biology 19:793–805.

Radeloff, V. C., D. P. Helmers, H. A. Kramer, M. H. Mockrin, P. M. Alexandre, A. Bar-Massada, V. Butsic, T. J. Hawbaker, S. Martinuzzi, A. D. Syphard, and S. I. Stewart. 2018. Rapid Growth of the US Wildland-Urban Interface Raises Wildfire Risk. Proceedings of the National Academy of Sciences 115:3314–3319.

Radoux, J., and P. Bogaert. 2017. Good Practices for Object-Based Accuracy Assessment. Remote Sensing 9:646.

Rebertus, A. J., B. R. Burns, and T. T. Veblen. 1991. Stand Dynamics of Pinus flexilis-Dominated Subalpine Forests in the Colorado Front Range. Journal of Vegetation Science 2:445–458.

Redmond, M. D., F. Forcella, and N. N. Barger. 2012. Declines in Pinyon Pine Cone Production Associated With Regional Warming. Ecosphere 3:1–14.

Redmond, M. D., P. J. Weisberg, N. S. Cobb, C. A. Gehring, A. V Whipple, and T. G. Whitham. 2016. A Robust Method to Determine Historical Annual Cone Production Among Slow-Growing Conifers. Forest Ecology and Management 368:1–6.

Rehfeldt, G. E., N. L. Crookston, M. V. Warwell, and J. S. Evans. 2006. Empirical Analyses of Plant-Climate Relationships for the Western United States. International Journal of Plant Sciences 167:1123–1150.

Reynolds, R. T., A. J. Sánchez Meador, J. A. Youtz, T. Nicolet, M. S. Matonis, P. L. Jackson, D. G. Delorenzo, A. D. Graves. 2013. Restoring Composition and Structure in Southwestern Frequent-Fire Forests : A Science-Based Framework for Improving Ecosystem Resiliency. RMRS GTR-310. USDA Forest Service, Rocky Mountain Research Station, Fort Collins, CO.

Riahi, K., S. Rao, V. Krey, C. Cho, V. Chirkov, and G. Fischer. 2011. RCP 8.5 - A Scenario of Comparatively High Greenhouse Gas Emissions. Climatic Change 109:33–57.

Richards, J. A. 2013. Remote Sensing Digital Image Analysis. 5th edition. Springer, New York.

Ritchie, M., and E. Knapp. 2014. Establishment of a Long-Term Fire Salvage Study in an Interior Ponderosa Pine Forest. Journal of Forestry 112:395–400.

Rocca, M. E., P. M. Brown, L. H. MacDonald, and C. M. Carrico. 2014. Climate Change Impacts on Fire Regimes and Key Ecosystem Services in Rocky Mountain Forests. Forest Ecology and Management 327:290–305.

Roccaforte, J. P., P. Z. Fulé, W. W. Chancellor, and D. C. Laughlin. 2012. Woody Debris and Tree Regeneration Dynamics Following Severe Wildfires in Arizona Ponderosa Pine Forests. Canadian Journal of Forest Research 42:593–604.

Roccaforte, J. P., A. Sánchez, A. E. M. Waltz, M. L. Gaylord, M. T. Stoddard, and D. W. Hu. 2018. Delayed Tree Mortality, Bark Beetle Activity, and Regeneration Dynamics Five Years

Following the Wallow Fire, Arizona, USA: Assessing Trajectories Towards Resiliency. Forest Ecology and Management 428:20–26.

Rodman, K. C., A. J. Sánchez Meador, M. M. Moore, and D. W. Huffman. 2017. Reference Conditions Are Influenced by the Physical Template and Vary by Forest Type: A Synthesis of Pinus ponderosa-Dominated Sites in the Southwestern United States. Forest Ecology and Management 404:316–329.

Rodman, K. C., T. T. Veblen, T. B. Chapman, M. T. Rother, A. P. Wion, and M. D. Redmond. *In Review*. Limitations to Recovery Following Wildfire in Dry Forests of Southern Colorado and Northern New Mexico, USA.

Rodman, K. C., T. T. Veblen, S. Saraceni, and T. B. Chapman. 2019. Wildfire Activity and Land Use Drove 20th Century Changes in Forest Cover in the Colorado Front Range. Ecosphere 10:e02594.

Rollins, M. G. 2009. LANDFIRE: A Nationally Consistent Vegetation, Wildland Fire, and Fuel Assessment. International Journal of Wildland Fire 18:235–249.

Romme, W. H., C. D. Allen, J. D. Bailey, W. L. Baker, B. T. Bestelmeyer, P. M. Brown, K. S. Eisenhart, M. L. Floyd, D. W. Huffman, B. F. Jacobs, R. F. Miller, E. H. Muldavin, T. W. Swetnam, R. J. Tausch, and P. J. Weisberg. 2009a. Historical and Modern Disturbance Regimes, Stand Structures, and Landscape Dynamics in Piñon – Juniper Vegetation of the Western United States. Rangeland Ecology and Management 62:203–222.

Romme, W. H., J. Clement, J. Hicke, D. Kulakowski, L. H. MacDonald, T. L. Schoennagel, and T. T. Veblen. 2006. Recent Forest Insect Outbreaks and Fire Risk in Colorado Forests: A Brief Synthesis of Relevant Research. Colorado Forest Restoration Institute, Fort Collins, CO.

Romme, W. H., M. L. Floyd, D. Hanna, E. J. Bartlett, M. Crist, D. Green, H. D. Grissino-Mayer, J. P. Lindsey, K. McGarigal, and J. S. Redders. 2009b. Historical Range of Variability and Current Landscape Condition Analysis: South Central Highlands Section, Southwestern Colorado & Northwestern New Mexico. Colorado Forest Restoration Institute, Fort Collins, CO.

Rother, M. T., and T. T. Veblen. 2016. Limited Conifer Regeneration Following Wildfires in Dry Ponderosa Pine Forests of the Colorado Front Range. Ecosphere 7:e01594.

Rother, M. T., and T. T. Veblen. 2017. Climate Drives Episodic Conifer Establishment after Fire in Dry Ponderosa Pine Forests of the Colorado. Forests 8:159.

Rother, M. T., T. T. Veblen, and L. G. Furman. 2015. A Field Experiment Informs Expected Patterns of Conifer Regeneration After Disturbance Under Changing Climate Conditions. Canadian Journal of Forest Research 45:1607–1616.

Sánchez Meador, A. J., M. M. Moore, J. D. Bakker, and P. F. Parysow. 2009. 108 Years of Change in Spatial Pattern Following Selective Harvest of a Pinus Ponderosa Stand in Northern Arizona, USA. Journal of Vegetation Science 20:79–90.

Savage, M., P. Brown, and J. J. Feddema. 1996. The Role of Climate in a Pine Forest Regeneration Pulse in the Southwestern United States. Ecoscience 3:310–318.

Savage, M., and J. N. Mast. 2005. How Resilient are Southwestern Ponderosa Pine Forests After Crown Fires? Canadian Journal of Forest Research 35:967–977.

Savage, M., J. N. Mast, and J. J. Feddema. 2013. Double Whammy: High-Severity Fire and Drought in Ponderosa Pine Forests of the Southwest. Canadian Journal of Forest Research 43:570–583.

Scheffer, M., S. R. Carpenter, T. M. Lenton, J. Bascompte, W. Brock, V. Dakos, J. van de Koppel, I. A. van de Leemput, S. A. Levin, E. H. van Nes, M. Pascual, and J. Vandermeer. 2012. Anticipating Critical Transitions. Science 338:344–348.

Schoennagel, T., R. L. Sherriff, and T. T. Veblen. 2011. Fire History and Tree Recruitment in the Colorado Front Range Upper Montane Zone: Implications for Forest Restoration. Ecological Applications 21:2210–2222.

Schoennagel, T., T. T. Veblen, and W. H. Romme. 2004. The Interaction of Fire, Fuels, and Climate Across Rocky Mountain Forests. BioScience 54:393–402.

Schubert, G. H. 1976. Silviculture of Southwestern Ponderosa Pine: The Status of Our Knowledge. Res. Pap. RM-123. USDA Forest Service, Rocky Mountain Forest and Range Experiment Station, Fort Collins, CO.

Scott, D. W. 1992. Multivariate Density Estimation. Theory, Practice, and Visualization. Wiley, New York.

Sen, P. K. 1968. Estimates of the Regression Coefficient Based on Kendall's Tau. Journal of the American Statistical Association 63:1379–1389.

Shatford, J. P. A., D. E. Hibbs, and K. J. Puettmann. 2007. Conifer Regeneration after Forest Fire in the Klamath-Siskiyous: How Much, How Soon? Journal of Forestry 105:139–146.

Shepperd, W. D., C. B. Edminster, and S. A. Mata. 2006. Long-Term Seedfall, Establishment, Survival, and Growth of Natural and Planted Ponderosa Pine in the Colorado Front Range. Western Journal of Applied Forestry 21:19–26.

Sherriff, R. L., R. V Platt, T. T. Veblen, T. L. Schoennagel, and M. H. Gartner. 2014. Historical, Observed, and Modeled Wildfire Severity in Montane Forests of the Colorado Front Range. PLoS one 9:1–17.

Sherriff, R. L., and T. T. Veblen. 2006. Ecological Effects of Changes in Fire Regimes in Pinus ponderosa Ecosystems in the Colorado Front Range. Journal of Vegetation Science 17:705–718.

Sherriff, R. L., and T. T. Veblen. 2007. A Spatially-Explicit Reconstruction of Historical Fire Occurrence in the Ponderosa Pine Zone of the Colorado Front Range. Ecosystems 10:311–323.

Sherriff, R. L., and T. T. Veblen. 2008. Variability in Fire-Climate Relationships in Ponderosa Pine Forests in the Colorado Front Range. International Journal of Wildland Fire 17:50–59.

Sherriff, R. L., T. T. Veblen, and J. S. Sibold. 2001. Fire History in High Elevation Subalpine Forests in the Colorado Front Range. Ecoscience 8:369–380.

Shive, K. L., H. K. Preisler, K. R. Welch, H. D. Safford, R. J. Butz, K. L. O'Hara, and S. L. Stephens. 2018. From the Stand-Scale to the Landscape-Scale: Predicting the Spatial Patterns of Forest Regeneration After Disturbance. Ecological Applications 28:1626–1639.

Sibold, J. S., and T. T. Veblen. 2006. Relationships of Subalpine Forest Fires in the Colorado Front Range to Interannual and Multi-Decadal Scale Climate Variations. Journal of Biogeography 33:833–842.

Sibold, J. S., T. T. Veblen, K. Chipko, L. Lawson, E. Mathis, and J. Scott. 2007. Influences of Secondary Disturbances on Lodgepole Pine Stand Development in Rocky Mountain National Park. Ecological Applications 17:1638–1655.

Sibold, J. S., T. T. Veblen, and M. E. González. 2006. Spatial and Temporal Variation in Historic Fire Regimes in Subalpine Forests Across the Colorado Front Range in Rocky Mountain National Park, Colorado, USA. Journal of Biogeography 33:631–647.

Simeone, C., M. P. Maneta, Z. A. Holden, G. Sapes, A. Sala, and S. Z. Dobrowski. 2019. Coupled Ecohydrology and Plant Hydraulics Modeling Predicts Ponderosa Pine Seedling Mortality and Lower Treeline in the US Northern Rocky Mountains. New Phytologist 221:1814–1830.

Simmons, V. M. 2000. The Ute Indians of Utah, Colorado, and New Mexico. University Press of Colorado, Boulder, CO.

Singleton, M., A. Thode, A. Sanchez Meador, and P. Iniguez. 2018. Increasing Trends in High-Severity Fire in the Southwestern USA from 1984-2015. Forest Ecology and Management 433:709–719.

Sohl, T., R. Reker, M. Bouchard, K. Sayler, J. Dornbierer, S. Wika, R. Quenzer, and A. Friesz. 2016. Modeled Historical Land Use and Land Cover for the Conterminous United States. Journal of Land Use Science 11:476–499.

Song, X.-P., M. C. Hansen, S. V. Stehman, P. V. Potapov, A. Tyukavina, E. F. Vermote, and J. R. Townshend. 2018. Global Land Change from 1982 to 2016. Nature 560:639–643.

Spracklen, D. V., L. J. Mickley, J. A. Logan, R. C. Hudman, R. Yevich, M. D. Flannigan, and A. L. Westerling. 2009. Impacts of Climate Change From 2000 to 2050 on Wildfire Activity and Carbonaceous Aerosol Concentrations in the Western United States. Journal of Geophysical Research 114:1–17.

Stahelin, R. 1943. Factors Influencing the Natural Restocking of High Altitude Burns by Coniferous Trees in the Central Rocky Mountains. Ecology 24:19–30.

Stephenson, N. L. 1998. Actual Evapotranspiration and Deficit: Biologically Meaningful Correlates of Vegetation Distribution Across Spatial Scales. Journal of Biogeography 25:855–870.

Stevens-Rumann, C. S., K. B. Kemp, P. E. Higuera, B. J. Harvey, M. T. Rother, D. C. Donato, P. Morgan, and T. T. Veblen. 2018. Evidence for Declining Forest Resilience to Wildfires Under Climate Change. Ecology Letters 21:243–252.

Stevens-Rumann, C. S., and P. Morgan. 2016. Repeated Wildfires Alter Forest Recovery of Mixed--Conifer -Ecosystems. Ecological Applications 26:1842–1853.

Stocker, T. F., Q. Dahe, G.-K. Plattner, L. V. Alexander, S. K. Allen, N. L. Bindoff, F.-M. Bréon, J. A. Church, U. Cubash, S. Emori, P. Forster, P. Friedlingstein, L. D. Talley, D. G. Vaughan, and S.-P. Xie. 2013. Climate Change 2013: The Physical Science Basis. Contribution of Working Group I to the Fifth Assessment Report of the Intergovernmental Panel on Climate Change. Cambridge University Press, New York.

Stoddard, M. T., D. W. Huffman, P. Z. Fulé, J. E. Crouse, and A. J. Sánchez Meador. 2018. Forest Structure and Regeneration Responses 15 Years After Wildfire in a Ponderosa Pine and Mixed-Conifer Ecotone, Arizona, USA. Fire Ecology 14:12.

Swetnam, T. W., and C. H. Baisan. 1996. Historical Fire Regime Patterns in the Southwestern United States Since AD 1700. Pages 11–32 in C. D. Allen, editor. Fire Effects in Southwestern Forests: Proceedings of the 2nd La Mesa Fire Symposium, Los Alamos, NM.

Telewski, F. W. 1993. Determining the Germination Date of Woody Plants: A Proposed Method for Locating the Root/Shoot Interface. Tree-Ring Bulletin 53:13–16.

Tepley, A. J., E. Thomann, T. T. Veblen, G. L. W. Perry, A. Holz, J. Paritsis, T. Kitzberger, and K. J. Anderson-Teixeira. 2018. Influences of Fire-Vegetation Feedbacks and Post-Fire Recovery Rates on Forest Landscape Vulnerability to Altered Fire Regimes. Journal of Ecology 106:1925–1940.

Tepley, A. J., J. R. Thompson, H. E. Epstein, and K. J. Anderson-Teixeira. 2017. Vulnerability to Forest Loss Through Altered Postfire Recovery Dynamics in a Warming Climate in the Klamath Mountains. Global Change Biology 23:4117–4132.

Tepley, A. J., and T. T. Veblen. 2015. Spatiotemporal Fire Dynamics in Mixed-Conifer and Aspen Forests in the San Juan Mountains of Southwestern Colorado, USA. Ecological Monographs 85:583–603.

Theil, H. 1950. A Rank-Invariant Method of Linear and Polynomial Regression Analysis. Nederlandse Akademie van Weinenschatpen A 53:1397–1412.

Theobald, D. M., D. Harrison-Atlas, and W. B. Monahan. 2015. Ecologically-Relevant Maps of Landforms and Physiographic Diversity for Climate Adaptation Planning. PLoS ONE 10:1–17.

Theobald, D. M., and W. H. Romme. 2007. Expansion of the US Wildland-Urban Interface. Landscape and Urban Planning 83:340–354.

Turner, M. G. 2010. Disturbance and Landscape Dynamics in a Changing World. Ecology 91:2833–2849.

Tylianakis, J. M., R. K. Didham, J. Bascompte, and D. A. Wardle. 2008. Global Change and Species Interactions in Terrestrial Ecosystems. Ecology Letters 11:1351–1363.

Urza, A. K., and J. S. Sibold. 2013. Nondestructive Aging of Postfire Seedlings for Four Conifer Species in Northwestern Montana. Western Journal of Applied Forestry 28:22–29.

United States Census Bureau, TIGER/Line Shapefiles. 2017. <https://www.census.gov/geo/maps-data/data/tiger-line.html>

United States Forest Service, National Agriculture Imagery Program. 2015. <http://www.fsa.usda.gov/programs-and-services/aerial-photography/imagery-programs/naip-imagery/>

United States Forest Service, R2 Aerial Detection Survey. 2015. <http://www.fs.usda.gov/detail/r2/forest-grasslandhealth/?cid=fsbdev3_041629>

United States Geological Survey, eMODIS Remote Sensing Phenology. 2015. <https://lta.cr.usgs.gov/emodis_phen>

United States Geological Survey, Federal Wildland Fire Occurrence Data. 2018. <https://wildfire.cr.usgs.gov/firehistory/data.html>

United States Geological Survey, Geospatial Multi-Agency Coordination (GeoMAC). 2018. <https://rmgsc.cr.usgs.gov/outgoing/GeoMAC/>

United States Geological Survey, Mineral Resource Data System. 2005. <https://mrdata.usgs.gov/mrds/>

United States Geological Survey, National Elevation Dataset. 1999. <https://nationalmap.gov/elevation.html>

United States Geological Survey, National Hydrography Dataset (NHDPlus). 2018.

<https://nhd.usgs.gov/>

USGCRP. 2017. Climate Science Special Report: Fourth National Climate Assessment. Page (D. J. Wuebbels, D. W. Fahey, K. A. Hibbard, D. J. Dokken, B. C. Stewart, and T. K. Maycock, Eds.). US Global Change Research Program, Washington, D.C.

Veblen, T. T. 1986. Age and Size Structure of Subalpine Forests in the Colorado Front Range. Bulletin of the Torrey Botanical Club 113:225–240.

Veblen, T. T., and J. A. Donnegan. 2005. Historical Range of Variability for Forest Vegetation of the National Forests of the Colorado Front Range. USDA Forest Service, Rocky Mountain Region and the Colorado Forest Restoration Institute, Golden, CO.

Veblen, T. T., K. S. Hadley, M. S. Reid, and A. J. Rebertus. 1991. The Response of Subalpine Forests to Spruce Beetle Outbreak in Colorado. Ecology 72:213–231.

Veblen, T. T., T. Kitzberger, and J. Donnegan. 2000. Climatic and Human Influences on Fire Regimes in Ponderosa Pine forests in the Colorado Front Range. Ecological Applications 10:1178–1195.

Veblen, T. T., and D. C. Lorenz. 1986. Anthropogenic Disturbance and Recovery Patterns in Montane Forests, Colorado Front Range. Physical Geography 7:1–24.

Veblen, T. T., and D. C. Lorenz. 1991. The Colorado Front Range: A Century of Ecological Change. University of Utah Press, Salt Lake City, UT.

Veblen, T. T., W. H. Romme, and C. M. Regan. 2012. Regional Application of Historical Ecology at Ecologically Defined Scales: Forest Ecosystems in the Colorado Front Range. Pages 149–165 *in* J. A. Wiens, G. D. Hayward, H. D. Safford, and C. Giffen, editors. Historical Environmental Variation in Conservation and Natural Resource Management. Wiley-Blackwell, Hoboken, NJ.

Villalba, R., T. T. Veblen, and J. Ogden. 1994. Climatic Influences on the Growth of Subalpine Trees in the Colorado Front Range. Ecology 75:1450–1462.

Vander Wall, S. B. 2008. On the Relative Contributions of Wind vs. Animals to Seed Dispersal of Four Sierra Nevada Pines. Ecology 89:1837–1849.

Walter, I. A., R. G. Allen, R. Elliot, B. Mecham, M. E. Jensen, D. Itenfisu, T. A. Howell, R. Snyder, P. Brown, S. Echings, T. Spofford, M. Hattendorf, R. H. Cuenca, J. L. Wright, and D. Martin. 2000. ASCE Standardized Reference Evapotranspiration Equation. Pages 209–215 in R. G. Evans, B. L. Benham, and T. P. Trooien, editors. Proceedings of the National Irrigation Symposium. Phoenix, AZ.

Waters, M. R., and T. W. Stafford Jr. 2007. Redefining the Age of Clovis: Implications for the Peopling of the Americas. Science 315:1122–1127.

Weiss, A. D. 2001. Topographic Position and Landforms Analysis. ESRI User Conference. San Diego, CA.

Welch, K. R., H. D. Safford, and T. P. Young. 2016. Predicting Conifer Establishment 5-7 years After Wildfire in Middle Elevation Yellow Pine and Mixed Conifer Forests of the North American Mediterranean-Climate Zone. Ecosphere 7:1–29.

Westerling, A. L. 2016. Increasing Western US Forest Wildfire Activity: Sensitivity to Changes in the Timing of Spring. Philosophical Transactions of The Royal Society B: Biological Sciences 371:1–10.

Westerling, A. L., M. G. Turner, E. A. H. Smithwick, W. H. Romme, and M. G. Ryan. 2011. Continued Warming Could Transform Greater Yellowstone Fire Regimes by Mid-21st Century. Proceedings of the National Academy of Sciences 108:13165–13170.

Williams, A. P., C. D. Allen, A. K. Macalady, D. Griffin, C. A. Woodhouse, D. M. Meko, T. W. Swetnam, S. A. Rauscher, R. Seager, H. D. Grissino-Mayer, J. S. Dean, E. R. Cook, C. Gangodagamage, M. Cai, and N. G. McDowell. 2012. Temperature as a Potent Driver of Regional Forest Drought Stress and Tree Mortality. Nature Climate Change 3:292–297.

Williams, A. P., R. Seager, A. K. Macalady, M. Berkelhammer, M. A. Crimmins, T. W. Swetnam, A. T. Trugman, N. Buenning, D. Noone, N. G. McDowell, N. Hryniw, C. I. Mora, and T. Rahn. 2015. Correlations Between Components of the Water Balance and Burned Area Reveal New Insights for Predicting Forest Fire Area in the Southwest United States. International Journal of Wildland Fire 24:14–26.

Williams, M. A., and W. L. Baker. 2012a. Comparison of the Higher-Severity Fire Regime in Historical (A.D. 1800s) and Modern (A.D. 1984-2009) Montane Forests Across 624,156 ha of the Colorado Front Range. Ecosystems 15:832–847.

Williams, M. A., and W. L. Baker. 2012b. Spatially Extensive Reconstructions Show Variable-Severity Fire and Heterogeneous Structure in Historical Western United States Dry Forests. Global Ecology and Biogeography 21:1042–1052.

Williams, M. I., and R. K. Dumroese. 2013. Preparing for Climate Change: Forestry and Assisted Migration. Journal of Forestry 111:287–297.

Woolsey, T. S. J. 1912. Permanent Sample Plots. Forestry Quarterly 10:38–44.

Wright, M. N., and A. Ziegler. 2017. ranger: A Fast Implementation of Random Forests for High Dimensional Data. Journal of Statistical Software 77:1–17.

Xu, C., and V. P. Singh. 2002. Cross Comparison of Empirical Equations for Calculating Potential Evapotranspiration with Data from Switzerland. Water Resources Management 16:197–219.

Young, D. J. N., C. M. Werner, K. R. Welch, T. P. Young, H. D. Safford, and A. M. Latimer. 2019. Post-Fire Forest Regeneration Shows Limited Climate Tracking and Potential for Drought-Induced Type Conversion. Ecology 100:e02571.

Ziegler, J. P., C. Hoffman, P. Fornwalt, C. Sieg, M. A. Battaglia, and J. M. Iniguez. 2017. Tree Regeneration Spatial Patterns in Ponderosa Pine Forests Following Stand-Replacing Fire: Influence of Topography and Neighbors. Forests 8:391.

Zier, J. L., and W. L. Baker. 2006. A Century of Vegetation Change in the San Juan Mountains, Colorado: An Analysis Using Repeat Photography. Forest Ecology and Management 228:251–262.

Zuur, A. F., E. N. Ieno, N. J. Walker, A. A. Saveliev, and G. M. Smith. 2009. Mixed Effects Models and Extensions in Ecology and R. Springer, New York.

APPENDIX A

SUPPLEMENTARY MATERIAL FOR CHAPTER 2 – WILDFIRE ACTIVITY AND LAND USE DROVE 20TH CENTURY CHANGES IN FOREST COVER IN THE COLORADO FRONT RANGE

A.1 Comparison Of Changes In Forest Cover With Interannual And Interdecadal Trends In Wildfire And Climate

Because of the potential importance of historical fire activity in driving broad-scale changes in forest cover, we created a fire activity index that quantifies interannual variability in fire activity in the study area c. 1800-2015 using a combination of field-derived fire history data (Sherriff et al. 2014) and burn perimeters from the Monitoring Trends in Burn Severity program (MTBS; Eidenshink et al. 2007). During the 1800-1983 time-period, this index reflects the proportion of montane fire history sites from Sherriff et al. (2014) that experienced spreading fires in a given year (i.e., at least 10% of samples and a minimum of two trees scarred within a stand). From 1984-2015, the index is based on the proportion of the montane zone intersecting MTBS fire perimeters in each year. We focused specifically on the montane zone because identifying important fire years in the subalpine zone would require extensive cohort mapping throughout the NFR, and because fire activity in the subalpine has been very limited through the last century. Given the widespread distribution of fire history sites throughout the NFR, fire history data are fairly compatible with remotely sensed data (i.e., MTBS data) and provide a useful approximation of important regional years of fire activity and general trends c. 1800-2015.

To develop time-series of winter precipitation (November-December$_{t-1}$ and January-May$_t$) and summer (June-August) drought stress (vapor pressure deficit [VPD] - the difference between the actual- and saturation-vapor pressure) 1896-2015, we extracted gridded data from the Parameter elevation Regression on Independent Slopes Model (PRISM; PRISM 2018), using

monthly values from each year 1895-2016. We used all 4 km PRISM cells intersecting the study area and created a time-series of monthly climate c. 1895-2015 for each cell. We standardized values in each cell over time using z-score transformations, and then calculated the average z-score across all 4-km cells in each year. These data describe relative summer drought stress and relative abundance of winter precipitation across the entirety of the study area, for each year 1896-2016. The first year of the record in PRISM, 1895, was excluded from the final time series because data were unavailable for the start of the water year (i.e., fall-early winter 1894). Winter precipitation and summer drought stress (i.e., summer VPD) are recognized as two of the strongest drivers of myriad processes important to forests (Williams et al. 2012, 2015). Independently and in tandem, these components of climate have been linked to bark beetle activity (Hart et al. 2014, 2017), wildfire activity (Littell et al. 2009), and tree regeneration (Rother and Veblen 2017, Andrus et al. 2018) throughout the Southern Rocky Mountains. We also obtained a long-term (1938-present; May 1st of each year) record of snow depth and snow water equivalent (SWE) from the University Camp snow course ([40.03 N, -105.57 W], 3,140 m; NRCS 2016). Though these data represent May 1st SWE at only a single point on the landscape, they are strongly correlated with similar snow course data in other parts of the NFR (Andrus et al. 2018).

To describe trends in climate prior to 1896, and to characterize the relationship between climate and tree growth in the NFR, we also obtained residual tree-ring chronologies describing interannual variability in tree growth for both ponderosa pine (*Pinus ponderosa*) and Engelmann spruce (*Picea engelmannii*). These are two of the most important tree species in the study area, and span much of the forested range of the NFR. Originally developed by Villalba et al. (1994) and Veblen et al. (2000) these chronologies were updated by new sampling in 2015 and 2008,

respectively; dendroclimatic signals were separated from local site factors and competition effects using linear and non-linear detrending of raw ring-width measurements, and autoregressive modelling using either the ARSTAN software (Cook and Holmes 1986) or *dplR* package in R (Bunn 2008). Using these data, we calculated Pearson correlation coefficients to quantify the strength of the dendroclimatic relationships among residual chronologies from each of the species with winter precipitation, summer VPD, and snowpack in late spring (May 1st SWE). This analysis is meant to demonstrate the importance of different components of interannual climate to tree radial growth across the range of life zones present in our study. Though non-stationarity in space is recognized limitations of these relationships (e.g., Villalba et al. 1994), these data are still useful in describing trends in growth and the ways in which climatic correlates vary among species present throughout the NFR. We also present climate and tree growth data that were smoothed using a 10-year mean to emphasize mid- and low-frequency climatic trends rather than high-frequency variability. These data allow graphical comparisons of interdecadal climate variability throughout the time-period of our analysis, as well as depictions of the 19th century climatic conditions leading to the forests present in 1938. Using these data, we identified pluvials as time periods in which 10-year running means of radial growth (for both *Pinus ponderosa* and *Picea engelmannii*) were above average in at least 5 consecutive years. Droughts were defined as the inverse – at least 5 consecutive years of negative growth departures for both species using the smoothed time series.

A.1.1 Interannual and Interdecadal Variability in Fire Activity, Climate, and Tree Growth

Fire activity in the study area varied widely throughout the 1800-2015 time-period (Fig. 2.2a). The proportion of sites recording spreading fires increased through the 1800s, then general declines were evident. While some sites recorded fire exclusion in the late 1800s, many

continued to burn until c. 1920, with some isolated fire activity after this date. Residual chronologies for Engelmann spruce and ponderosa pine were correlated with components of interannual climate (Fig. 2.2b, 2.2c). In the 1896-2015 period, the Engelmann spruce residual chronology was negatively correlated with summer vapor pressure deficit (VPD; r = -0.45) and showed a slight negative correlation with winter precipitation (r = -0.10). In contrast, the ponderosa pine residual chronology was positively correlated with winter precipitation (r = 0.58) and had a slight negative correlation with summer VPD (r = -0.08). May 1st SWE was positively related to residual chronologies of ponderosa pine (r = 0.36) and less so for Engelmann spruce (r = 0.16). These trends reflect general differences in relationships between radial growth and climate for mature ponderosa pine and Engelmann spruce in our study area, and the correlation between the chronologies for the two species was low (r = 0.12). Summer drought stress increased from 1896 to 2015 (correlation of year and VPD = 0.33), with the period of greatest summer VPD occurring in the early 2000s. During this same period, winter precipitation increased slightly (r = 0.15). From 1938-2015 (the period of available data), SWE from the University Camp Snow Course declined (r = -0.23) likely reflecting increasing spring and summer temperatures (and earlier snowmelt) rather than a reduction in winter precipitation.

A.1.2 Influences of Interannual and Interdecadal Climate Variability on Forest Cover

Though climate was not a direct focus of this study, previous literature suggests that interannual and interdecadal variability in climate likely played a role in changes in forest cover through the 20th century. Tree growth, pulses of establishment, fire activity, and bark beetle outbreaks – important drivers of forest change in the Southern Rocky Mountains – are all closely tied to climate. Pluvial periods in the early 1900s and 1980s-1990s (Fig. 2.2; in conjunction with fire exclusion and altered livestock grazing practices) may have helped to trigger pulses of

establishment in the lower montane zone (Mast et al. 1998, Sherriff and Veblen 2006). These pulses of establishment (e.g., early 1900s, 1980s-1990s) were also identified in a montane site in the southern Front Range (Boyden et al. 2005), suggesting that interdecadal periods of beneficial climate may lead to synchronous recruitment across broad spatial scales. Ponderosa pine in particular is known to establish episodically during years with beneficial climatic conditions (League and Veblen 2006, Rother and Veblen 2017). In contrast, tree establishment in more mesic upper montane sites may be more strongly limited by growing space than by climate (*sensu* Ehle and Baker 2003), as evidenced by the abundant establishment of conifers following wildfires during a period of relative drought in the 1800s (Sherriff and Veblen 2006, Schoennagel et al. 2011, Battaglia et al. 2018). In the subalpine zone of the NFR, Engelmann spruce and subalpine fir tend to establish with relative synchrony during years of above average snowpack and/or cool, wet summers, again suggestive of broad-scale climatic controls (Andrus et al. 2018).

Wildfire activity, the largest driver of forest loss in our study area from 1938-2015, is known to correlate strongly with temperature and/or precipitation. In the NFR, sites within the lower montane zone historically experienced broad-scale and synchronous fire activity during dry years with antecedent moisture, primarily because these prior wet years led to abundant fine fuels in a relatively fuel-limited system (Veblen et al. 2000, Sherriff and Veblen 2008). In contrast, upper montane and subalpine forests primarily burn in years of extreme drought, and are not as dependent on antecedent precipitation (Sibold and Veblen 2006, Sherriff and Veblen 2008). Bark beetle (e.g., *Dendroctonus* and *Ips* spp.) activity is also heavily influenced by climate, and insect outbreaks have been triggered by recent droughts throughout the Southern Rocky Mountains (Chapman et al. 2012, Hart et al. 2014, 2017). Episodic tree mortality is also

driven by extreme drought events in the NFR and sometimes lagged by ten years or so following droughts (Bigler et al. 2007), representing an additional link between climate and tree death. We theorize that interannual and interdecadal periods of drought act as important controls on broad-scale forest cover in the NFR, primarily by triggering broad-scale disturbance and mortality events that respond to climate.

A.2 Image Processing, Segmentation and Classification

Image texture and contrast can aid in the classification of remotely sensed imagery (Richards 2013). To provide ancillary data for use in our image classifications, we used an expanding-window approach (*sensu* Coburn and Roberts 2004) to calculate two metrics relating to texture and edge contrast. Moving window processing was conducted across many spatial scales (3x3, 5x5, 7x7, 9x9, 11x11, 13x13, and 15x15 pixel windows) surrounding each c. 1 m cell, thus providing relevant information for forest patches of different sizes.

Our first metric identifies pixels that are darker than their surroundings (hereafter "local minima"). To identify local minima, we calculated the mean and standard deviation of pixel brightness at each scale (3-15 pixel windows). A pixel was considered to be darker than its surroundings if its brightness value was lower than the window mean minus two standard deviations. These calculations were made for each window size for each pixel, then summed across all window sizes (thus, local minima values range 0-7, where 7 indicates that a pixel is darker than its surroundings across all moving window sizes; Fig. 2.3b). Local minima values were helpful in classifying individual trees on brightly lit ridgetops, south-facing hillslopes, or in grassland-dominated areas.

For the second metric, we calculated the sum of standard deviation values across all window sizes (Fig. 2.3c). Standard deviation of pixel brightness is a simple version of local

texture that can improve forest classification in high-resolution imagery. While standard deviation is more computationally efficient than many other texture metrics (e.g., entropy based on grey-level co-occurrence matrices), it may still yield comparable performance in classification (Coburn and Roberts 2004). Standard deviation appeared helpful in separating dark forest stands (low brightness, moderate variance) from more homogenous areas (low brightness, low variance; i.e., water bodies, shadows).

We combined these three layers (brightness, local minima, and standard deviation) to create a three-band composite image (Fig. 2.3d). We completed these image processing steps in Python 2.7 using the GDAL (Geospatial Data Abstraction Library 2017), SciPy (Oliphant 2007), and NumPy (Hugunin 1995) modules. NAIP imagery was processed similarly (minima and standard deviation calculated using a greyscale image of the average brightness across all bands).

Prior to classification, we also performed an image segmentation on the three-band composite imagery (brightness, local minima, standard deviation) using the segment mean shift algorithm in ArcGIS 10.4 (ESRI 2016). Segmentation is a useful procedure when attempting to identify homogeneous areas or features (i.e., objects) in data with high spatial resolution, where pixels are smaller than the objects of interest (such as individual trees and forest stands in high-resolution aerial imagery; Blaschke 2010). We selected segmentation parameters iteratively on a subset of the imagery to create a segmentation that identified individual trees in open areas as objects, but also considered large homogeneous areas of forest cover to be objects. In this sense, we prioritized spectral similarity rather than sensitivity to scale, and primarily used segmentation as a noise-reduction technique to reduce misclassification of individual pixels within homogeneous areas. Final segmentation parameters were the same for both time periods. We

allowed objects to be as small as 3 contiguous pixels, a size threshold (2-3 m in diameter) at which an adult tree might be realistically separated from an individual shrub.

Following segmentation, we identified training areas for classification of four distinct forest and non-forest cover types. These classes were: 1) dense, dark, and homogeneous forests, 2) smaller forest patches with moderate brightness values and high values for local minima and standard deviation, 3) very bright surfaces (roads, bare ground) and, 4) moderately bright grassland or non-forest vegetation. Using these training areas, and ancillary data from DEM hillshade values (for historical air photos) and a red-green index (NAIP), we performed a supervised classification of the segmented image using support vector machines. Support vector machines (SVMs) are a statistical learning algorithm commonly used in remote sensing, that can identify non-linear decision boundaries between classes in multi-dimensional space, making few distributional assumptions (Hastie et al. 2009). Following classification, we merged all distinct forest classes (1 and 2), and all distinct non-forest classes (3 and 4), to create a binary forest/non-forest layer at c. 1 m resolution. We then identified shadows as pixels with brightness and standard deviation values less than 10 and buffered these pixels by 7 m in all directions (equivalent to the largest window size used in our image processing; Fig. 2.3e). Shadows in either time period were combined with spatial data identifying lakes, reservoirs (USGS 2018), incorporated urban areas, and elevations above 3500 m (USGS 1999), and these areas were masked from the analysis for both 1938 and 2015. In addition, we manually removed areas of degraded imagery that could not be reliably classified in the 1938 imagery (i.e., fading, creases, handwriting on original prints). Of the total study area, 93.9% (2713.19 km^2) was left unmasked and classified and was included in later analysis. Finally, we manually reclassified a small number of forest areas that were, by visual interpretation, bare ground on dark hillsides or in lush

meadows. This manual reclassification had relatively minor effects, resulting in net reductions of estimated 1938 forest cover and 2015 forest cover by 1.09% and 0.45%, respectively. Forest cover in recently burned areas (for the 2015 classification) was also corrected using a systematic photointerpretation that was completed for another study meant to identify the presence of live seed trees in recent burn areas (T. Chapman, unpublished data). Initial estimates of classification accuracy in this project exceed 97%. Following processing and classification, the 1938 classification was resampled from 1.1 to 1 m using nearest neighbor interpolation to facilitate direct comparison with 2015 NAIP.

A.3 Accuracy Assessment and Uncertainty Modeling

To permit comparisons with previous studies, we performed a traditional accuracy assessment of our image classifications for both historical and contemporary imagery (*sensu* Congalton 1991, Olofsson et al. 2014). Because we used a combination of object- and pixel-based classification techniques, where segmentation was primarily used to reduce noise and enhance pixel-level classification accuracy, we based our methods for accuracy assessment on the recommendations of Olofsson et al. (2014) and Radoux and Bogaert (2017) for enhanced pixel-level accuracy assessments. First, we randomly located 2,000 points through each classified map (4,000 total), with a minimum spacing of 400 m to prevent points from being located within the same segmented object. We then used manual photointerpretation at each point to identify the cover type of a specific 1 m pixel (forest/non-forest) and compared this reference to the predicted cover type from the final classification. Indicator variograms of classification accuracy (correct/incorrect) for points at a minimum 400 m spacing had nugget to sill ratios near 1, indicating little spatial dependence of classification error at scales greater than

400 m. Overall agreement between the reference class and predicted class was 90.2% for the 1938 imagery, and 89.4% for the 2015 imagery (Table A1).

Table A1. Confusion matrices of classification accuracy of 1938 and 2015 aerial imagery in the northern Front Range, CO, based on manual photointerpretation at 2,000 randomly located points. Cell values are given for proportion of total map area in each class. Area proportions, accuracy metrics, and 95% confidence intervals were calculated following the recommended protocol of Olofsson et al. (2014).

		1938 Classification		
		Reference Class		
		Non-Forest	Forest	User's Acc.
Predicted Class	Non-Forest	0.371	0.064	85.29 ± 2.36
	Forest	0.034	0.531	93.98 ± 139
	Prod.'s Acc.	91.61 ± 1.78	89.24 ± 1.78	90.20 ± 1.29

		2015 Classification		
		Reference Class		
		Non-Forest	Forest	User's Acc.
Predicted Class	Non-Forest	0.310	0.048	86.63 ± 2.51
	Forest	0.058	0.584	90.90 ± 1.57
	Prod.'s Acc.	84.12 ± 1.36	92.44 ± 2.07	89.37 ± 1.35

Accurate results of change detection analyses are contingent upon spatial alignment (i.e., co-registration error) and accurate thematic representations of cover types (i.e., classification accuracy; Leyk et al. 2018). To account for these effects, we performed an uncertainty analysis in which we used a combination of Monte Carlo simulations of co-registration error and spatial models of classification accuracy (derived from binomial GLMs; *sensu* Leyk and Zimmermann 2004, 2007) to develop lower and upper estimates of forest cover for each 250 m cell in each time period. We used binomial GLMs to predict classification accuracy for each 1m pixel using the following: 1) raw pixel brightness (unsegmented) across all bands, 2) segmented pixel values across all bands, 3) the difference between segmented and unsegmented values in each band

(essentially the effect of smoothing on each pixel), as well as 4) the predicted class and relevant interaction terms. We extracted these independent predictors at each of the manual photointerpretation points used in the traditional accuracy assessment, as well as the binary dependent variable of correct/incorrect classification. We selected final variables for each GLM using Akaike's Information Criterion (AIC) and likelihood ratio tests. For each of these binomial models, we used c-log-log link functions to account for unbalanced sampling of the dependent variable that was heavily skewed in favor of correct classification (Zuur et al. 2009). Following fitting of the final models, we tested for homogeneity of variance and spatial independence of residuals in each GLM using the "DHARMa" package in R (Hartig 2018), and found no evidence for violations of model assumptions. Adjusted deviance squared (following Guisan and Zimmermann 2000) for the final GLMs were 0.32 for 1938 imagery, and 0.28 for the 2015 imagery. We used these models to make predictions of the probability of an accurate classification for each 1 m cell across each date, and then calculated the overall accuracy, forest accuracy, and non-forest accuracy using all predicted values within each 250 m grid cell. Overall accuracy in each grid cell was calculated as the mean probability of a correct classification across all classified pixels, while forest and non-forest accuracies were the mean values for all pixels assigned to each class (Fig. A1a-d).

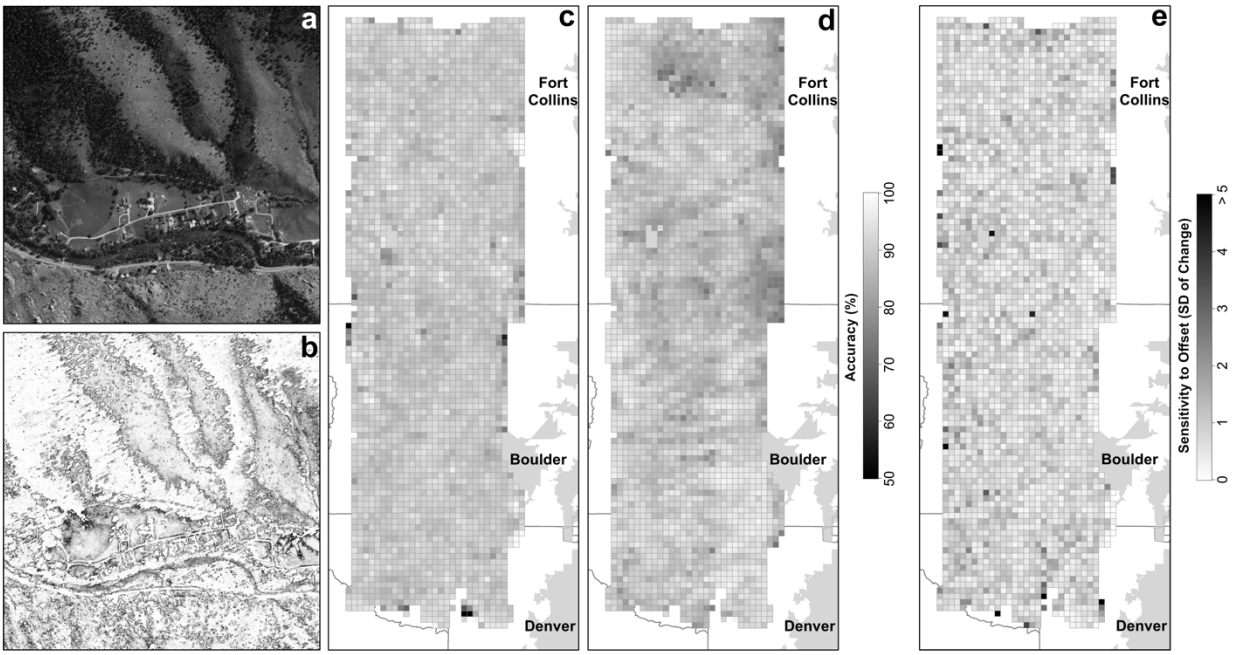

Fig. A1. Steps to identify cells with significant increases or decreases in forest cover in the northern Front Range of Colorado 1938-2015. Classification accuracy was modeled locally for each cell in 1 m imagery (a, b) using generalized linear models meant to predict the probability of a correct classification in a given grid cell (b). Overall accuracy (c, d; 1938 and 2015, respectively), as well as the accuracy for forest and non-forest classes were taken as the mean probability across all classified 1 m cells in each 250 m grid cell. Lastly, 1938 imagery was randomly shifted 200 times to simulate the effects of co-registration error (e; values given as the standard deviation of net forest change 1938-2015 across all simulations). Example shown is for 1 km grid cells, but the final analysis was also performed at the 250 m resolution.

We also quantified and incorporated the sensitivity of forest cover estimates to error in image co-registration. Using an independent set of tie points not used in co-registration (n = 100), we fit several potential distribution functions to the values of co-registration error (normal, exponential, Weibull, gamma, and log-normal). Through comparisons of root-mean-square error and visual interpretation of histograms and qqplots, we determined that distances of co-registration error were best approximated with a log-normal distribution (mean = 2.92 and sd = 0.73 on the log scale). We then drew 200 random samples of offset distance from this log-normal distribution, as well as 200 random azimuth values (0-360 from a uniform distribution) to perform a Monte Carlo simulation of sensitivity to co-registration error. Over these 200

simulations, each of the 250 m aggregated cells was shifted by a random distance and azimuth to extract the estimate of percent forest canopy cover in 1938 from that new location. We used the 6th and 195th ranked simulations (out of 200) to construct 95% confidence intervals of forest cover for each 250 m grid cell in the 1938 imagery.

Lastly, we combined modeled classification accuracy and the simulations of co-registration error using a series of decision rules to determine if forest cover change exceeded potential error in each 250 m grid cell. Error bounds were defined as follows:

$$LowerForest_{1938} = (\%Acc_{Forest} * ForestArea_{6th})/ClassifiedArea_{6th}$$

$$UpperForest_{1938} = (ForestArea_{195th} + (NonForestArea_{195th} * (1 - \%Acc_{NonForest})))/ClassifiedArea_{195th}$$

$$LowerForest_{2015} = (\%Acc_{Forest} * ForestArea)/ClassifiedArea$$

$$UpperForest_{2015} = (ForestArea + (NonForestArea * (1 - \%Acc_{NonForest})))/ClassifiedArea$$

Where *LowerForest* and *UpperForest* are the lower and upper estimates for forest cover at a given date ($_{1938}$ or $_{2015}$), *%Acc* is the estimated classification accuracy for a given cover type, *ForestArea* and *NonForestArea* are the total area classified (by SVMs) as forest and non-forest, respectively, and *ClassifiedArea* is the total area classified as either cover type. Subscripts $_{6}$ and $_{195}$ correspond to the 6th and 195th ranked estimates of forest cover (95% bounds) across the Monte Carlo simulations of co-registration error for the 1938 imagery. All values in the above formulas were specific to each grid cell, thus identifying potential ranges of forest cover in each 250 m area at each date (1938 or 2015).

We determined that a grid cell had experienced a significant change in forest cover 1938-2015 if the potential ranges of forest cover in 1938 and 2015 did not overlap. In other words, if a maximum estimate of 1938 forest cover was lower than the minimum estimate of 2015 forest cover, a grid cell was classified as Forest Gain. Likewise, if the maximum estimate of 2015 forest cover was lower than minimum estimate of 1938 canopy cover, a grid cell was classified

as Forest Loss. If the error bounds for the two time-periods overlapped, a cell was then classified as Little Change (generally less than 15% net change). Following thresholding, we manually reclassified 1,331 Forest Loss grid cells (3.0% of the total area) to Little Change because designation as Forest Loss in these cells was primarily due to lighting conditions in the 1938 imagery (i.e., overestimates of 1938 forest cover due to topographic shading).

A.4 Data Processing and Selection of Variables that Potentially Drive Forest Change

To assess the relative influences of several potential drivers of forest change, we performed a Random Forest analysis at the 250 m scale to predict forest change class (Little Change, Forest Gain, Forest Loss) as a function of 13 landscape variables relating to land use, land management, ownership designation, the physical environment, and historical and recent wildfire activity (Table 2.2). The following is a description of these datasets, and the ways in which they were processed prior to performing our analyses.

Related to land use, we acquired mine location data for the study area from the USGS Mineral Resource Data System (USGS 2005). We then created a spatial kernel estimate of mine density using Scott's rule of thumb for bandwidth selection, which is appropriate for illustrating gradual trends in density of point locations through space (Scott 1992, Baddeley and Turner 2005). We used the spatstat package in R to perform kernel density estimation (Baddeley and Turner 2005). We also acquired estimates of land cover type in 1938 in each 250 m cell from a spatially explicit model of historical land cover (Sohl et al. 2016). This model was created using backcasting at a 250 m spatial resolution and annual time scale, with the National Land Cover Dataset and numerous historical data sources (e.g., Census of Agriculture, historical housing density) as inputs (Sohl et al. 2016). Visual comparison of this model with our data suggested a good match between predicted cover types and those present in the 1938 imagery. We also

included the proportion of developed land in each grid cell from the most recent iteration (2011) of the National Land Cover Dataset (Homer et al. 2015). Proportion treated area was extracted from a regional database of silvicultural treatment activities (e.g., thinning and prescribed fire) c. 2006-2016, but including some activities prior to this date (Caggiano 2017). We excluded any silvicultural treatments occurring outside the time period of image coverage (1938-2015), and treatments that were related to invasive weed management or other activities that would have minimal influence on the forest overstory. Lastly, we calculated road density using the TIGER primary and secondary road layers (USCB 2017) as the linear distance of TIGER roads (m) per grid cell.

We extracted four variables related to land ownership designation from the COMaP (Colorado Ownership, Management, and Protection) dataset. COMaP is the most comprehensive dataset of land ownership at the state level, and incorporates data from numerous agency partners (COMaP 2010). We derived four variables from this dataset for each grid cell – proportion city/county open space, proportion National Park Service land, proportion private land, and proportion US Forest Service land. These are the four largest land ownership categories in the study area and represent four differing sets of land-use histories and management strategies.

To describe characteristics of the physical environment, we used 10 m digital elevation models from the National Elevation Dataset (USGS 1999). We extracted the mean elevation (m) from each grid cell, as well as the mean heat load index (calculated at a 10 m resolution). Heat load index (HLI) is a combined variable incorporating transformed aspect (NE to SW), slope, and latitude. HLI is typically used to estimate moisture stress and radiant intensity on a given site, with higher values representing steep, SW-facing slopes, and low values representing steep NE-facing slopes (McCune and Keon 2002). We calculated HLI using the spatialEco (Evans

2017) and raster (Hijmans 2015) packages in R, and used an exponential transformation of equation 1 defined in McCune and Keon (2002).

Finally, we obtained spatial data describing recent and historical fire activity. We acquired spatial data identifying recent fire perimeters from the monitoring trends in burn severity program (all fires larger than c. 400 ha occurring 1984-2015; Eidenshink et al. 2007), "historical perimeters" from the USGS geospatial multi-agency coordination dataset (all fires larger than 40 ha 2000-2015; USGS 2018), and other data from local and regional land management offices (extending the record to 1978). We merged these datasets into a single layer, removing fires represented multiple times, and used the merged data to calculate the proportion of each grid cell that burned 1978-2015. We acknowledge that records for large fires since 1984 are more complete than for other events, however, previous research has documented very little fire activity in this region c. 1938 – late 1970s (Veblen and Donnegan 2005, Collins et al. 2006; Fig. 2.2). Furthermore, while the exclusion of fires less than 40 ha may ignore many individual fire events, large events make up the majority of the area burned in the NFR. A simple comparison with the national wildland fire occurrence database (USGS 2018; which includes many smaller fires without polygonal data identifying fire perimeters) suggested that our dataset omitted less than 5% of total area burned on public lands in the NFR during the 1980-2015 period. To assess the influence of historical fire regimes on 20th century forest change, we also incorporated the spatial model of low severity fire created by Sherriff et al. (2014). This dataset, at 30 m resolution in raster format, was created using 232 fire history sites through the Colorado Front Range and is currently the most detailed model of montane fire history in our study area. We calculated proportion low severity as the proportion of each 250 m grid cell predicted to have been dominated by frequent, low severity fire prior to the onset of fire exclusion c. 1920.

In addition to these variables, we also explored factors such as bark beetle (*Dendroctonus* and *Ips* spp.) presence and severity, climate (PRISM 2011), and satellite-derived growing season length and amplitude (USGS 2015). These variables were excluded either because they explained a very small proportion of total variance (bark beetle activity) or because they were strongly correlated with elevation and thus added no additional explanatory power (gridded climate data and satellite-derived phenology). While bark beetle outbreaks have occurred in portions of our study area, the severity and extent of infestation are generally much lower than in other portions of Colorado, such as the western slope of the Front Range and in the San Juan Mountains (USFS 2015).

A.5 Summary of Changes in Forest Cover and Results of Random Forest Analyses

Table A2. Summary of net changes in forest cover c. 1938-2015 in the northern Front Range of Colorado. Unless otherwise stated, values given are in percent forest cover out of the total mapped area for a given date. "Unburned Areas" represent the entire study area after excluding locations within known fire perimeters (1978-2015). "Grid Cells" are 250 m cells (n = 44,464) that we classified as Forest Gain, Forest Loss, and Little Change based on directional changes in forest cover exceeding the influence of inaccurate classification and co-registration error. Montane and subalpine fire histories are for stands within the study area with stand-specific fire history records, where lower and upper bounds represent minimum and maximum values in the change detection (based on sensitivity to inaccurate classification and co-registration error).

Forest Cover	1938	2015	Net Change
Entire Study Area	56.5	64.3	7.8
Burned Areas	56.6	19.7	-36.9
Unburned Areas	57.2	71.6	14.4
Lower Montane (1700-2400 m)	46.6	51.1	4.5
Upper Montane (2400-2800 m)	62.2	69.6	7.4
Subalpine (2800-3500 m)	65.4	81.4	16
Grid Cells	**Forest Gain**	**Little Change**	**Forest Loss**
Entire Study Area	39.4	47.6	13.0
Montane Fire History	**Lower Bound**	**Net Change**	**Upper Bound**
Low-Severity Class	4.4	15.7	26.4
Mixed-Severity Class	-2.4	11.7	20.2
Subalpine Fire History	**Lower Bound**	**Net Change**	**Upper Bound**
Last Fire Before 1650	3.8	13.4	19.5
Last Fire 1650-1850	0	9.6	16.2
Last Fire 1850-1900	6.5	19.9	27.6
Last Fire 1900-1938	14.6	27.2	34.1
Last Fire 1938-2015	-42.7	-31.9	-17.3

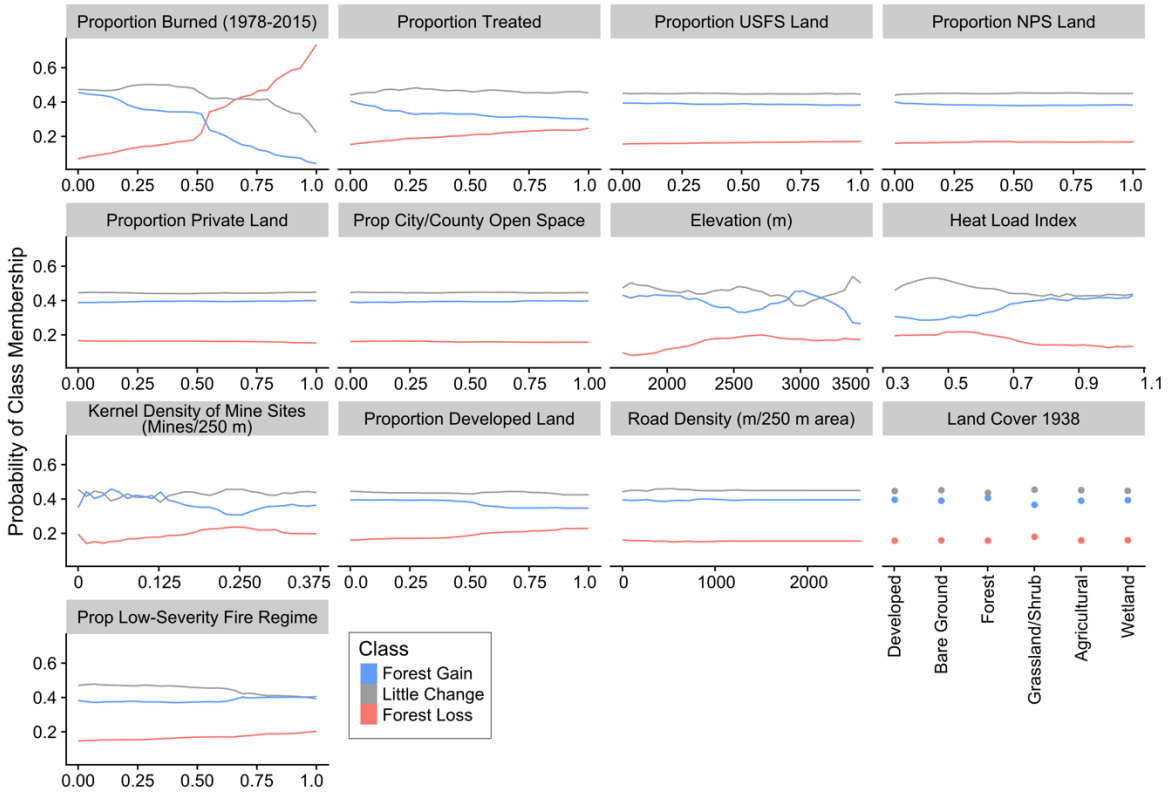

Fig. A2. Further results of Random Forest analysis at 250 m resolution. Partial dependence of forest change class (significant gain, significant loss, little change) on 13 landscape variables relating to land use, ownership, abiotic environment, historical fire regime, and recent (1978-2015) fire activity. The four variables of greatest relative importance at this scale of analysis (proportion burned, elevation, density of mine sites, and proportion low severity fire regime) are also presented in Fig. 2.6 in the manuscript.

Table A3. Confusion matrix from Random Forest classification based on 13 landscape predictors of forest change class (1938-2015) in the study area in the Colorado Front Range. Cell values are the number of 250m grid cells included in the final analysis.

		Reference Class			
		Forest Loss	Little Change	Forest Gain	User's Acc. (%)
Predicted Class	Forest Loss	4290	922	143	80.11
	Little Change	1259	14570	6765	64.49
	Forest Gain	230	5656	10629	64.36
	Prod.'s Acc (%)	74.23	68.90	60.61	Overall = 66.32

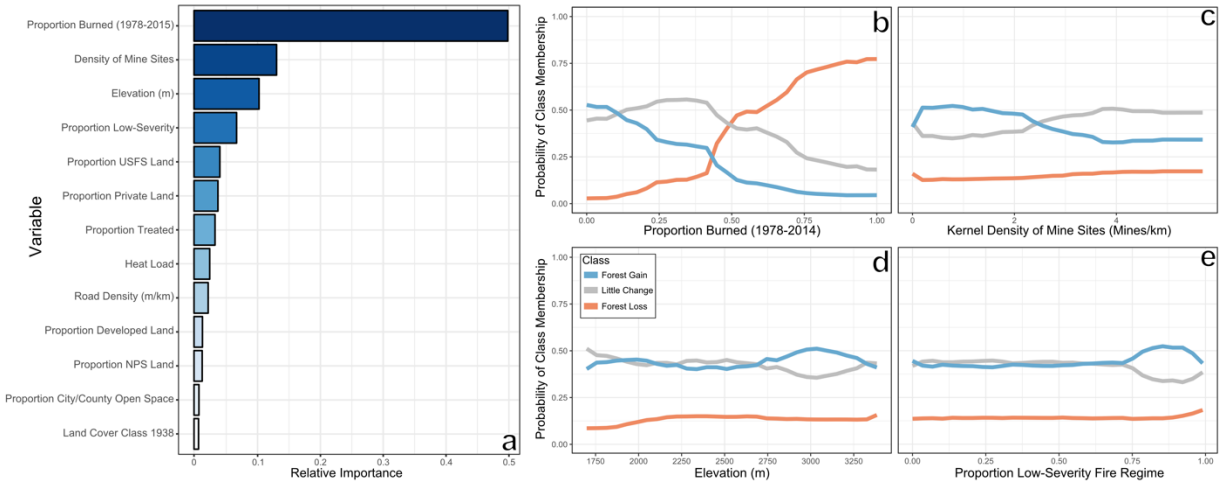

Fig. A3. Random Forest analysis of several potential drivers of forest cover change in the northern Front Range of Colorado, 1938-2015 at a 1 km scale of analysis. Results are presented at this scale (in addition to the 250 m scale included in the main text) for comparison and assessment of scale-dependent relationships. Variable importance plot (a) gives the relative importance of each variable in the ensemble model, and partial dependence plots (b-e) show the marginal effects of each of the top four predictors across their respective ranges.

APPENDIX B

SUPPLEMENTARY MATERIAL FOR CHAPTER 3 – LIMITATIONS TO RECOVERY FOLLOWING WILDFIRE IN DRY FORESTS OF SOUTHERN COLORADO AND NORTHERN NEW MEXICO, USA

B.1 Description of Climate Downscaling Methods and Water Balance Calculations

To characterize climate and moisture availability throughout each fire, we performed a statistical downscaling of gridded climate data and combined these data with a monthly water balance model. First, we used spatial gradient and inverse distance squared interpolation (GIDS; following Nalder and Wein 1998, Flint and Flint 2012) of monthly climate data from the Parameter-Elevation Regression on Independent Slopes Model (PRISM; PRISM 2018). GIDS-products developed using similar methods have been shown to be tightly correlated with independent validation data (McCullough et al. 2016). To describe long-term average climate across each site, we used monthly 30-year climate normals (800 m initial resolution) of maximum temperature, minimum temperature, and precipitation for the 1981-2010 period. To describe climatic conditions following each fire, we also used PRISM annual data (4 km initial resolution) for all months during the first three years following fire. This three-year time-period has been shown to be important for the prediction of post-fire conifer establishment in related studies (Harvey et al. 2016, Stevens-Rumann et al. 2018). Post-fire data were first downscaled to 800 m, then all layers (post-fire climate and 30-year climate normals) were downscaled from 800 m to 270 m to 90 m to 30 m using GIDS with digital elevation models from the national elevation dataset (USGS 1999) as ancillary data.

Following statistical downscaling, we calculated monthly actual evapotranspiration (AET), potential evapotranspiration (PET) and climatic water deficit (CWD; the difference between PET and AET) using the modified Thornthwaite water balance model described by Lutz

et al. (2010). We obtained soils data from POLARIS (Chaney et al. 2016), and calculated available water capacity (one of the inputs in the water balance model) as the product of soil depth and fractional water capacity in the top 200 cm of soil. We also calculated heat load index (HLI) (*sensu* McCune and Keon 2002) – a proxy for topographic variation in incoming shortwave radiation and heating – and used these data as a terrain modifier on PET following Lutz et al. (2010). AET, PET, and CWD were developed at a monthly time step and we derived predictors from these data using: 1) the summed annual values of AET and CWD from 30-year normal (Fig. 3.5, Fig. 3.6), 2) the average annual values of AET and CWD in the three years following a given fire, and 3) the percent deviation between 1 and 2 as an index of relative post-fire drought (Table 3.2).

Important limitations of these methods should be acknowledged. The water balance model of Lutz et al. (2010) relies on a modified Thornthwaite-Mather estimate of potential evapotranspiration (PET) to calculate PET, AET, and CWD. This method of estimating of PET is primarily based on temperature, however, solar radiation-based (e.g., Priestley-Taylor) and combination (e.g., Penman-Montieth) methods of calculating PET may provide more realistic estimates of evaporative demand than do temperature-based approaches. However, radiation-based and combination approaches require detailed inputs of incoming solar radiation, relative humidity, and/or wind speed (Xu and Singh 2002, Chen et al. 2005). These data are not available at the 30 m resolution used in this study and would be computationally intensive to model at this resolution across broad landscapes. Furthermore, the Lutz et al. (2010) equations incorporate heat load index (McCune and Keon 2002) to modify PET estimates by accounting for aspect-driven differences in incoming radiation - this partially accounts for the drawbacks of the Thornthwaite-Mather approach.

B.2 Description of Aerial Image Classifications to Quantify Mature Conifer Canopy Cover Throughout Each Fire

We created thematic maps of the cover of surviving mature conifers throughout each fire using image classification of 4-band aerial imagery collected in 2014 (for NM) or 2015 (for CO) (NAIP; USFS 2015). To add supplementary information describing image texture and image texture, we processed the 4-band imagery using multi-scaled moving windows (following Coburn and Roberts 2004, Rodman et al. 2019; summed values from window sizes of 3, 5, 7, 9, 11, 13, and 15 pixels). Following image processing, this led to a 7-band image composite consisting of the following: visible bands (red, green, and blue wavelengths), near-infrared, NDVI (normalized difference vegetation index), local standard deviation of brightness in the visible bands, and local standard deviation of NDVI (Fig. B1). Local standard deviation of NDVI was particularly helpful in the classification as it helped to identify vegetated areas (high NDVI) near shadows (low NDVI), which is typical of large mature trees in aerial imagery.

We then classified this 7-band composite image as forest/non-forest using a semi-supervised workflow within each fire. First, each 1 m pixel was assigned to one of 12-20 classes using an ISODATA (Iterative Self-Organizing Data Analysis Technique) unsupervised cluster algorithm. We then merged these classes into forest/non-forest categories and used a 3x3 pixel majority filter for post-classification correction. Following classification, we removed non-vegetated areas from the forest class using NDVI (normalized difference vegetation index) thresholding at a 1 m resolution. Lastly, we removed areas that had no live seed trees using a 30 m manual photointerpretation completed for a previous study (initial accuracy >97%; T. Chapman unpublished data), with RdNBR thresholding, and a final manual photointerpretation to identify any additional misclassified areas. Following classification, we performed an

accuracy assessment using a total of 1,000 randomly-located points. These points were stratified throughout each fire (where the number of points in a fire was based on fire area), and with balanced sampling based on predicted cover type (i.e., forest/non-forest). At each point, we performed manual photointerpretations of NAIP imagery (USFS 2015), supplemented by higher resolution satellite imagery (c. 0.4 m) available through ArcGIS 10.4 (ESRI 2016) to determine reference classes. We then developed a confusion matrix of area proportions in each cover type following the methods of (Olofsson et al. 2014). Overall accuracy was 90.2% and user's accuracies exceeded 90% for each cover type (Table B1). Producer's accuracy for the forest class was lower (68.2%); however, this was primarily due to use of area proportions and the greater prevalence of the non-forest cover type as compared to forest cover. Calculation of this same value using raw counts of photointerpretation points led to a producer's accuracy > 90%.

Following image classifications, we then quantified canopy cover throughout each fire at a range of neighborhood sizes (30 – 600 m radii in 30 m increments) surrounding each 30 m grid cell. We did this in an effort to better understand the importance of different scales of canopy cover in predicting conifer seedling abundance (Table 3.2, Fig. 3.5, Fig. 3.6). At each scale (i.e., circular radius around the center of each grid cell), canopy cover was calculated as the following:

$$Percent\ CC_{scale\ i} = \frac{classified\ forest\ area_i}{(classified\ forest\ area_i) + (classified\ nonforest\ area_i)}$$

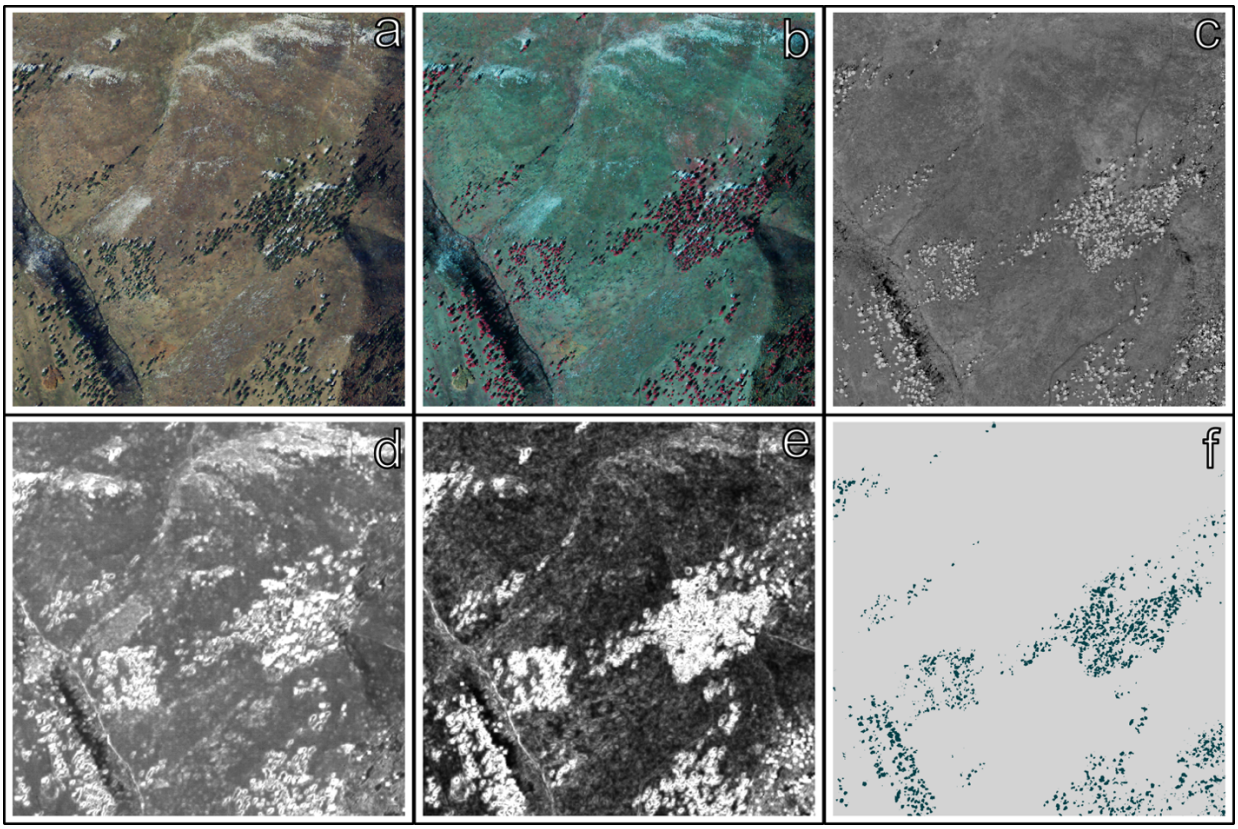

Fig. B1. Steps involved in image processing and classification of 2014 and 2015 NAIP imagery for each fire. Panels of (a) true color and (b) false color composites show the four spectral bands in green, blue, red, and near-infrared wavelengths. To improve pixel-level classification of mature conifer trees in each fire, we processed these data to calculate (c) the normalized difference vegetation index (NDVI), (d) the local standard deviation of visible bands, and (e) the local standard deviation of NDVI. The (f) final classified image shows tree (green) and non-tree (grey) pixels following image classification and thresholding using systematic photointerpretation and RdNBR (Landsat-derived fire-severity; relative differenced Normalized Burn Ratio) thresholding. Example scene is from the Mato Vega fire at 105.27 W, 37.59 N.

Table B1. Accuracy assessment from image classifications of 2014 and 2015 NAIP Imagery throughout each fire. We used c. 1000 points of manual image interpretation stratified by predicted class and throughout each fire. Values given are area proportions (proportion of total mapped area estimated to belong to each combination), as well as percent overall, user's, and producers's accuracies following Olofsson et al. (2014).

		Reference Class		
		Non-Forest	Forest	User's Acc.
Predicted Class	Non-Forest	0.730	0.080	90.13
	Forest	0.019	0.172	90.24
	Prod.'s Acc.	97.52	68.21	Overall = 90.15

B.3 Results of Cross-Validation, Sensitivity Analysis, and Spatial Models of Ponderosa Pine and Douglas-fir Seedling Abundance

Table B2. Sensitivity analysis of different stocking levels and the results of spatial models of post-fire ponderosa pine seedling abundance. “Balanced Accuracy” gives the balanced classification accuracy results from cross-validation at each stocking threshold. Selected thresholds discussed in the main text are delineated with (*).

	Stocking Threshold Seedlings/ha	Percent Area Below Threshold ("Low Regeneration")	Percent Area Canopy Limited	Balanced Accuracy (%) - CV
Total Area	5	4.75	3.94	61.92
	*25	41.77	25.39	70.55
	50	73.12	32.62	67.27
	100	92.82	12.92	64.62
	200	98.3	0.48	56.22
High Severity Only	5	6.28	5.15	N/A
	25	57.27	38.47	N/A
	50	83.12	50.17	N/A
	100	98.09	18.17	N/A
	200	99.56	0.72	N/A

Table B3. Sensitivity analysis of different stocking levels and the results of spatial models of post-fire Douglas-fir seedling abundance. “Balanced Accuracy” gives the balanced classification accuracy results from cross-validation at each stocking threshold.

	Stocking Threshold Seedlings/ha	Percent Area Below Threshold ("Low Regeneration")	Percent Area Canopy Limited	Balanced Accuracy (%) - CV
Total Area	2	20.46	20.45	72.8
	*10	68.49	67.56	77.33
	20	83.82	81.51	75.52
	40	94.64	90.08	69.52
	80	97.68	87.37	63.46
High Severity Only	2	33.77	33.76	N/A
	*10	79.35	78.28	N/A
	20	89.97	87.36	N/A
	40	99.58	94.47	N/A
	80	99.84	89.14	N/A

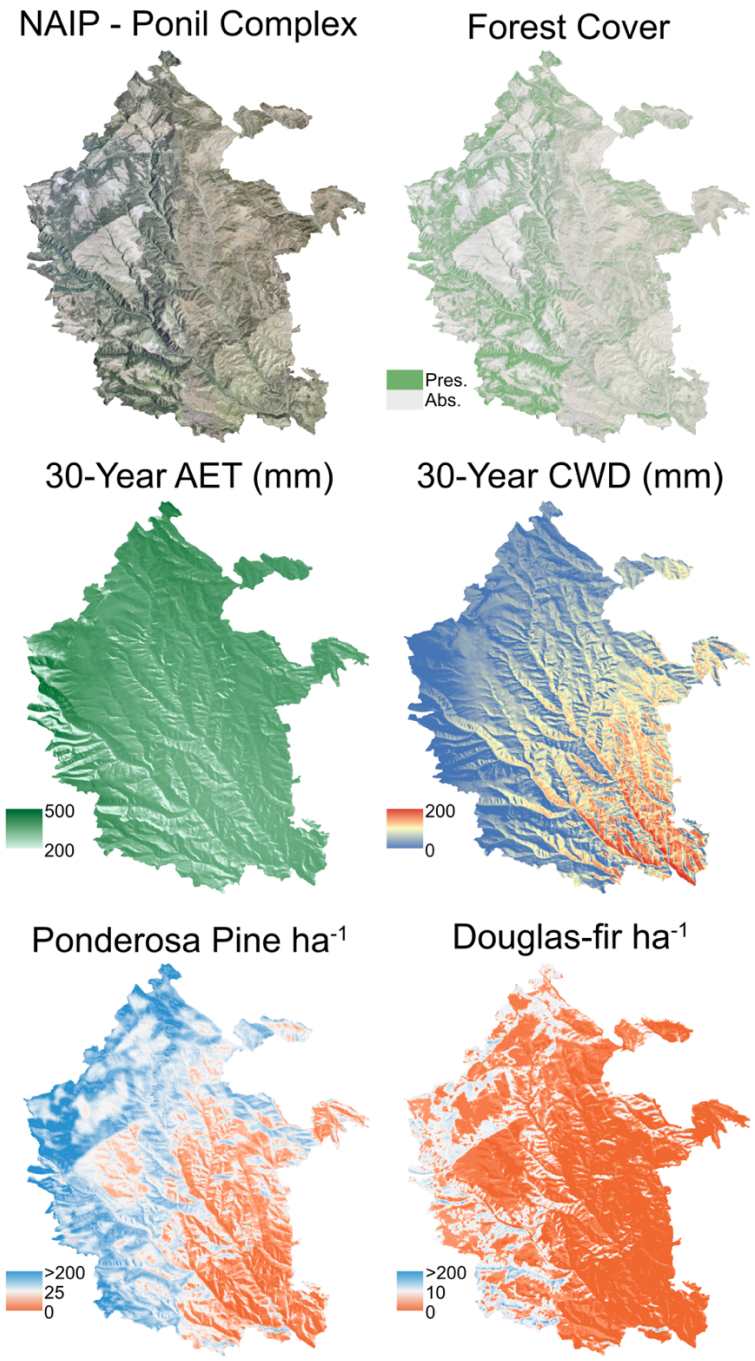

Fig. B2. An example showing the spatially continuous predictor datasets used in spatial modeling of post-fire seedling abundance for the Ponil Complex fire near Raton, NM. Forest cover (based on classifications of aerial imagery), 30-year averages of annual actual evapotranspiration (AET), and annual climatic water deficit (CWD) were used to model post-fire seedling abundance for each species at 30 m resolution across each fire.

APPENDIX C

SUPPLEMENTARY MATERIAL FOR CHAPTER 4 – A CHANGING CLIMATE IS SNUFFING OUT POST-FIRE FOREST RECOVERY IN THE SOUTHERN ROCKY MOUNTAINS

C.1 Description of Vegetation Classes in Montane Zone

Table C1. LANDFIRE vegetation types included in the definition of the montane zone used in this study. Data were from the 2014 LANDFIRE classification of environmental site potential (ESP). ESP represents neither the current or historical vegetation type, but rather the potential vegetation that could be supported on a site given the current biophysical environment.

ID Code	Name
1011	Rocky Mountain Aspen Forest and Woodland
1024	Madrean Lower Montane Pine-Oak Forest and Woodland
1050	Rocky Mountain Lodgepole Pine Forest
1051	Southern Rocky Mountain Dry-Mesic Montane Mixed Conifer Forest and Woodland
1052	Southern Rocky Mountain Mesic Montane Mixed Conifer Forest and Woodland
1054	Southern Rocky Mountain Ponderosa Pine Woodland
1061	Inter-Mountain Basins Aspen-Mixed Conifer Forest and Woodland
1107	Rocky Mountain Gambel Oak-Mixed Montane Shrubland
1117	Southern Rocky Mountain Ponderosa Pine Savanna
1166	Middle Rocky Mountain Montane Douglas-fir Forest and Woodland
1167	Rocky Mountain Poor-Site Lodgepole Pine Forest
1179	Northwestern Great Plains-Black Hills Ponderosa Pine Woodland and Savanna

C.2 Study Area Map and Table Describing Sites and Sample Depth

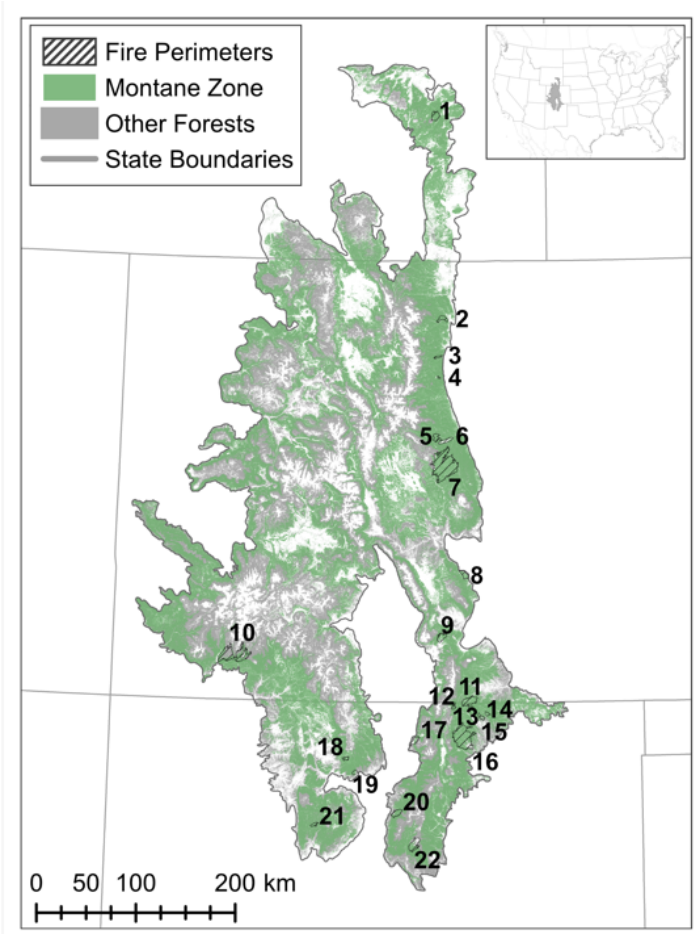

Fig. C1. The locations of the 22 recent (1988-2010) wildfires that occurred in the Southern Rocky Mountains Ecoregion (EPA Level III Ecoregion 21). Numbers on map correspond to "Map ID" in Table C2.

Table C2. A summary of post-fire field surveys of conifer establishment and abundance throughout 22 recent wildfires in the Southern Rocky Mountains Ecoregion. “Map ID” corresponds to numbers in Fig. C1. “N. destructive samples” denotes the number of seedlings collected within each fire perimeter for the analysis of annual establishment. “Field Plots” gives the number of individual plots used to survey post-fire seedling abundances of ponderosa pine and Douglas-fir in each fire.

Map ID	Fire Name	Area (ha)	Fire Year	N. Destructive Samples		Field Plots
				Ponderosa Pine	Douglas-Fir	
1	Hensel	5843.3	2002	0	0	39
2	Bobcat	3695.2	2000	0	0	117
3	Overland	1308.0	2003	86	5	94
4	Eldorado	404.9	2000	75	8	50
5	High Meadows	3887.9	2000	62	12	89
6	Buffalo Creek	3962.7	1996	81	5	120
7	Hayman	52373.2	2002	68	11	205
8	Mason	4461.0	2005	16	2	37
9	Mato Vega	5311.8	2006	3	6	36
10	Miss. Ridge	27890.5	2002	12	5	33
11	Spring	9730.3	2002	25	0	45
12	H12	1777.7	2010	32	0	40
13	York	1313.8	2001	16	0	40
14	Saw	1258.7	1988	7	10	38
15	West Fork	2199.8	2008	4	2	40
16	Ponil Complex	36050.8	2002	19	1	39
17	Hondo	3338.8	1996	1	0	31
18	Montoya	1665.5	2002	1	0	45
19	Pine Canyon	1656.1	2005	38	0	39
20	Borrego	5211.1	2002	44	1	45
21	Lakes	1742.4	2002	18	13	48
22	Viveash	9093.4	2000	17	17	31
	Total	**184176.8**	**1988-2010**	**625**	**98**	**1301**

C.3 Methods of Developing and Downscaling Climate Datasets for the Historical Period and for Future Scenarios

To develop gridded datasets of annual AET (actual evapotranspiration), annual CWD (climatic water deficit), and precipitation during the growing season (April-September) used in the final analyses, we first developed all datasets (1980-2015 historical data and 2006-2099 GCM estimates) at a 4 km spatial resolution. We then quantified trends in each of the 19 GCMs to reduce the number of GCMs analyzed to 3. Finally, we downscaled historical and future climate grids to c. 250 m resolution using the high-resolution climate grids of Holden et al. (2016) and 250 m digital elevation models from the national elevation dataset (USGS 1999). AET, CWD, and growing season precipitation are three different but biologically-relevant constraints on the distribution of vegetation. AET is an indicator of site productivity because it identifies areas with simultaneous availability of energy and moisture, key limitations to plant growth. CWD describes relative drought stress through the landscape, as influenced by broad-scale climatic factors of precipitation and temperature, as well as fine- and mid-scale drivers of incoming solar radiation and available water capacity of the soil (Stephenson 1998, Lutz et al. 2010). Growing season precipitation may be beneficial to seedling establishment across a broad elevational and geographic range (Rother and Veblen 2017, Andrus et al. 2018, Davis et al. 2019).

Our approach of developing these climatic datasets has several important methodological advantages over previous approaches in species distribution modeling. First, given the topographic complexity inherent to the study area, data resolutions that better capture aspect-level differences are needed to accurately reflect the spatial variability in climate that is experienced by plants (Flint and Flint 2012, Franklin et al. 2013). In mountainous landscapes,

resolutions of 270 m or higher have been recommended for this purpose (Franklin et al. 2013). To our knowledge, the future projections of AET, CWD, and growing season precipitation developed in the present study are the highest-resolution data of this kind in the Southern Rocky Mountains Ecoregion. Lastly, because the historical data (GridMET) we used in our analyses were used for bias correction and downscaling of our future projections (Abatzoglou and Brown 2012), and all 4 km data (historical climate and future projections) were processed and further downscaled using the same steps (described below), historical and future climate data should be directly comparable.

C.3.1 Developing AET and CWD Layers at 4 km Resolution

We obtained monthly or daily datasets of maximum temperature, minimum temperature, precipitation, and potential evapotranspiration (PET) from the GridMET dataset (Abatzoglou 2013) for the 1980-2015 period. PET was calculated using the Penman-Montieth method, which estimates reference evapotranspiration using incoming solar radiation, temperature, humidity, and wind speed (Walter et al. 2000). These same variables were obtained from statistically-downscaled datasets (MACA; Abatzoglou and Brown 2012) derived from 19 coupled atmosphere-ocean general circulation models (GCMs) and two representative concentration pathways (RCPs 4.5 and 8.5) from the fifth Coupled Model Intercomparison Project (CMIP5). These data were acquired from model runs in 2006-2099. All datasets that were acquired at daily temporal resolution were aggregated to monthly values either based on the mean (e.g., temperature) or sum (e.g., precipitation) of daily values. Growing season precipitation in each year was calculated as the sum of monthly precipitation values from April-September.

Next, we used historical climate data and future projections to develop annual estimates of AET and CWD for the historical (1981-2015) period and for each future scenario (from 2006-

2099). In conjunction with PET data from GridMET and MACA, we used the monthly water balance equations of Dobrowski et al. (2013) to model monthly AET and CWD across the Southern Rocky Mountains Ecoregion at a 4 km resolution. Available water capacity in the top 200 cm of soil was derived as the product of fractional water capacity and soil depth from POLARIS (Chaney et al. 2016). The resulting soil layer was then aggregated to a 4 km resolution and aligned with GridMET. For the first year in the historical period (1981) and in each GCM (2006), snow depth and soil moisture were initiated in each 4 km cell with December values from a prior year of water balance modeling. Monthly values of AET and CWD were summed in each 4 km cell by calendar year to develop annual grids.

C.3.2 Selecting GCMs Based on Predicted Trends

Due to limitations of computation and data storage, we reduced the number of GCMs considered in further analyses from 19 to 3. We did this by analyzing the direction and magnitude of trends in AET and CWD across the region in each GCM and emissions scenario. First, we calculated the annual mean value across all 4 km grid cells in the Southern Rocky Mountains for each variable, in each GCM and RCP. We then assessed trends in each GCM and RCP combination through time using the Theil-Sen slope estimator (Theil 1950, Sen 1968). The Theil-Sen slope is the median slope of lines between all pairs of points, and is a common non-parametric technique used to assess the magnitude of trends through time. Next, to rank GCMs according to future projections, we calculated the mean Theil-Sen slope for each GCM in RCP 4.5 and 8.5. We then selected the GCMs that had the lowest ranked (Dunne et al. 2012), median ranked (Jeffrey et al. 2013), and highest ranked (Dufresne et al. 2013) averages of Theil-Sen slopes of CWD through time (Table C3, Table C4). CWD was used in GCM selection because a preliminary analysis indicated that this variable was a more important predictor in our analyses

than was AET. We selected these three GCMs in an effort to show the broadest range of potential climate trajectories in the region a necessarily limited sample. We did not use an ensemble of all GCMs because this masks the simulated interannual variability in future climate and interannual variability was a key component of our modeling framework.

C.3.3 Statistical Downscaling From 4 km to 250 m

Lastly, we used gradient and inverse distance squared (GIDS) interpolation (Nalder and Wein 1998, Flint and Flint 2012) to statistically downscale the 4 km climate variables (i.e., AET, CWD, and growing season precipitation) from the historical period and future projections. For AET and CWD, we used as ancillary data the average values of AET and CWD during the 1981-2015 historical period from the 250 m grids described in Holden et al. (2016, 2018). For growing season precipitation, we used 30 m digital elevation models from the national elevation dataset (NED; USGS 1999), aggregated and aligned to the grids of Holden et al. (2016, 2018) as ancillary data in downscaling. When compared to station data and independent validation data, GIDS outputs have been shown to better represent local climate conditions in complex terrain than do coarse-scale climate grids (Flint and Flint 2012, McCullough et al. 2016). Furthermore, visual assessment of downscaled data demonstrates that GIDS preserves spatial variability of climate patterns present in each year (e.g., wet conditions in the northern end of the study area and dry conditions in the south) better than interpolators that use a single global relationship (i.e., robust regression). The local flexibility of the method also allows for an improved representation of localized factors such as cold-air pooling.

Table C3. Trends in actual evapotranspiration (AET; evaporation constrained by moisture availability) across the Southern Rocky Mountains using 19 coupled atmosphere-ocean general circulation models (GCMs) and two representative concentration pathways (RCPs). RCPs 4.5 and 8.5 indicate different levels of change in radiative forcing (Δ W/m^2) and represent two potential future trajectories - a peak in anthropogenic emissions in 2040, or rapid increases in emissions through 2100, respectively. AET was calculated at a 4 km resolution throughout the Southern Rocky Mountains, and trends were calculated using Theil-Sen slopes of annual mean AET across the region for each year (2006-2099). "Average" gives the mean of slopes from both RCPs. GCMs selected for later analyses are shown in bold.

Actual Evapotranspiration

GCM	RCP 4.5		RCP 8.5		Average	
	Theil-Sen Slope	Rank	Theil-Sen Slope	Rank	Theil-Sen Slope	Rank
BCC_CSM 1.1(m)	0.1	16	0.6	11	0.35	12
BNU-ESM	0.25	14	0.87	5	0.56	10
CanESM2	0.99	2	1.79	1	1.39	1
CCSM 4.0	0.61	7	0.6	10	0.61	9
CNRM-CM5	0.59	8	0.78	8	0.69	6
CSIRO-Mk 3.6.0	**0.47**	**9**	**0.87**	**6**	**0.67**	**8**
GFDL-ESM2G	**0.85**	**4**	**0.91**	**4**	**0.88**	**4**
GFDL-ESM2M	-0.22	18	0.41	13	0.10	16
HadGEM2-CC365	0.38	11	0.26	16	0.32	13
HadGEM2-ES365	0.27	13	0.35	14	0.31	14
INMCM 4.0	0.31	12	-0.85	18	-0.27	18
IPSL-CM5A-LR	0.04	17	0.14	17	0.09	17
IPSL-CM5A-MR	**-0.43**	**19**	**-1.55**	**19**	**-0.99**	**19**
IPSL-CM5B-LR	0.45	10	0.59	12	0.52	11
MIROC-ESM-CHEM	1.12	1	1.09	2	1.11	2
MIROC-ESM	0.86	3	0.96	3	0.91	3
MIROC5	0.17	15	0.3	15	0.24	15
MRI-CGCM3	0.67	6	0.7	9	0.69	6
NorESM1-M	0.71	5	0.79	7	0.75	5

Table C4. Trends in climatic water deficit (CWD; unmet evaporative demand of the atmosphere) across the Southern Rocky Mountains based on 19 coupled atmosphere-ocean general circulation models (GCMs) and two representative concentration pathways (RCPs). RCPs 4.5 and 8.5 indicate different levels of change in radiative forcing (Δ W/m^2) and represent two potential future trajectories - a peak in anthropogenic emissions in 2040, or continuous increases in emissions through 2100, respectively. CWD was calculated at a 4km resolution throughout the Southern Rocky Mountains and trends were calculated using Theil-Sen slopes of annual mean CWD across all cells in the region for each year (2006-2099). "Average" gives the mean of slopes from both RCPs. Selected GCMs are shown in bold.

Climatic Water Deficit

GCM	RCP 4.5		RCP 8.5		Average	
	Theil-Sen Slope	Rank	Theil-Sen Slope	Rank	Theil-Sen Slope	Rank
BCC_CSM 1.1(m)	1.28	9	2.45	12	1.87	12
BNU-ESM	1.19	10	2.3	15	1.75	13
CanESM2	0.43	17	1.65	19	1.04	18
CCSM 4.0	0.8	14	2.39	13	1.60	15
CNRM-CM5	1.3	8	2.99	9	2.15	7
CSIRO-Mk 3.6.0	**1.42**	**6**	**2.64**	**11**	**2.03**	**10**
GFDL-ESM2G	**-0.59**	**19**	**1.89**	**18**	**0.65**	**19**
GFDL-ESM2M	1.35	7	2.73	10	2.04	9
HadGEM2-CC365	1.57	5	4.46	3	3.02	3
HadGEM2-ES365	1.75	4	4.15	4	2.95	4
INMCM 4.0	0.66	15	4.12	5	2.39	6
IPSL-CM5A-LR	1.92	3	4.5	2	3.21	2
IPSL-CM5A-MR	**2.38**	**1**	**6.45**	**1**	**4.42**	**1**
IPSL-CM5B-LR	1.1	11	2.15	16	1.63	14
MIROC-ESM-CHEM	0.63	16	3.35	7	1.99	11
MIROC-ESM	1.04	12	3.2	8	2.12	8
MIROC5	1.95	2	3.79	6	2.87	5
MRI-CGCM3	0.36	18	1.96	17	1.16	17
NorESM1-M	0.84	13	2.35	14	1.60	16

Table C5. Results of Mann-Kendall trend tests for climate variables derived from each of the selected GCMs under each emissions scenario. Kendall's correlation coefficients (τ) were calculated between each climate variable and time, and p is the p-value of the test for a monotonic trend after accounting for serial autocorrelation.

RCP 4.5

	AET		**CWD**	
	τ	**p**	**τ**	**p**
GFDL	0.25	0.007	-0.15	0.018
CSIRO	0.14	0.077	0.11	0.092
IPSL	0.01	0.921	0.18	0.020

RCP 8.5

	AET		**CWD**	
	τ	**p**	**τ**	**p**
GFDL	0.20	< 0.001	0.18	0.003
CSIRO	0.16	0.034	0.37	< 0.001
IPSL	-0.31	< 0.001	0.61	< 0.001

C.4 Development of Other Spatial Datasets Used In Predicting Post-Fire Abundance

In addition to gridded climate data (described in Appendix C.3), we developed or acquired several spatial datasets for use in predictive models of post-fire seedling abundance throughout the Southern Rocky Mountains Ecoregion. These additional datasets related to topography, soils, or fire severity, and are discussed below. We selected these datasets because these variables have known influences on plant growth, the distribution of vegetation, and, specifically, tree seedling establishment and abundance.

We first developed terrain variables of heat load index (HLI) and topographic position index (TPI). HLI is a proxy for aspect-driven solar heating, while TPI helps to quantify exposure and moisture availability. Climatic variables of AET and CWD include some of these effects, they are generally calculated at a coarser spatial scale, and thus including terrain variables allowed us to incorporate fine and mid-scale topographic effects to identify potential hot spots of

post-fire abundance. HLI combines slope, folded aspect, and latitude to estimate solar heating at a given location. To calculate HLI, we used equation 1 of McCune and Keon (2002) with 30 m digital elevation models (DEMs) from the national elevation dataset (NED; USGS 1999). We then aggregated these data to 60 m to align with the resolution of final spatial models. Higher values are typical on southwesterly slopes, while low values are common on northeasterly slopes. Moderate values are common in flatter terrain and on northwesterly and southeasterly aspects. Next, we calculated TPI at two spatial scales that characterize fine-scale (3 x 3 cell neighborhood) and coarse-scale (15 x 15 cell neighborhood) topographic effects. TPI was also developed using 30 m DEMs from NED, and is calculated as the difference between the elevation of a cell and the mean elevation in its surrounding neighborhood (i.e., a 3 x 3 or 15 x 15 cell neighborhood; Weiss 2001). Higher TPI indicates that a cell is at a relatively higher topographic position than its surroundings (i.e., ridgetops), while lower values are indicative of topographic low points such as valley bottoms or depositional basins. Importantly, TPI is scale-dependent. Calculation in larger window sizes identifies coarse-scale topographic features, while calculation in small window sizes identifies localized depressions and high points in fine-scale topography.

We also acquired data describing soil characteristics and fire severity. Soils data were acquired from POLARIS (Chaney et al. 2016) at a 30 m spatial resolution. POLARIS has important advantages over many spatial datasets describing soil characteristics in the continental United States because it is spatially contiguous (i.e., does not have the large gaps present in NRCS gSSURGO data) and provides a broad suite of chemical, textural, and structural variables (Chaney et al. 2016). We extracted percent clay content and soil pH as two additional predictors because of their potential influence on seedlings (Puhlick et al. 2012). Both variables were

extracted at a 30 m resolution and later aggregated to 60 m. We also acquired data on fire severity from the Monitoring Trends in Burn Severity interagency program (MTBS; Eidenshink et al. 2007). MTBS provides fire perimeters, thematic maps of burn severity, and LANDSAT-derived burn-severity indices for all fires larger than 400 ha in the United States. Specifically, we used the relative differenced Normalized Burn Ratio (RdNBR) (Miller and Thode 2007). As a relativized index, RdNBR better accounts for the initial state of vegetation in heterogeneous environments than other burn severity indices such as dNBR (Miller et al. 2009a) or dNDVI. Following acquisition, we aggregated these data to 60 m.

Table C6. Summary of variables included in analyses of post-fire conifer abundance. Variables are grouped into categories representing a range of potential factors driving post-fire recovery. Expected relationships among each variable and species (Douglas-fir – *Pseudotsuga menziesii*, and ponderosa pine – *Pinus ponderosa*) combination are indicated with a + or -. "Citation(s)" give a selection of recent studies that have investigated the influence of a specific variable on conifer establishment or post-fire recovery dynamics.

			Expected Relationship		
Category	**Variable**	**Description**	**Douglas-Fir**	**Ponderosa Pine**	**Citation(s)**
Time Since Fire	Time Since Fire	Number of years between fire occurrence and time of field surveys	-	-	(Tepley et al. 2017, Shive et al. 2018)
Fire Severity/ Forest Cover	Minimum Distance to Seed Tree	Field-derived distance to closest mature conifer. When not possible to collect in the field (n = 48), distances were derived from aerial image interpretation. Values were square root transformed prior to analysis to incorporate a non-linear effect.	-	-	(Chambers et al. 2016, Rother and Veblen 2016)
	RdNBR	Relative differenced Normalized Burn Ratio (RdNBR), an index of fire severity derived from LANDSAT imagery in the near-infrared and shortwave-infrared portions of the spectrum	-	+/-	(Welch et al. 2016)

Topography/Terrain	Heat Load Index	Index combining slope, aspect, and latitude to estimate differences in solar heating due to terrain variability. Higher values indicate greater solar heating. Calculated following equation 2 from McCune and Keon (2002) using 30 m digital elevation models and aggregated to 60 m.	-	+/-	(Stevens-Rumann et al. 2018)
	Topographic Position Index (3 x 3)	Elevation of an area relative to its surroundings. Higher values indicate ridgetops and lower values indicate valley bottoms. Calculated following Weiss (2001) using 30 m digital elevation models and aggregated to 60 m. 3 x 3 cell window is indicative of local topographic position.	-	+/-	(Owen et al. 2017, Ziegler et al. 2017)
	Topographic Position Index (15 x 15)	Elevation of an area relative to its surroundings. Higher values indicate ridgetops and lower values indicate valley bottoms. Calculated following Weiss (2001) using 30 m digital elevation models and aggregated to 60 m. 15 x 15 cell window is indicative of broader-scale topographic position.	-	+/-	(Owen et al. 2017, Ziegler et al. 2017)
Soils	Soil pH	A measure of acidity and alkalinity of soils. Derived from POLARIS soils database	-	-	(Puhlick et al. 2012)
	Soil Texture - Percent Clay Content	A measure of soil texture. Clay content leads to greater water holding capacity and cation exchange capacity, but shrink/swell may also reduce seedling survival. Derived from POLARIS soils database	-	-	(Puhlick et al. 2012)

Average Climate	30-Year Average Climatic Water Deficit (CWD)	The difference between potential and actual evapotranspiration (in mm) based on downscaled monthly GridMET normals (aggregated from daily data; 1981-2010), Penman-Montieth equations of PET, the water balance model of Dobrowski et al. (2013). Higher values are common on sites experiencing strong moisture limitation (warm and dry), while low values are common on sites with little moiture limitation (i.e., cool/wet sites, or warmer sites with high available moisture).	-	-	(Dobrowski et al. 2015, Tepley et al. 2017)
	30-Year Average Actual Evapotra-nspiration (AET)	Estimated annual actual evapotranspiration (in mm) based on downscaled monthly GridMET normals (aggregated from daily data; 1981-2010), Penman-Montieth equations of PET, the water balance model of Dobrowski et al. (2013). High values are typical on warm sites with little moisture limitation, while low values are typical on warm sites with strong moisture limitation, or on cool sites with minimal evapotranspiration.	+/-	+	(Dobrowski et al. 2015, Shive et al. 2018)
	30-Year Average Growing Season Precipitation (PPT-GS)	Average total precipitation (in mm) from April-September based on downscaled monthly GridMET normals (aggregated from daily data; 1981-2010).	+	+	(Welch et al. 2016, Rother and Veblen 2017)
Post-Fire Climate[a]	Average CWD in First Five Years After Fire	Mean annual CWD from five years after fire occurrence. Calculated using same methods as 30-year average CWD.	-	-	(Harvey et al. 2016, Stevens-Rumann et al. 2018)[b]
	Average AET in First Five Years After Fire	Mean annual AET from five years after fire occurrence. Calculated using same methods as 30-year average AET.	+/-	+	None

	Average PPT-GS in First Five Years After Fire	Mean total precipitation from April-September in first five years after fire.	+	+	None
	Maximum PPT-GS in First Five Years After Fire	Total precipitation from April-September in wettest of first five years after fire.	+	+	None
	Minimum PPT-GS in First Five Years After Fire	Total precipitation from April-September in driest of first five years after fire.	+	+	(Young et al. 2019)
	Maximum CWD in First Five Years After Fire	Annual CWD in driest of first five years after fire.	-	-	None
	Minimum CWD in First Five Years After Fire	Annual CWD in wettest of first five years after fire.	-	-	None
	Maximum AET in First Five Years After Fire	Maximum value of annual AET in first five years after fire.	+/-	+	None
	Minimum AET in First Five Years After Fire	Minimum value of annual AET in first five years after fire.	+/-	+	(Young et al. 2019)

[a]: All values for post-fire climate were scaled and centered to z-scores specific to each 250 m climate grid cell (relative to 1981-2015 historical period) prior to analysis.

[b]: Cited studies show a relationship with 3-year post-fire climate. However, we used a 5-year time period because observed establishment for Douglas-fir and ponderosa pine continued after for several years following fire in our sites, and because 5-year post-fire climate variables led to an improved model fit and higher cross-validated accuracy.

Table C7. Comparison of predictive accuracy for BRTs (boosted regression trees) and GLMMs (generalized linear mixed models) of post-fire abundances for ponderosa pine and Douglas-fir. RMSE (root mean squared error) and ρ (Pearson's correlation coefficient) are based on comparisons between observed and predicted values in the full dataset (i.e., full) and in spatially stratified cross-validation (i.e., test; 22 folds). Lower RMSE and higher *r* indicate a stronger relationship between observed and predicted values and a better model fit.

	Ponderosa Pine				**Douglas-Fir**			
Method	RMSE (Full)	RMSE (Test)	*r* (Full)	*r* (Test)	RMSE (Full)	RMSE (Test)	*r* (Full)	*r* (Test)
BRT	10.75	10.51	0.39	-0.12	8.34	8.58	0.75	0.11
GLMM	**9.72**	**10.40**	**0.46**	**0.22**	**7.09**	**8.00**	**0.61**	**0.25**
Hybrid	9.21	10.33	0.47	0.19	6.66	8.21	0.61	0.20

Table C8. Model summary table from GLMMs of post-fire ponderosa pine seedling abundance. We used zero-inflated models with a generalized Poisson error structure and random intercepts by fire. Variables were not scaled prior to analysis, therefore coefficients represent the predicted change in seedling abundance for each unit change in a given predictor.

	Model Term	**Coefficient**	**P-Value**
Conditional Model	Intercept	-2.384	0.210
	Distance to Seed Tree	-0.094	< 0.001
	Years Since Fire	-0.121	0.001
	30-Year Average Precipitation	0.009	0.014
	Topographic Position Index (TPI)	-0.055	0.130
	30-Year Climatic Water Deficit (CWD)	-0.003	0.005
	Max Post-fire CWD (Z-Score)	-1.459	< 0.001
	Average Precipitation * TPI	< 0.001	0.210

	Model Term	**Coefficient**	**P-Value**
Zero-Inflation Model	Intercept	-2.055	< 0.001

Table C9. Model summary table from GLMMs of post-fire Douglas-fir seedling abundance. We used zero-inflated models with a generalized Poisson error structure and random intercepts by fire. Variables were not scaled prior to analysis, therefore coefficients represent the predicted change in seedling abundance for each unit change in a given predictor.

	Model Term	Coefficient	P-Value
Conditional Model	Intercept	-2.384	0.210
	Distance to Seed Tree	-0.184	< 0.001
	30-Year Climatic Water Deficit (CWD)	-0.010	< 0.001
	Topographic Position Index (TPI)	-0.032	< 0.001
	Heat Load Index (HLI)	-4.513	< 0.001
	Max Post-fire CWD (Z-Score)	-1.098	0.011
Zero-Inflation Model	**Model Term**	**Coefficient**	**P-Value**
	Intercept	-2.235	0.003

C.5 Justification for Use of Historical Density Thresholds to Assess Resilience to Wildfire

In this study, we elected to use tree density thresholds that represent near-minimum historical densities in the montane zone of the Southern Rocky Mountains as a method of assessing resilience to wildfire. We were motivated to do this for several reasons. First, silvicultural stocking thresholds on many forests are currently based on timber management principles, and these stocking densities tend to be unreasonably high (Welch et al. 2016, North et al. 2019). Timber production on federally-owned lands has declined since the 1980s (Howard and Jones 2016), and is generally a lower priority than many other management goals in the Southern Rocky Mountains. Many studies use "replacement density" (i.e., the mature overstory density of forests on each site prior to the fire; e.g., Rother and Veblen 2016, Stevens-Rumann et al. 2018) as a logical threshold as the assessment of resilience. However, tree density (i.e., stems ha^{-1}) is not broadly quantified throughout montane forests in the region. Furthermore, density reduction treatments are a common practice in montane forests throughout the region (Reynolds

et al. 2013, Addington et al. 2018), and pre-fire tree densities may be higher than those desired by forest managers (Dickinson et al. 2014).

Historical minimum tree densities, as used in this study, are a useful alternative approach because they represent the lowest stem densities that might be considered to be ponderosa pine or mixed-conifer forests in the Southern Rocky Mountains. Because there is also no consideration of seedling mortality or recruitment rates, historical tree densities represent a very low threshold for resilience and conservatively estimate the area that is experiencing regeneration failure. Any potential biases using these thresholds would be in failing to detect areas that are unlikely to regenerate to a forested state. We set these thresholds by combining data from three published studies that used tree-ring reconstructions to estimate late 1800s tree density in montane forests throughout the Southern Rocky Mountains (Fulé et al. 2009, Rodman et al. 2017, Battaglia et al. 2018). From these data, we used the 5^{th} percentile of species-specific densities for Douglas-fir and ponderosa pine (5 and 20 trees ha^{-1}, respectively) from plots with species presence (i.e., excluding zero counts). In Table C10, we present the means and ranges of values reported in these studies, as well as a summary of similar studies that reconstructed stand densities in the montane zone of the Southern Rocky Mountains using tree-ring methods, general land office records, tree morphology, and/or early forest inventory data (*sensu* Woolsey 1912).

Table C10. Summary of stand density reconstructions in Colorado and New Mexico, USA using four different techniques (i.e., tree-ring reconstructions, tree morphology, early forest inventory data, and General Land Office (GLO) data). Values given are reported or calculated mean, with total range in parentheses.

Citation	PIPO	PSME	Total Density	Sizes	Year(s)	Method	Study Area
Fulé et al. (2009) [a]	67.4 (60.8-78.8)	20.7 (18.3-26.7)	141.6 (127.1-146.7)	> 0 cm DBH	1870	Tree rings	San Juan Mountains, Colorado
Romme et al. (2009)[b]	NA	NA	43.6 (11-98)	Unspecificed	1900	Tree morphology	San Juan Mountains, Colorado
Williams and Baker (2012)[c]	NA	NA	216.9 (0-?)	> 10 cm DBH	c. 1880	General Land Office records	Front Range, Colorado
Matonis et al. (2014)[d]	NA	NA	49.5 (12.4-135.9)	> 15.2 cm DBH	1875	Tree rings	Uncompahgre Plateau, Colorado
Brown et al. (2015)[e]	96 (0-320)	0	96 (0-320)	> 0 cm DBH	1860	Tree rings	Front Range, Colorado
Rodman et al. (2017)[f]	181.9 (114.3-250.4)	8.9 (0-29.5)	140.9 (35-314.3)	> 0 cm DBH	1880; 1890	Tree rings; early forest inventories	Northern and Western New Mexico
Baker et al. (2017) - Pine	NA	NA	168.0 (64.2-306.4)	> 10 cm DBH	1881-1902	General Land Office records	Uncompahgre Plateau, Colorado
Baker et al. (2017) - Dry Mixed-Conifer	NA	NA	195.2 (84.0-353.4)	> 10 cm DBH	1881-1902	General Land Office records	Uncompahgre Plateau, Colorado
Baker et al. (2017) - Wet Mixed-Conifer	NA	NA	422.5 (64.2-998.3)	> 10 cm DBH	1881-1902	General Land Office records	Uncompahgre Plateau, Colorado
Battaglia et al. (2018)	98.8 (0-344.8)	34.1 (0-555.4)	142.4 (0-767.8)	> 4 cm DBH	1860	Tree rings	Front Range, Colorado

[a]: Reported values taken from site-level means, where each site was composed of several individual plots that likely had a wider range.
[b]: True minimum and maximum range of values were not reported. Minimum and maximum values are the site-level means +- two standard errors.
[c]: Minimum value was taken from map showing some previously unforested area in the study area. The maximum value was not reported.
[d]: Reported densities exclude aspen and other angiosperms due to more rapid decomposition.
[e]: Sites included in this study are also included in Battaglia et al. (2018), but minimum tree sizes included are different in each study. Therefore, both are reported here.
[f]: Many of these sites were also included in Reynolds et al. (2013) and Moore et al. (2004)